Thomas Gamse, Amra Perva, Zeljko Knez (eds.)

# Book of Abstracts

## GEHPT and ESS-HPT 2022

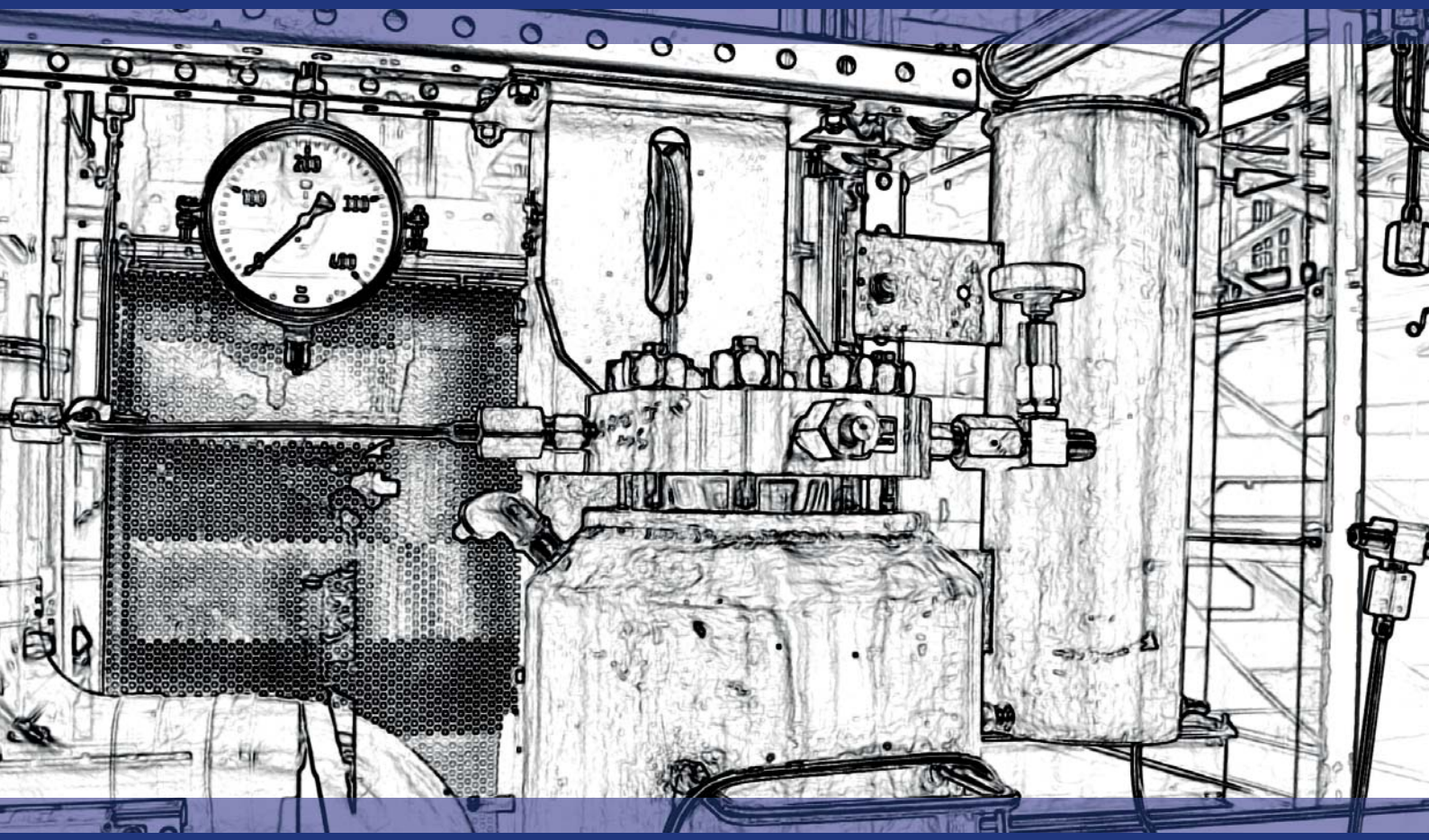

**Green Engineering by High Pressure Technology**

3.7. – 10.7.2022

**The European Summer School in High Pressure Technology**

11.7. – 17.7.2022

TU Graz
Graz University of Technology

University of Maribor
Faculty of Chemistry and Chemical Engineering

EFCE
European Federation of Chemical Engineering
Europäische Föderation für Chemie-Ingenieur-Wesen
Fédération Européenne de Génie Chimique

# Imprint

Organisation: Thomas Gamse
Institute of Chemical Engineering and Environmental Technology
**Graz University of Technology**
**Inffeldgasse 25/C, A-8010 Graz, Austria**
Tel. +43 (0)316 873-7477
E-Mail: thomas.gamse@tugraz.at

Zeljko Knez
Amra Perva
Faculty of Chemistry and Chemical Engineering
Laboratory for Separation Processes
**University of Maribor, Smetanova ulica 17, 2000 Maribor, Slovenia**
E-Mail: zeljko.knez@um.si; amra.perva@um.si

Editors: Thomas Gamse, Amra Perva
Layout: Thomas Gamse
Cover: Verlag der Technischen Universität Graz,
Thomas Gamse

2022 Verlag der Technischen Universität Graz
www.tugraz-verlag.at

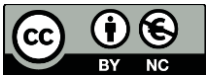



Book of Abstracts, GEHPT and ESS-HPT 2022
“Green Engineering by High Pressure Technology”
"The European Summer School in High Pressure Technology"
3.7.-17.7.2022, University of Maribor and Graz University of Technology

ISBN (e-book) 978-3-85125-903-2

DOI 10.3217/978-3-85125-903-2

# Preface

The European Summer School in High Pressure Technology (ESS-HPT) is the continuation of many years of high pressure intensive courses. The history of this very successful series of courses started in 1995, when the first intensive course took place in Monselice, Italy. Most of these Intensive Courses were supported by SOCRATES and later Life Long Learning, as shown in following overview:

SOCRATES IP "Current Trends in High Pressure Technology and Chemical Engineering"
- 1995 Monselice / Italy
- 1996 Nancy / France
- 1997 Erlangen / Germany

SOCRATES IP "High Pressure Technology in Process and Chemical Engineering"
- 1999 Abano Terme / Italy
- 2000 Valladolid / Spain
- 2001 Maribor / Slovenia and Graz / Austria

SOCRATES IP "High Pressure Chemical Engineering Processes: Basics and Applications"
- 2002 Graz / Austria and Maribor / Slovenia
- 2003 Budapest / Hungary
- 2004 Barcelona / Spain

SOCRATES IP "Basics, Developments, Research and Industrial Applications in High Pressure Chemical Engineering Processes"
- 2005 Prague / Czech Republic
- 2006 Lisbon / Portugal
- 2007 Albi / France

Life Long Learning IP "SCF- GSCE: Supercritical Fluids – Green Solvents in Chemical Engineering"
- 2008 Thessaloniki / Greece
- 2009 Istanbul / Turkey
- 2010 Budapest / Hungary

EFCE Intensive Course "High Pressure Technology - From Basics to Industrial Applications"
- 2011 Belgrade / Serbia

Life Long Learning IP "PIHPT: Process Intensification by High Pressure Technologies – Actual Strategies for Energy and Resources Conservation"
- 2012 Maribor / Slovenia and Graz / Austria
- 2013 Darmstadt / Germany
- 2014 Glasgow / Great Britain

Unfortunately the financial support for these Intensive Programmes was cancelled within ERASMUS+. The EFCE Working Party "High Pressure Technology" decided in September 2014 to go on with this course in the form of a Summer School.

ESS-HPT "The European Summer School in High Pressure Technology"

| | |
|---|---|
| ESS-HPT 2015 | Maribor / Slovenia and Graz / Austria |
| ESS-HPT 2016 | Maribor / Slovenia and Graz / Austria |
| ESS-HPT 2017 | Maribor / Slovenia and Graz / Austria |
| ESS-HPT 2018 | Maribor / Slovenia and Graz / Austria |
| ESS-HPT 2019 | Maribor / Slovenia and Graz / Austria |
| ESS-HPT 2021 | Online Course, Graz / Austria |
| GEHPT and ESS-HPT 2022 | Maribor / Slovenia and Graz / Austria |

The ESS-HPT takes place every year within the first 2 weeks of July at University of Maribor, Slovenia and Graz University of Technology, Austria.

This year the first week in Maribor / Slovenia is organised as a COST training school "GEHPT – Green Engineering by High Pressure Technology", financed by the COST action "GREENERING -Green Chemical Engineering Network towards upscaling sustainable processes", COST action CA18224.


All participants have to give an oral presentation and the abstracts of these presentations, which are peer-reviewed by the EFCE WP Members, are published in this book of abstracts.

The editor

Thomas Gamse
Organiser of GEHPT and ESS-HPT 2022

Many thanks to our sponsors, COST action CA18224 "GREENERING", NATEX Prozesstechnologie GesmbH and Tourismusverband Stadt Graz.



# Contents

## Abstracts of Participants Presentations

| | Tuesday, 5 July 2022 | | |
|---|---|---|---|
| 11 | 17:15 - 17:30 | **Laura Euler Bueno, Robin Dursun, Markus Busch, Jan Duchateau**<br>Propargyl Methacrylate - A Bifunctional Comonomer in the High Pressure Polymerization of Ethene | 44 |
| | | | |
| 12 | 17:30 - 17:45 | **Jeta Lica, Lorenci Gjurgjaj, Iris Çaçani, Carla Ferreri, Altin Mele**<br>The Fatty Acid Analysis of Vitex Agnus Castus Extracts Obtained by Liquid $CO_2$ | 48 |
| | | | |
| 13 | 17:45 - 18:00 | **Enkeledo Menalla, Maria Jose Cocero**<br>Understanding the Role of Sub/Supercritical Water in the Hydrolysis of the Ester Link in Polyesters | 53 |
| | | | |
| 14 | 18:00 - 18:15 | **Lena Gockel, Markus Busch**<br>Influence of Mixing on the Initiator Efficiency in High-Pressure Polymerization Reactors | 56 |
| | | | |
| 15 | 18:15 - 18:30 | **Vid Ravnik, Marko Jukić, Urban Bren**<br>Inverse Molecular Docking of Cannabinoids | 59 |

| | Wednesday, 6 July 2022 | | |
|---|---|---|---|
| 16 | 15:30 - 15:45 | **Moritz Imhoff, Markus Busch**<br>Ventilated Deflagrations of Polymerization Mixtures | 64 |
| | | | |
| 17 | 15:45 - 16:00 | **Elisa Mialich**<br>Optimization of $scCO_2$ Drying of Tuna Fillets | 68 |
| | | | |
| 18 | 16:00 - 16:15 | **Alexander Klimeck, Markus Busch**<br>Group Contribution Method for Transfer Activity in the LDPE Process | 73 |
| | | | |
| 19 | 16:25 - 16:40 | **Altin Mele, Jeta Lica, Lorenci Gjurgjaj, Dorina Mele, Ardita Mele**<br>Presentation of P,V,T,x Phase Equilibria on Mole Volume – Composition Diagram in the Example of the $CO_2$ – $C_2H_5OH$ System | 76 |
| | | | |
| 20 | 16:40 - 16:55 | **Julija Strunčnik**<br>Solvent Absorption Study of Cross-Linked Polymers | 81 |
| | | | |
| 21 | 16:55 - 17:10 | **Isabel M. Kronshorst, Laura Ständecke, Julia Eigenseer, Markus Busch**<br>A Mini-Plant as a Tool for Understanding the Solution Polymerisation Process | 84 |
| | | | |

| | | | |
|---|---|---|---|
| 22 | 17:15 - 17:30 | **Zala Štukovnik, Urban Bren**<br>Development and Optimization of an Electrochemical-Impedimetric Biosensor Based on Whole Cells for the Detection of Active Compounds | 87 |
| | | | |
| 23 | 17:30 - 17:45 | **Ka Loi Lin, Thomas Ernst Müller**<br>$CO_2$ and Biomass as Feedstock for the Production of Chemical Intermediates | 92 |
| | | | |
| 24 | 17:45 - 18:00 | **Patience Nnenna Abugu**<br>Nano-Silica Grafting with Aminosilanes in Supercritical Carbon Dioxide for Polymer Nanocomposites Preparation | 96 |
| | | | |
| 25 | 18:00 - 18:15 | **Dennis Panke, Thomas E. Müller**<br>Conversion of Lignin to Phenolic Base Chemicals | 102 |

| | **Thursday, 7 July 2022** | | |
|---|---|---|---|
| 26 | 17:15 - 17:30 | **Aaron Röblitz, Markus Busch**<br>Visualization of Relief and Decomposition Phenomena in High-Pressure Systems | 106 |
| | | | |
| 27 | 17:30 - 17:45 | **Alina Satpayeva, Juan Garcia-Serna, Danilo Cantero**<br>Evaluation of Chemical Reaction of Biomass under Partial Oxidation in Supercritical Water | 110 |
| | | | |
| 28 | 17:45 - 18:00 | **Lorenz Schmidt, Markus Busch**<br>Influence of Initiators on Temperature Distribution in High-Pressure Polyethylene Autoclaves | 113 |
| | | | |
| 29 | 18:00 - 18:15 | **Inês Vasconcelos Silva, Raquel Costa, Ana Leite Oliveira**<br>Using Supercritical Carbon Dioxide to Process Biological Tissue into Preserved and Highly Functional Matrices for Tissue Healing and Regeneration | 117 |
| | | | |
| 30 | 18:15 - 18:30 | **Azra Osmić, Matjaž Finšgar, Gal Slaček, Taja Žitek, Maša Knez Marevci, Željko Knez**<br>Extraction of Active Components from Cranberry (Vaccinium vitis-ideaea) and Determination of Antimicrobial Potential | 124 |

**Registered Lecturers** **130**

**Registered Participants** **132**

# Development of self-assembled aerogel silk particles for wound healing

Beatriz G. Bernardes[1,2], Sara Baptita-Silva[1], Carlos Illanes-Bordomás[2], Rui Magalhães[1], Raquel Costa[*3,4,5], Carlos A. García-Gonzaléz[*2], Ana Leite Oliveira[*1]

[1] Universidade Católica Portuguesa, CBQF - Centro de Biotecnologia e Química Fina – Laboratório Associado, Escola Superior de Biotecnologia, Porto, Portugal

[2] Department of Pharmacology, Pharmacy and Pharmaceutical Technology, I+D Farma group (GI-1645), iMATUS and Health Research Institute of Santiago de Compostela (IDIS), Universidade de Santiago de Compostela, E-15782 Santiago de Compostela, Spain

[3] Instituto de Investigação e Inovação em Saúde, Universidade do Porto (i3S), Porto, Portugal

[4] Department of Biomedicine, Biochemistry Unit, Faculdade de Medicina, Universidade do Porto, Porto, Portugal

[5] Escola Superior de Saúde, Instituto Politécnico do Porto, Porto, Portugal

*raquel.costa@i3s.up.pt; carlos.garcia@usc.es; aloliveira@ucp.pt

## Introduction

Chronic wounds are one of the major therapeutic and healthcare challenges. The wound healing process is divided in three important stages (haemostasis, inflammation and proliferation/maturation) that deploy a series of biochemical reactions which induce the repair of the injury. In chronic wounds, healing is prolonged in the inflammatory phase without reaching the required anatomic and functional integrity to attain the proliferation phase.[1] A fluid (exudate) can be produced as a natural response towards healing. However, its excessive production can be detrimental, as it promotes bacterial growth, delaying the inflammatory phase. Nowadays, the design and development of biocompatible, biodegradable and adaptable materials that promote the tissue repair, prevent the infection and inflammation and ensure the management of exudate are a constant need for wound management.

Aerogels are nanostructured materials with high porosity, large surface and low bulk density.[2] They can provide advanced performance for wound healing due to their high porosity and large surface area, which can be tailored for a fast and directional fluid transfer of the exudate. Bio-based aerogels, from natural polymer sources are assessed

as drug carriers because of their biocompatibility, biodegradability, low toxicity, high loading capacity, enhanced stability upon storage and tuneable drug release.[3,4] Silk fibroin (SF) protein, obtained from *Bombyx Mori,* is an excellent carrier of bioactive compounds while supporting cell proliferation, being presently used in wound healing and regeneration. In this work, we propose the use supercritical $CO_2$ technology to develop SF aerogel particles for wound treatment.

## Experimental

Silk fibroin extracted from *Bombyx mori* cocoons was used for the aerogel particles' production. Different SF aqueous solutions (3, 5 and 7% (w/v)) were added dropwise to a mixture of ethanol and sorbitan oleate (Span 80) (3 wt.% with respect to SF), followed by supercritical $CO_2$ drying (120 bar, 39ºC, 3.5 h). SF aerogel particles were characterized concerning particle size distribution by laser diffraction. The average diameter and the dispersion increased with increasing SF concentration. These particles presented also high surface area and low skeletal density (Figure 1A). Fourier Transform Infrared with Attenuated Total Reflectance spectroscopy (FTIR-ATR) was used to study the chemical structure, in particular secondary structure formation. It was possible to verify the presence of the main characteristic bands of SF assigned to the presence of β-sheet structure (Figure 1B). Textural properties were analyzed by helium pycnometry and N2 adsorption-desorption presenting high surface area and low skeletal density.

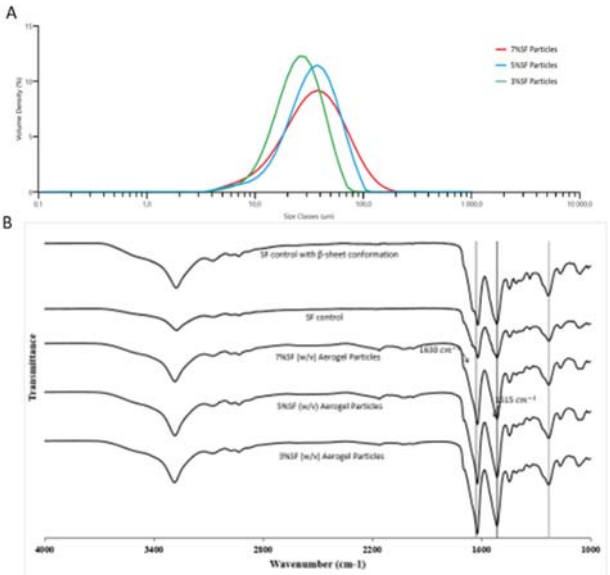


Figure 1 - A) Laser diffraction of different concentrations of S aerogel particles. B) FTIR-ATR of SF aerogel particles and controls of natural SF and SF with β-sheet conformation.

Aerogel particles' biocompatibility was evaluated by direct contact with Human Dermal Fibroblasts (HDF's) and observed by Scanning Electron Microscope (SEM). Figure 2A, represents the SF Aerogel particles by SEM. Quantitative data were subjected to an analysis of variance (one-way ANOVA, Tukey's test; α=0.05. SF aerogel particles were tested by MTT assay and the cell viability increases consistently with time. After 24 h of incubation, all the aerogels presented a cell viability of 50% and there were significant differences between the cells in contact with the aerogel particles and the control group (Figure 2A). This cell response to the presence of aerogel particles, could be related with the initial adaptation of the cells to the contact with the particles. After 48 h, the cell viability increased considerably to 100%, having no significant differences between the control group, demonstrating that the cells were able to adapt to the aerogel particles. After 7 days of incubation, it was possible to verify that the aerogel particles had a marked effect on promoting cell proliferation.

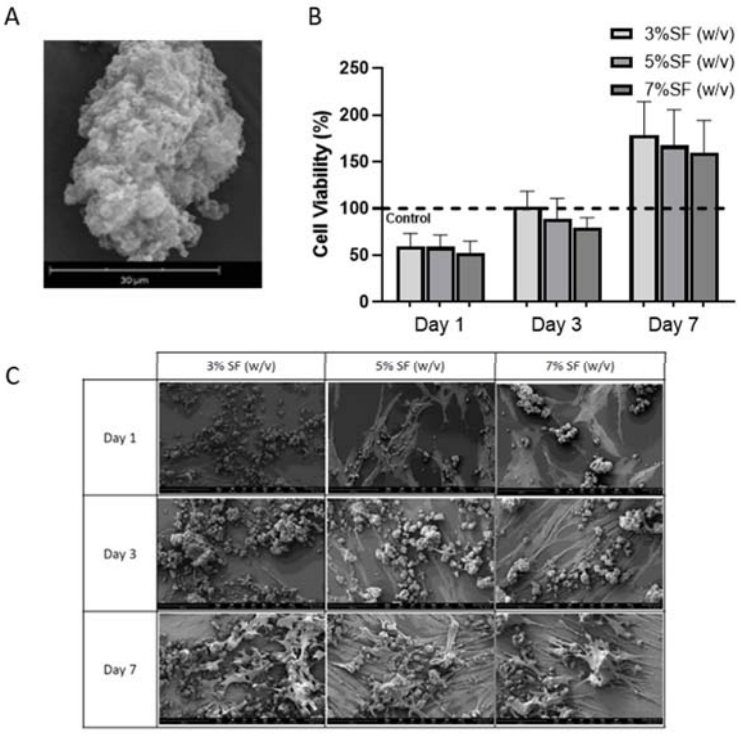


Figure 2 – A) SEM micrographs of SF Aerogel particles. B) Cell viability after MTT assay of control group of NDF's cells and cells cultured with aerogel particles. After Tuckey's analysis of variance there were no statistical difference between groups for the same time point ($\alpha < 0.05$). C) SEM micrographs of HDF's cell adhesion and culture on the SF Aerogel particles for 1, 3, and 7 days. Magnification of 1050× were used.

Following these promising results, studies are ongoing to use these particles as a controlled release system of adenosine, a nucleoside that is expected to trigger the healing process of chronic wounds, promoting angiogenesis and regeneration.[5]

## Summary

Wound exudate is a natural response to heal. However, its excess production can compromise and delay the inflammatory phase, which often is associated with chronicity. Novel biocompatible, biodegradable and adaptable dressings are sought to promote tissue regeneration, prevent infection and control inflammation. Aerogels are nanostructured materials with high porosity, large surface area, low bulk density and water uptake that can provide advanced performance for wound healing, especially considering the management of exudate. Silk fibroin (SF) aerogels can act as promising carriers of bioactive molecules while supporting cell proliferation. Hereupon, SF aerogel particles were developed as carriers for controlled release of bioactive molecules such as adenosine for promoting wound healing and regeneration.

## Acknowledgments

This research was funded by MICINN [PID2020-120010RB-I00], Xunta de Galicia [ED431C 2020/17], Agencia Estatal de Investigación [AEI] and FEDER funds. This work was also supported by National Funds from Fundação para a Ciência e a Tecnologia (FCT), through project UID/Multi/50016/2020, Doctoral Research Grant 2021.05717.BD and Post-Doctoral research grant SFRH/BPD/116024/2016. Work carried out in the framework of the COST Action CA18224 “Green Chemical Engineering Network towards upscaling sustainable processes” (GREENERING), funded by the European Commission; and project TEX4WOUNDS (POCI-01-0247-FEDER-047029), financed under the Incentive System for Research and Technological Development, R&DT Projects in co-promotion (Notice SI/17/2019).

## References

[1] S.A. Shah, M. Sohail, S. Khan, M.U. Minhas, M. de Matas, V. Sikstone, Z. Hussain, M. Abbasi, M. Kousar, Biopolymer-based biomaterials for accelerated diabetic wound healing: A critical review, International Journal of Biological Macromolecules. 139 (2019) 975–993. https://doi.org/10.1016/j.ijbiomac.2019.08.007.

[2] C. López-Iglesias, J. Barros, I. Ardao, F.J. Monteiro, C. Alvarez-Lorenzo, J.L. Gómez-Amoza, C.A. García-González, Vancomycin-loaded chitosan aerogel particles for chronic wound applications, Carbohydrate Polymers. 204 (2019) 223–231. https://doi.org/10.1016/j.carbpol.2018.10.012.

[3] H. Maleki, L. Durães, C.A. García-González, P. del Gaudio, A. Portugal, M. Mahmoudi, Synthesis and biomedical applications of aerogels: Possibilities and challenges, Advances in Colloid and Interface Science. 236 (2016) 1–27. https://doi.org/10.1016/j.cis.2016.05.011.

[4] B.G. Bernardes, P. del Gaudio, P. Alves, R. Costa, C.A. García-Gonzaléz, A.L. Oliveira, Bioaerogels: Promising Nanostructured Materials in Fluid Management, Healing and Regeneration of Wounds, Molecules. 26 (2021) 3834. https://doi.org/10.3390/molecules26133834.

[5] M.C. Montesinos, A. Desai, J.-F. Chen, H. Yee, M.A. Schwarzschild, J.S. Fink, B.N. Cronstein, Adenosine Promotes Wound Healing and Mediates Angiogenesis in Response to Tissue Injury Via Occupancy of A2A Receptors, The American Journal of Pathology. 160 (2002) 2009–2018. https://doi.org/10.1016/S0002-9440(10)61151-0.

# High-Pressure Polymerization of Ethylene: From Tubular Reactors, Autoclaves and the Urge to Design a Multi-Zone Autoclave on Laboratory Scale

*Nicola Schreiner, Lena Gockel, Markus Busch**
TU Darmstadt, Darmstadt/Germany
*e-mail: markus.busch@pre.tu-darmstadt.de

## Introduction

Everyday life without plastics is hard to imagine. Whether the toothbrush at home, the car interior on the way to work or functional clothing during sports, plastics are omnipresent. They owe their special position as a material of the 21st century to their lower density with stabilities like materials such as steel, glass, or wool. In 2018, 359 million tons of plastics were produced worldwide. With 61.8 million tons, Europe is the third-largest producer after China and the NAFTA countries. Just under 30 % of the plastics produced here are polyethylene.[1]

Polyethylene is differentiated by its microstructure into low-density polyethylene (LDPE), linear low-density polyethylene (LLDPE), and high-density polyethylene (HDPE). The properties based on the microstructure and the resulting fields of application are determined by the manufacturing process. The synthesis of LDPE follows the mechanism of radical polymerization. For this purpose, temperatures of up to 330 °C and pressures of up to 3500 bar are reached. The long- and short-chain branching that occurs in this process is largely responsible for the properties of the polymer and justifies the cost-intensive high-pressure synthesis.[2,3,4]

## Experimental

For the industrial production of LDPE, both autoclaves and tubular reactors can be used. Tubular reactors show conversions of up to 40 % due to the favorable surface-to-volume ratio. Industrial autoclave reactors on the other hand are limited in their conversions to about 20 %. This is due to the poorer heat dissipation of the heat of polymerization, caused by a lower surface-to-volume ratio.[5,6] Figure 1 shows a schematic illustration of the setup of an autoclave and a tubular reactor.

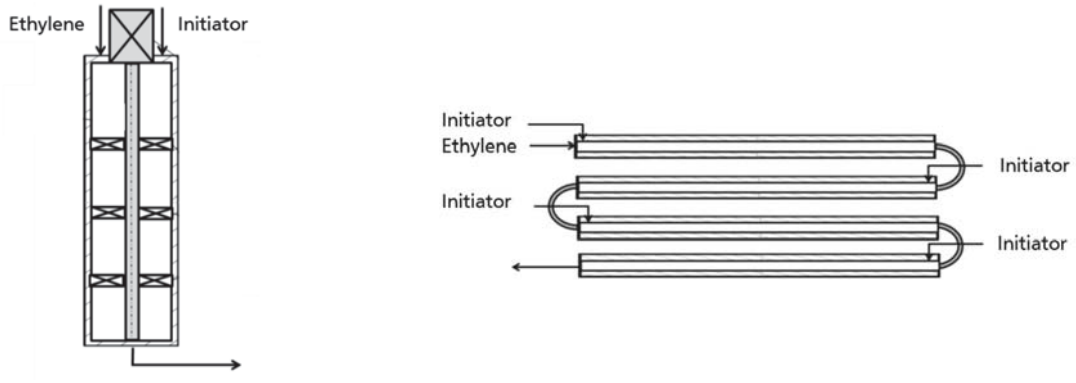


Fig. 1.: Schematic illustration of an autoclave and tubular reactor used in the high-pressure polymerization of ethylene.

During this work both a tubular reactor and an autoclave are used to perform the radical polymerization of ethylene on a laboratory scale. The obtained samples are then analyzed and compared regarding their microstructure. Both reactors show a contrary residence time behavior, which results in different microstructures of LDPE. Due to back mixing, autoclave products show a broad molecular weight distribution. Compared to tubular products, the number of long-chain branches is increased, and the polymer chains look tree-like branched. Both criteria are essential for extrusion coating applications. Tubular products, on the other hand, show a narrow molecular weight distribution with a lower number of long-chain branches. The polymer chains are more comb-like structured. Both structures are depicted in Figure 2.

Fig. 2.: The microstructure of LDPE produced in autoclaves (lef) and tubular reactors (right). Due to the back-mixing behavior of an autoclave, its product is tree-like branched. Tubular products are comb-like branched.

To combine the preferred unique structure of autoclave products and the higher conversion of tubular reactors, multi-zone autoclaves are a promising approach. In this

process, several fresh ethylene feeds and a gradual increase in reaction temperature lead to a conversion close to the tubular reactor scale. However, due to back-mixing, the microstructure of an autoclave can be maintained.[6,7,8]

This is where, the second part of the present work takes place: The first steps towards the realization of a 300 mL multi-zone autoclave designed for 3500 bar and 300 °C on a laboratory scale are presented. Figure 3 shows the CAD drawing of the planned 300 mL multi-zone autoclave.

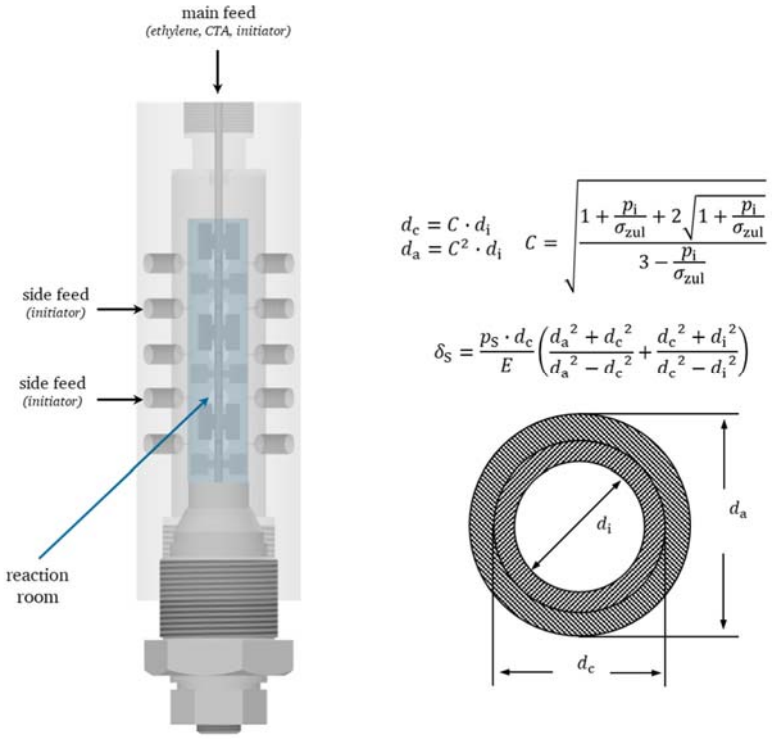


Fig. 3.: CAD-drawing of the 300 mL multi-zone autoclave with 30 boreholes to introduce thermocouples and side feeds. On the right: Method to design a shrink construction.

## Summary

The present work used an autoclave as well as a tubular reactor to conduct the high-pressure polymerization of ethylene. The obtained LDPE is investigated regarding its microstructure. Furthermore, the first steps towards the realization of a multi-zone-autoclave are shown.

We acknowledge the generous support of SCG Chemicals.

## References

[1] PlasticsEurope, **2019**.

[2] M. D. Lechner, K. Gehrke, E. H. Nordmeier, *Makromolekulare Chemie*, **2014**.

[3] N. Maraschin, *Encyclopedia of Polymer Science and Technology: Ethylene Polymers*, **2002**.

[4] Uhde High Pressure Technologies GmbH, Broschüre zum Thema LDPE, **2012**.

[5] K. S. Whiteley, in *Ullmann's Encyclopedia of Industrial Chemistry: Polyethylene*, **2000**.

[6] I. Neuhaus, PhD Thesis, TU Darmstadt **2014**.

[7] R. Kuhn, H. Kröner, G. Roßmanith, *Angew. Makro. Chem.* **1974**, *40*, 361.

[8] C. Kiparissides, J. F. MacGregor, G. Verros, *J. Macromol. Sci. Rev. Macromol. Chem. Phys.* **1993**, *33*, 437.

# Hydrothermal $CO_2$ Reduction by Glucose as Reducing Agent and Metals and Metal Oxides as Catalysts

Maira I. Chinchilla, Fidel A. Mato, Ángel Martín, María D. Bermejo*

Press Technologies Group, Department of Chemical Engineering and Environmental Technology, BioEcoUva Research Institute on Bioeconomy, Universidad de Valladolid.

mairaivette.chinchilla@alumnos.uva.es (M.I.C.); fidel@iq.uva.es (F.A.M.); mamaan@iq.uva.es (Á.M.); * Correspondence: mdbermejo@iq.uva.es

## Introduction

In this work aims to investigate the hydrothermal reduction of $CO_2$ previously captured in basic solutions in presence of metals and metal oxide catalysts and molecules derived from biomass, to obtain high value-added products such as formic acid (FA) that is a hydrogen vector and could be used directly as high energy density carrier for fuel cells [1].

Hydrothermal reduction of $CO_2$ is one of many research techniques to produced formic acid and is part of the Carbon Utilization initiatives that are being developed to mitigate greenhouse emissions by using $CO_2$ as raw material to obtain high value-added products [2–8].

In the hydrothermal reduction of $CO_2$, water at high pressures and temperatures[9–11] is used as hydrogen donor medium [12]. Several metals and metal oxides have been suggested as $CO_2$ reducers (Zn [13]) and catalysts (Pd/C[10,14], $Fe_2O_3$ [15]), that improve the hydrothermal reduction of the carbon source and increase the yield of formic acid which is one of the most frequent products obtained from these reactions. Some works state that organic compounds containing alcohol groups such as isopropanol[16], glycerol[17], glucose, C2 and C3 alcohols, saccharides, lignin derivatives[18] could be used as reducing agents because these molecules contain alcohol groups that oxidate to intermediate species of that could lead to the production of formic acid.

In this research, all these variables have been taken in account and the influence that different catalysts (Cu, Ni, Pd/C 5%, Ru/C 5%, $Fe_3O_4$, $Fe_2O_3$ and activated carbon) have on the production of formic acid by means of hydrothermal conversion of $CO_2$ by using glucose as reducing agent, and sodium bicarbonate ($NaHCO_3$) as carbon source was studied.

## Experimental

Different set of experiments were carried out in order to study the possibility to obtain FA from the reduction of $CO_2$ captured in a basic solution, by using glucose as reducing agent and metal and metal oxides as catalysts.

The procedure was carried out in horizontal tubular batch reactors of 10 ml volume that were filled with, 4.6 ml of a solution of sodium bicarbonate (SB) 0.5 M which was the carbon source and glucose (0.05 M) as reducing agent. Powder of Cu (400 μm), Ni (9 μm), Pd/C 5% (25 μm), Ru/C 5% water paste (175 μm), $Fe_3O_4$ (90 μm) and $Fe_2O_3$ (100 μm) as well as activated carbon were used as catalysts. The reactions took place for 30, 60 and 120 minutes at 200 and 250°C. A fluidized bed heater was used to achieve the working temperature. All solutions were prepared with deionized water. The reaction was stopped by introducing the reactors immediately in a water bath at 15 °C.

The yield of the reaction was calculated as:

$$Y_{product} = \frac{C_{Product}}{C_{Reductant,i}} * 100\%$$

Where $C_{Product}$ is the molar concentration of formic acid at the end of the reaction, and $C_{reductant,i}$ is the initial molar concentration of the organic reductant.

Concentration of FA in the liquid product was measured in HPLC. FA can be generated by following two paths: from the oxidation of sugars at low temperatures in basic aqueous media [19–22]; or by the reduction of sodium bicarbonate at high temperatures [18]. Because of these possibilities several reactions in which $NaH^{13}CO_3$ (SB-$^{13}$C) was used as carbon source were performed in order to investigate the origin of FA. This samples were analysed with $^{13}$C-NMR.

## Summary

In all the reactions FA, acetic acid and lactic acid were obtained in major proportion. In minor quantity were identified other products that derive typically from the reduction of glucose in basic media, such as: glyceraldehyde, glycolaldehyde, formaldehyde, ethylenglycol, acetone, pyruvaldehyde, galacturonic acid or 5-HMF.

Regarding the production of total FA, $Fe_3O_4$ is the catalyst that provides the highest yield of FA: 49% at 250°C and 2 hours of reaction.

From the NMR results it was observed that Pd/C 5%, Ru/C 5% and Ni favoured the formation of FA derived from the reduction of SB-$^{13}$C over that produced by the reduction

of glucose. The fractions of FA coming from SB-$^{13}$C for these catalysts were 0.81, 0.76, and 0.69, respectively.

It was observed that metal supported catalysts such as Pd/C 5% and Ru/C 5% presented highest catalytic effect to reduce SB-$^{13}$C in comparison to the activated carbon support (C), which reach fraction of FA of 0.81, 0.76 and 0.34 each.

There were catalysts that did not improved the reduction of SB-$^{13}$C, in fact, the reaction without catalyst (fraction FA-$^{13}$C: 0.37) showed slightly higher capability to reduce $^{13}CO_2$ than Cu, $Fe_3O_4$ and $Fe_2O_3$ (0.37, 0.32 and 0.34, respectively).

The performance of the catalysts to reduce $CO_2$ captured as SB-$^{13}$C was: Pd/C 5% > Ru/C 5% > Ni > Cu > C ≈ $Fe_2O_3$ > $Fe_3O_4$.

## Acknowledgment

This research was funded by Ministerio de Ciencia y Universidades by project RTI2018-097456-B-I00 and by the Regional Government of Castilla y León and the EU-FEDER program (CLU-2019-04)

M.I.C. acknowledges Universidad de Valladolid and Banco de Santander for the predoctoral grant. The authors acknowledge Laboratorio de Técnicas Instrumentales UVa for their assistance in the NMR and SEM analysis.

## References

1. Uhm, S.; Chung, S.T.; Lee, J. Characterization of Direct Formic Acid Fuel Cells by Impedance Studies: In Comparison of Direct Methanol Fuel Cells. *Journal of Power Sources* **2008**, *178*, 34–43, doi: 10.1016/J.JPOWSOUR.2007.12.016.
2. Intergovernmental Panel on Climate Change Global Warming of 1.5 ºC Available online: https://www.ipcc.ch/sr15/ (accessed on 21 December 2021).
3. United Nations El Acuerdo de París | CMNUCC Available online: https://unfccc.int/es/process-and-meetings/the-paris-agreement/el-acuerdo-de-paris (accessed on 27 January 2022).
4. Khezri, M.; Heshmati, A.; Khodaei, M. Environmental Implications of Economic Complexity and Its Role in Determining How Renewable Energies Affect CO2 Emissions. *Applied Energy* **2022**, *306*, 117948, doi: 10.1016/J.APENERGY.2021.117948.

5. Ritchie H; Roser M CO2 and Greenhouse Emisions Available online: https://ourworldindata.org/co2-and-other-greenhouse-gas-emissions (accessed on 26 January 2022).
6. Rafiee A; Rajab Khalilpour K; Milani D; Panahi M Trends in CO2 Conversion and Utilization: A Review from Process Systems Perspective. *J Environ Chem Eng* **2018**, *6*, 5571–5794, doi: 10.1016/j.jece.2018.08.065.
7. Quintana-Gómez, L.; Martínez, L.; Román-González, D.; Segovia, J.J.; Martín, Á.; Bermejo, M.D. Energy and Economic Analysis of the Hydrothermal Reduction of CO2into Formate. *Industrial and Engineering Chemistry Research* **2021**, *60*, 14038–14050, doi:10.1021/ACS.IECR.1C01961/SUPPL_FILE/IE1C01961_SI_001.PDF.
8. Sakakura, T.; Choi, J.C.; Yasuda, H. Transformation of Carbon Dioxide. *Chemical Reviews* **2007**, *107*, 2365–2387, doi:10.1021/CR068357U.
9. Foustoukos, D.I.; Seyfried, W.E. Hydrocarbons in Hydrothermal Vent Fluids: The Role of Chromium-Bearing Catalysts. *Science* **2004**, *304*, 1002–1005, doi:10.1126/SCIENCE.1096033.
10. del Río, J.I.; Pérez, E.; León, D.; Martín, Á.; Bermejo, M.D. Catalytic Hydrothermal Conversion of CO2 Captured by Ammonia into Formate Using Aluminum-Sourced Hydrogen at Mild Reaction Conditions. *Journal of Industrial and Engineering Chemistry* **2021**, *97*, 539–548, doi: 10.1016/J.JIEC.2021.03.015.
11. Etiope, G.; Sherwood Lollar, B. ABIOTIC METHANE ON EARTH. *Reviews of Geophysics* **2013**, *51*, 276–299, doi:10.1002/ROG.20011.
12. Centi, G.; Quadrelli, E.A.; Perathoner, S. Catalysis for CO 2 Conversion: A Key Technology for Rapid Introduction of Renewable Energy in the Value Chain of Chemical Industries. *Energy & Environmental Science* **2013**, *6*, 1711–1731, doi:10.1039/C3EE00056G.
13. Roman-Gonzalez, D.; Moro, A.; Burgoa, F.; Pérez, E.; Nieto-Márquez, A.; Martín, Á.; Bermejo, M.D. 2Hydrothermal CO2 Conversion Using Zinc as Reductant: Batch Reaction, Modeling and Parametric Analysisof the Process. *The Journal of Supercritical Fluids* **2018**, *140*, 320–328, doi: 10.1016/J.SUPFLU.2018.07.003.
14. Su, J.; Lu, M.; Lin, H. High Yield Production of Formate by Hydrogenating CO2 Derived Ammonium Carbamate/Carbonate at Room Temperature. *Green Chemistry* **2015**, *17*, 2769–2773, doi:10.1039/C5GC00397K.

15. Chen, Q.; Qian, Y. Carbon Dioxide Thermal System: An Effective Method for the Reduction of Carbon Dioxide. *Chemical Communications* **2001**, 1402–1403, doi:10.1039/B100183N.
16. Shen, Z.; Zhang, Y.; Jin, F. The Alcohol-Mediated Reduction of CO2 and NaHCO3 into Formate: A Hydrogen Transfer Reduction of NaHCO3 with Glycerine under Alkaline Hydrothermal Conditions. *RSC Advances* **2012**, *2*, 797–801, doi:10.1039/C1RA00886B.
17. Farnetti, E.; Crotti, C. Selective Oxidation of Glycerol to Formic Acid Catalyzed by Iron Salts. *Catalysis Communications* **2016**, *84*, 1–4, doi: 10.1016/J.CATCOM.2016.05.014.
18. Andérez-Fernández, M.; Pérez, E.; Martín, A.; Bermejo, M.D. Hydrothermal CO2 Reduction Using Biomass Derivatives as Reductants. *The Journal of Supercritical Fluids* **2018**, *133*, 658–664, doi: 10.1016/J.SUPFLU.2017.10.010.
19. Yun, J.; Yao, G.; Jin, F.; Zhong, H.; Kishita, A.; Tohji, K.; Enomoto, H.; Wang, L. Low-Temperature and Highly Efficient Conversion of Saccharides into Formic Acid under Hydrothermal Conditions. *AIChE Journal* **2016**, *62*, 3657–3663, doi:10.1002/AIC.15287.
20. Sundqvist, B.; Karlsson, O.; Westermark, U. Determination of Formic-Acid and Acetic Acid Concentrations Formed during Hydrothermal Treatment of Birch Wood and Its Relation to Colour, Strength and Hardness. *Wood Science and Technology* **2006**, *40*, 549–561, doi:10.1007/S00226-006-0071-Z/FIGURES/5.
21. Gao, P.; Li, G.; Yang, F.; Lv, X.N.; Fan, H.; Meng, L.; Yu, X.Q. Preparation of Lactic Acid, Formic Acid and Acetic Acid from Cotton Cellulose by the Alkaline Pre-Treatment and Hydrothermal Degradation. *Industrial Crops and Products* **2013**, *48*, 61–67, doi: 10.1016/J.INDCROP.2013.04.002.
22. Ding, K.; Le, Y.; Yao, G.; Ma, Z.; Jin, B.; Wang, J.; Jin, F. A Rapid and Efficient Hydrothermal Conversion of Coconut Husk into Formic Acid and Acetic Acid. *Process Biochemistry* **2018**, *68*, 131–135, doi: 10.1016/J.PROCBIO.2018.02.021.

# Investigation of Boundary Layers in Mini-Plant LDPE Tubular Reactors

Jonas Degenkolb, Markus Busch*

TU Darmstadt, Darmstadt/Germany, *markus.busch@pre.tu-darmstadt.de

## Introduction

Low-density polyethylene (LDPE) is industrially produced under harsh conditions of temperatures up to 300 °C and pressures up to 3000 bar. The reaction takes places as a substance polymerization, where the produced LDPE is dissolved in the supercritical ethene. Besides autoclaves, the majority of LDPE is produced in kilometer-long tubular reactors. The length of the reactor is mainly due to the need of cooling, as the heat of the highly exothermic polymerization reaction must be carried out. In case of the tubular reactor, this is done by a coolant led inside an annular gap. However, a polymer-rich layer can form on the inner wall of the reactor, known as fouling, which impedes the heat transfer. This not only leads to less conversion as less heat is carried out but can also result in safety risks due to increased temperature inside the reactor. Furthermore, the product properties may be affected due to the differing material formed at the boundary layer. Since this phenomenon is poorly understood so far, a deeper understanding on the formation and the evolution throughout the reactor would be helpful and is thus the focus of this work. For this purpose, fouling is first investigated in a mini-plant setup using lab-scale tubular reactors. The data obtained from this serve as a basis for the model developed in parallel to rigorously describe the boundary layer using computational fluid dynamics (CFD).

## Experimental

To investigate the process of fouling, the fluid dynamic profile is crucial. Therefore, three different double-tube reactors were constructed, which cover the fluid dynamic states of laminar flow, transition state and turbulent flow. Whereas the laminar case should favor the most fouling, and thus is focused for the studies. To exclude asymmetric secondary flows of gravitation, the reactors are designed to be used vertical with a flow

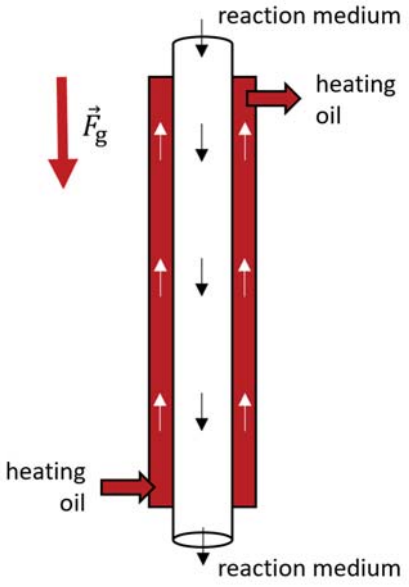


Figure 1: Schematic representation of the designed reactors.

from top to bottom. Samples may then be analyzed by gel permeation chromatography (GPC) to determine their molecular weight distributions (MWDs). Especially for the samples with highly pronounced fouling (i.e., in the laminar reactor) this should lead to a signifcant amount of high-molecular weight material, originated in the boundary layer. Furthermore, the setup can also be used to investigate the influence of the process parameters such as temperature, initiator flows and in particular the chain-transfer agent (CTA).

## Modeling

In literature, modeling of the LDPE process is well-established.[1] Ideal reactor models such as the plug flow reactor are usually used for this purpose. However, these models do not provide any information about the boundary layer since the radial resolution is not solved at all. The next logical step would be the use of a radial model, i.e., the extension by one dimension. While these have been successfully applied in literature[2,3], they rely on some assumptions and are limited to very few geometries. To obtain a complete spatial picture, computational fluid dynamics simulations are used in this work. The model is designed to depict the reactor described in the experimental part. Therefore, the data obtained by experiments serve as a basis for validation as well. However, the most significant result of the experiments is the MWD. Though, by using the method of moments for polymeric species in the CFD, only mean values and not a full MWD are obtained. To overcome this issue, an interface to the hybrid Monte-Carlo approach[4] established in the working group is implemented. For that, the reaction rates along individual pathways through the reactor (trajectories) are exported and are then simulated by the Monte-Carlo algorithm as individual tubular reactors. In each Monte-Carlo simulation, an ensemble of macromolecules is generated by simulating the evolution of one molecule after the other, what ultimately results in a full MWD. By merging the trajectories’ MWDs the results may be compared with the experiment. In addition, by only looking at several trajectories, for example at the boundary layer, the product resulting from there may simulatively be analyzed as well.

## Summary

In this work, the formation and evolution of fouling in tubular reactors in the LDPE process is investigated. For that, three tubular reactors were constructed to extend an existing continuous LDPE mini-plant. These are primarily used for the investigation of boundary layer phenomena. The data obtained thereby is used as a basis for complementary simulations. To get a better picture of fouling, a spatial simulation using CFD is established. In addition, a coupling to a stochastic method allows a comparison of experimental and modelled MWDs.

## References

[1] T. Herrmann, Modellierung Technischer Hochdruck-LDPE-Reaktoren, Technische Universität Darmstadt, **2011**.

[2] J. W. Hamer, W. H. Ray, *Chem. Eng. Sci.* **1986**, *41*, 3083–3093.

[3] S. Fries, Modelling of Fouling Mechanisms in the LDPE Synthesis, Technische Universität Darmstadt, **2020**.

[4] E. Neuhaus, T. Herrmann, I. Vittorias, D. Lilge, G. Mannebach, A. Gonioukh, M. Busch, *Macromol. Theory Simulations* **2014**, *23*, 415–428.

# Unravelling the Potential of Marine Microalga *Porphyridium Cruentum* for Wound Healing and Regeneration

Marta M Duarte, Rui Morais*, Ana Leite Oliveira*

Universidade Católica Portuguesa, CBQF - Centro de Biotecnologia e Química Fina – Laboratório Associado, Escola Superior de Biotecnologia, Porto, Portugal

*rcmorais@uco.pt; aloliveira@ucp.pt

## Introduction

Wound healing is a dynamic process, that involves complex cellular, biochemical, and physiological events that are dependent on local and systemic factors, as well as many cell types and mediators [1]. After the healing process, the injury site should have connective tissue repaired and re-epithelialized and returned to its normal anatomical structure and function. The increasing number of patients with chronic wounds caused by diseases, such as diabetes, malignant tumors, infections, and vasculopathy, has caused severe economic and social burdens [2][3]. Nowadays, the design and development of new bioactive materials for wound management, able to promote the repair of damaged tissue and restore its integrity constitute a constant challenge, especially in a scenario of chronicity [4].

Marine microalgae and their metabolites have been widely recognized for their bioactive properties with applications in various industries, such as the pharmaceutical, biomedical, cosmetics, and food [5]. In the biomedical field, these therapeutic molecules and biomaterials become highly relevant in the creation of sophisticated controlled drug delivery systems or integrated on advanced tissue regeneration. Their properties are mainly due to the structure and several physicochemical characteristics, according to the organism they are produced by [6].

The red unicellular microalgae from the genus *Porphyridium (Porphyridiales, Rhodophyta)* is a natural source for a variety of interesting bioactive compounds, including carotenoids, phycoerythrin, oligosaccharides, phycobiliproteins, and sulfated polysaccharides [7], [8]. These molecules have a wide range of applications and are used in several industries.

**Table 1.** Biomolecules extracted from *Porphyridium* cultures and their applications [8], [9].

| Biomolecules | Application | Industrial sector |
|---|---|---|
| Sulfated Polysaccharides | antioxidant, anti-inflammatory, antimicrobial agent | Cosmetic, Nutraceutic |
| Oligosaccharide | Vasoconstriction of blood vessels | Cosmetic |
| B-phycoerythrin | Diagnostics, molecular biology, and fluorescence techniques | Biomedical |
| Phycobiliproteins | Medical Diagnostic | Biomedical |
| Pigments | Diagnostics, molecular biology, and fluorescence techniques | Biomedical |
| Biomass | Biofuel, feed (for animals) | Energy, Aquaculture |

Among these molecules of interest, sulfated polysacharides have been shown to possess several biological properties of high value for wound healing and regeneration. These polysacharides have been described/studied as anti-allergic and anti-inflammatory agents [10] and as nutraceuticals due to their antioxidant, hypolipidaemic and hypoglicaemic activities [11], [12]. Moreover, they have potential to be used as therapeutic agents [13] due to anti-bacterial [14], antiviral [15], anti-inflammatory and anti-tumour activities [10], [16], [17]. However, to our knowledge, these molecules have never been explored as active components for the creation of wound dressing materials for skin wound healing and regeneration.

This work proposes to evaluate the potential of the extracted molecules from *Porphyridium cruentum* for skin wound healing and regeneration, with a focus on sulfated polysaccharides. In this work, a sequential valorization process will be applied to *P. cruentum* culture and biomass, using both membrane and $scCO_2$ processes, directed towards the extraction of phycoerythrin, carotenoids and sulfated polysaccharides. The resulting compounds will be fully characterized and their physicochemical and mechanical properties investigated, as well as their *in vitro* biocompatibility, regenerative capacity and cell laden possibilities in the context of wound healing.

## Experimental

Culture of *Porphyridium cruentum*

*Porphyridium cruentum*. *P. cruentum* strain was provided by Allmicroalgae - Natural Products, S.A and cultured at their facilities. A protocol optimization was achieved as described in Raposo *et al*. [7], to increase the sulfate content of the produced sulfated

exopolysaccharides (EPS). Culture was kept outdoors, in flat-panel photobioreactor systems, under constant aeration. pH was kept between 6.5 and 8 by $CO_2$ injection. Samples were taken from each replicate daily for pH and growth measurements. Cultures were collected when stationary phase was reached. *P. cruentum* culture media and biomass are separated via centrifugation.

**Figure 1.** *P. cruentum* culture in flat-panel photobioreactors.

Extraction and purification of EPS

This task will consist of the development and optimization of extraction protocols for sulfated exopolysaccharides (EPS) and other molecules of interest using both membrane separation and $scCO_2$ technologies.

Exopolysaccharides will be extracted from microalgae culture via ultrafiltration, using a membrane with a molecular weight cut-off of 300 kDa. Intracellular polysaccharides, phycoerythrin, and carotenoids will be extracted from *P. cruentum* biomass via a sequential extraction process using $scCO_2$ technology, as described in Gallego *et al.* [18]

The extraction protocols will be optimized towards obtaining a balance between maximum yield and the best preservation of extracted molecules.

Characterization of *P. cruentum* Sulfated Polysaccharides

For the biochemical characterization, the total carbohydrate, protein, and lipid composition percentage will be determined through the Phenol-Sulfuric Acid [19], Kjedahl [20], and Soxhlet [21] methods, respectively. Total uronic acid will be determined through the spectrophotometric method described by Blumenkrantz and Asboe-Hansen method [19]. Sulfate content will be obtained turbidimetrically, as barium sulfate, according to the method described by Dodgson and Price [22]. Inorganic content will be measured through inductively coupled plasma mass spectrometry (ICP-MS). Monosaccharide composition

will be done through high-performance liquid chromatography (HPLC), while the main organic functional groups will be determined through Fourier Transform Infrared Spectroscopy (FT-IR). The molecular weight of the polysaccharides will be obtained through size exclusion chromatography.

The biological characterization will focus on the determination of cytotoxicity, and the antioxidant, antibacterial, antitumoral, immunomodulatory, and antiviral capacity of EPS. Antioxidant capacity will be determined via ABTS colorimetric assay according to [23]. Antibacterial capacity will be determined via bacterial growth inhibition assay as described by Raposo *et al.* [7]. The biocompatibility of EPS will be evaluated through the direct contact method, using human Dermal Neonatal Fibroblasts (hDNFs), following ISO10993-5:2009 guidelines. While antitumoral activity will be determined using tumoral cell lines. Cell viability will be determined directly through a DNA quantification assay, and indirectly through the quantification of metabolic activity using an MTT assay. Cell morphology will be observed through confocal and scanning electron microscopy (SEM). Immunomodulatory activity will be determined through a macrophage (RAW 264.7) proliferation assay, and a cytokine (TNF-α and IL-6) production assay, as described by Díaz *et al.*, and Casas-Arrojo *et al*. [24], [25].

## Summary

Recently, there has been an interest for the use of materials from natural origin that are capable of stimulating or promoting events in wound healing. Within this vast range of biomaterials, the metabolites from marine microalgae have been widely recognized for their bioactive properties with applications in the biomedical field.

These polysaccharides have already been shown to possess antioxidant, antimicrobial, antitumor, and immunomodulatory properties. All these properties show the potential of these compounds to be used as a therapeutic agent. The author proposes to explore these properties through a skin wound healing focus, to evaluate their potential as building blocks for a wound-dressing product for future work.

## Acknowledgment

This research was funded by National Funds from Fundação para a Ciência e a Tecnologia (FCT), through project UID/Multi/50016/2020, Doctoral Research Grant UI/BD/151391/2021. Work carried out in the framework of the COST Action CA18224 “Green Chemical Engineering Network towards upscaling sustainable processes” (GREENERING), funded by the European Commission. The authors acknowledge the

expertise and resources provided by Allmicroalgae, Natural Products, S.A throughout the microalgae culturing process.

## References

[1] M. C. Robson, D. L. Steed, and M. G. Franz, "Wound healing: Biologic features and approaches to maximize healing trajectories," *Current Problems in Surgery*, vol. 38, no. 2, pp. A1-140, Feb. 2001, doi: 10.1067/msg.2001.111167.

[2] X. Zhang, W. Shu, Q. Yu, W. Qu, Y. Wang, and R. Li, "Functional Biomaterials for Treatment of Chronic Wound," *Frontiers in Bioengineering and Biotechnology*, vol. 8, no. June, pp. 1–15, 2020, doi: 10.3389/fbioe.2020.00516.

[3] K. Järbrink *et al.*, "The humanistic and economic burden of chronic wounds: A protocol for a systematic review," *Systematic Reviews*, vol. 6, no. 1, pp. 1–7, Jan. 2017, doi: 10.1186/S13643-016-0400-8/PEER-REVIEW.

[4] R. Z. Murray, Z. E. West, A. J. Cowin, and B. L. Farrugia, "Development and use of biomaterials as wound healing therapies," *Burns & Trauma*, vol. 7, Dec. 2019, doi: 10.1186/S41038-018-0139-7.

[5] G. Pierre *et al.*, "What Is in Store for EPS Microalgae in the Next Decade?," *Molecules*, vol. 24, no. 23, p. 4296, Nov. 2019, doi: 10.3390/molecules24234296.

[6] M. de Jesus Raposo, A. de Morais, and R. de Morais, "Marine Polysaccharides from Algae with Potential Biomedical Applications," *Marine Drugs*, vol. 13, no. 5, pp. 2967–3028, May 2015, doi: 10.3390/md13052967.

[7] M. F. D. J. Raposo, A. M. M. B. de Morais, and R. M. S. C. de Morais, "Influence of sulphate on the composition and antibacterial and antiviral properties of the exopolysaccharide from Porphyridium cruentum," *Life Sciences*, vol. 101, no. 1–2, pp. 56–63, Apr. 2014, doi: 10.1016/j.lfs.2014.02.013.

[8] C. Gaignard *et al.*, "New horizons in culture and valorization of red microalgae," *Biotechnology Advances*, vol. 37, no. 1, pp. 193–222, Jan. 2019, doi: 10.1016/J.BIOTECHADV.2018.11.014.

[9] H. M. Kim, C. H. Oh, and H. J. Bae, "Comparison of red microalgae (Porphyridium cruentum) culture conditions for bioethanol production," *Bioresource Technology*, vol. 233, pp. 44–50, Jun. 2017, doi: 10.1016/J.BIORTECH.2017.02.040.

[10] M. S. Matsui, N. Muizzuddin, S. Arad, and K. Marenus, "Sulfated Polysaccharides from Red Microalgae Have Antiinflammatory Properties In Vitro and In Vivo," *Applied Biochemistry and Biotechnology*, vol. 104, no. 1, pp. 13–22, 2003, doi: 10.1385/ABAB:104:1:13.

[11] T. Tannin-Spitz, M. Bergman, D. Van-Moppes, S. Grossman, and S. (Malis) Arad, "Antioxidant activity of the polysaccharide of the red microalga Porphyridium sp," *Journal of Applied Phycology*, vol. 17, no. 3, pp. 215–222, May 2005, doi: 10.1007/s10811-005-0679-7.

[12] G. Jiao, G. Yu, J. Zhang, and H. Ewart, "Chemical Structures and Bioactivities of Sulfated Polysaccharides from Marine Algae," *Marine Drugs*, vol. 9, no. 2, pp. 196–223, Feb. 2011, doi: 10.3390/md9020196.

[13] S. Geresh, A. Mamontov, and J. Weinstein, "Sulfation of extracellular polysaccharides of red microalgae: preparation, characterization and properties," *Journal of Biochemical and Biophysical Methods*, vol. 50, no. 2–3, pp. 179–187, Jan. 2002, doi: 10.1016/S0165-022X(01)00185-3.

[14] M. A. Guzman-Murillo and F. Ascencio, "Anti-adhesive activity of sulphated exopolysaccharides of microalgae on attachment of red sore disease-associated bacteria and Helicobacter pylori to tissue culture cells," *Letters in Applied Microbiology*, vol. 30, no. 6, pp. 473–478, Jun. 2000, doi: 10.1046/j.1472-765x.2000.00751.x.

[15] M. F. D. J. Raposo, A. M. M. B. de Morais, and R. M. S. C. de Morais, "Influence of sulphate on the composition and antibacterial and antiviral properties of the exopolysaccharide from Porphyridium cruentum," *Life Sciences*, vol. 101, no. 1–2, pp. 56–63, Apr. 2014, doi: 10.1016/j.lfs.2014.02.013.

[16] M. Huheihel, V. Ishanu, J. Tal, and S. (Malis) Arad, "Activity of Porphyridium sp. polysaccharide against herpes simplex viruses in vitro and in vivo," *Journal of Biochemical and Biophysical Methods*, vol. 50, no. 2–3, pp. 189–200, Jan. 2002, doi: 10.1016/S0165-022X(01)00186-5.

[17] S. (Malis) Arad and O. Levy-Ontman, "Red microalgal cell-wall polysaccharides: biotechnological aspects," *Current Opinion in Biotechnology*, vol. 21, no. 3, pp. 358–364, Jun. 2010, doi: 10.1016/j.copbio.2010.02.008.

[18] R. Gallego, M. Martínez, A. Cifuentes, E. Ibáñez, and M. Herrero, "Development of a Green Downstream Process for the Valorization of Porphyridium cruentum Biomass," *Molecules*, vol. 24, no. 8, p. 1564, Apr. 2019, doi: 10.3390/molecules24081564.

[19] Michel. DuBois, K. A. Gilles, J. K. Hamilton, P. A. Rebers, and Fred. Smith, "Colorimetric Method for Determination of Sugars and Related Substances," *Microb Cell Fact*, vol. 8, p. 59, 2002, doi: 10.1021/AC60111A017.

[20] J. Kjeldahl, "Neue Methode zur Bestimmung des Stickstoffs in organischen Körpern," *Zeitschrift für analytische Chemie 1883 22:1*, vol. 22, no. 1, pp. 366–382, Dec. 1883, doi: 10.1007/BF01338151.

[21] F. Soxhlet, "Soxhlet, über gewichtsanalytische Bestimmung des Milchfettes.," *Polytechnisches Journal*, vol. 232, 1879.

[22] K. DODGSON and R. PRICE, "A note on the determination of the ester sulphate content of sulphated polysaccharides," *Biochemical Journal*, vol. 84, no. 1, pp. 106–110, Jul. 1962, doi: 10.1042/bj0840106.

[23] R. Re, N. Pellegrini, A. Proteggente, A. Pannala, M. Yang, and C. Rice-Evans, "Antioxidant activity applying an improved ABTS radical cation decolorization assay," *Free Radical Biology and Medicine*, vol. 26, no. 9–10, pp. 1231–1237, May 1999, doi: 10.1016/S0891-5849(98)00315-3.

[24] V. Casas-Arrojo, J. Decara, M. de los Ángeles Arrojo-Agudo, C. Pérez-Manríquez, and R. T. Abdala-Díaz, "Immunomodulatory, Antioxidant Activity and Cytotoxic Effect of Sulfated Polysaccharides from Porphyridium cruentum. (S.F.Gray) Nägeli," *Biomolecules*, vol. 11, no. 4, p. 488, Mar. 2021, doi: 10.3390/biom11040488.

[25] R. T. A. Díaz, M. Chabrillón, A. Cabello-Pasini, J. L. Gómez-Pinchetti, and F. L. Figueroa, "Characterization of polysaccharides from Hypnea spinella (Gigartinales) and Halopithys incurva (Ceramiales) and their effect on RAW 264.7 macrophage activity," *Journal of Applied Phycology*, vol. 23, no. 3, pp. 523–528, Jun. 2011, doi: 10.1007/S10811-010-9622-7/FIGURES/3.

# Supercritical Solvent Impregnation of Starch Xero- and Aerogels with Carnosic Acid

Ahmed Elrashidy

Chemistry department, Wroclaw university of science and technology,
ahmedelrashidy.jr@gmail.com

## Introduction

Aerogels produced from organic material are of unique characteristics that allow them to be used in food and medicine areas where safe and stable products are needed (Milovanovic et al., 2015) . This master's thesis investigates starch hydrogels' production, their transformation to aceto- and alcogels, and consecutive drying to obtain xero- and aerogels. The temperature of hydrogel preparation, solvent exchange method, supercritical drying conditions, and supercritical impregnation conditions will be investigated. The selected starch gels will be impregnated with carnosic using supercritical carbon dioxide. Physicochemical characterization of the obtained materials will be performed using FTIR and SEM-FIB techniques.

## Experimental

### Materials

In order to perform the experiments intended the Potato starch was obtained from a local supermarket,and the distilled water was acquired from reverse osmosis at the university facilities, 99.99% ethanol 99.99% Acetone were bougtht from Stanlab company and lastly the Carnosic acid was from Sigma-aldrich.

### Methods

Hydrogels were prepared by mixing 10 g of the starch with 100 mL of distilled water. After the mixture was dissolved at room conditions, it was heated to the desired temperature using a heating plate and oil bath while mixing continuously for 20 min at 900 rpm. The hydrogel was spread evenly on a petri dish in the next step. Experimental conditions considered are presented in Table 1.

*Table 1: Hydrogel production conditions*

| Experiment number | Gel temperature | Solvent |
|---|---|---|
| 1 | 85°C | Acetone |
| 2 | 90°C | Ethanol |
| 3 | 100°C | Ethanol |

The acetogel (experiment 1) was obtained by soaking the hydrogel with pure Acetone for 24 hours. Alcogels (experiments 2 and 3) were obtained by soaking the hydrogel in 20, 40, 60, 80, and 100% ethanol consecutively. In each solvent concentration, the gel was left for 24 h, except for the 100%, where it was left for 48 h. After the solvent substitution process ended, the gels were cut into uniformly shaped pieces (1x1 cm) and dried in air or supercritical carbon dioxide.

For the supercritical drying process, acetogels and alcogels were put inside a 280 mL high-pressure vessel under. The investigated pressures were 15 and 20 MPa and temperatures 35°C and 50°C. The drying med consisted of 2 h of batch drying and 30 min of supercritical carbon dioxide flow (1L/min measured at ambient conditions). The decompression was performed at a rate of 0.3 MPa/min.

Hydrogels demonstrated a higher contraction when acetone was used as a solvent for water replacement. Consequently, gels obtained from alcogels were more porous (Fig. 1.). As expected, aerogels were more porous than xerogels. 20 MPa and 35°C were appropriate drying conditions for the selected drying mode. SEM investigation combined with ion beam microscopy (SEM-FIB) will provide an insight into the obtained structures.

The porosity tests using a pycnometer showed that the aerogels were porous 25-43%. However, a more accurate measurement method is needed due to the possible presence of small pores.

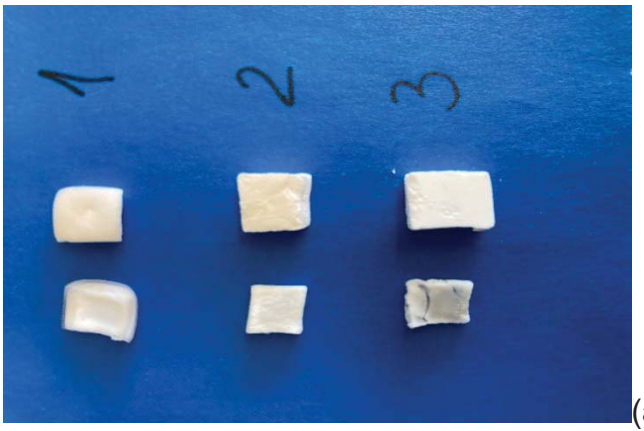

(a)

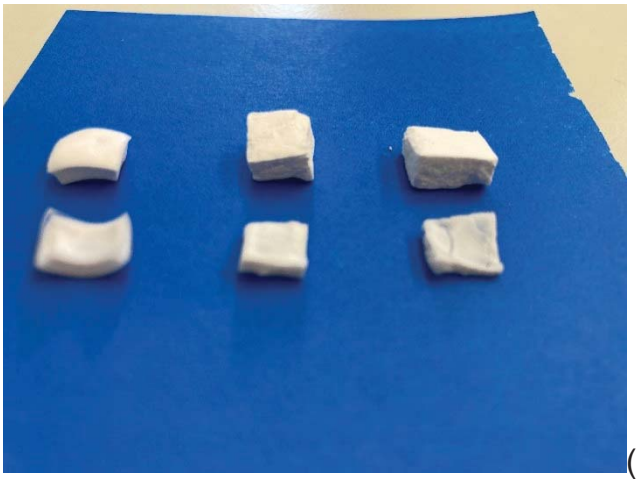
(b)

Fig. 1. Aerogels (top three) and xerogels (bottom three), top (a) and side (b) view

**Summary**

The experiments indicated the temperature of 90°C for search gelatination, ethanol as the water replacement solvent, step replacement method, and drying conditions of 20 MPa and 35°C as appropriate for potato starch aerogels production. The aerogels will be further characterized and impregnated with carnosic acid using supercritical carbon dioxide.

**Acknowledgment**

I would like to thank and acknowledge the help of the chemistry department at Wroclaw university of science and technology with special thanks to my supervisor Prof.Irena Zizovic and her doctoral students Dr.Mariusz Nowak and Dr.Marcin Tynka.

**References**

Milovanovic, S., Jankovic-Castvan, I., Ivanovic, J., & Zizovic, I. (2015). Effect of starch xero- and aerogels preparation on the supercritical CO2 impregnation of thymol [https://doi.org/10.1002/star.201400134]. *Starch - Stärke*, *67*(1-2), 174-182. https://doi.org/https://doi.org/10.1002/star.201400134

# How Methoxyphenol Effects the High-Pressure Polyethylene Polymerization

Denise Eryildirim, Markus Busch*

Ernst-Berl-Institut, Technische Universität Darmstadt,

*markus.busch@pre.tu-darmstadt.de

## Introduction

Stabilizers are added to chemical compounds to ensure their stability and thus slow down decomposition, cross-linking, auto-initiating polymerization or depolymerization.
Therefore, the influence of them should be well investigated in terms of slow down the reaction and the properties of the product, to know if there are effects given from the stabilizers during the process.
Stabilizers are commonly used in various application areas. For instance, different types of stabilizers are used in the plastics industry depending on the application to inhibit accelerate aging of monomers during storage.[1] In many well-known processes like the acrylic acid process, stabilizers are beside storage reasons also used for safety reasons, to prevent runaway reactions due to the auto-initiation of the monomer.[2] The property of slow down a reaction leads to the fact that, stabilizers must be separated at the beginning of a process at high costs, or they remain in the process and are overrun by an increased addition of initiators and high process temperatures. If stabilizers are removed at the beginning of a process, a premature reaction, can occur in the pipes or pumps upstream of the reactor. If they are not separated, operating costs are higher due to increased addition of initiators.

## Experimental

The influence of stabilizers during the homo-polymerization of ethylene must be investigated. To examine this, a fixed amount of initiator was added, and therefore, was checked if stabilized radicals were present or if the effectiveness of the stabilizer was no longer given at process conditions. For the continuous experiments an autoclave with a volume of 100 mL is used and the hole experimental set-up can be seen in Figure 1. Furter, a HPLC pump is used which fed the stabilizer directly into the third compressor stage. In this manner ethylene and methoxyphenol (MeHQ) gets premixed into the reactor. The last component which is needed for the investigation of the stabilizer is the fixed

amount of initiator. Here, the initiator *tert*-butylperoxypivalate TBPPI is used. The initiator is fed through a syringe pump into the system.

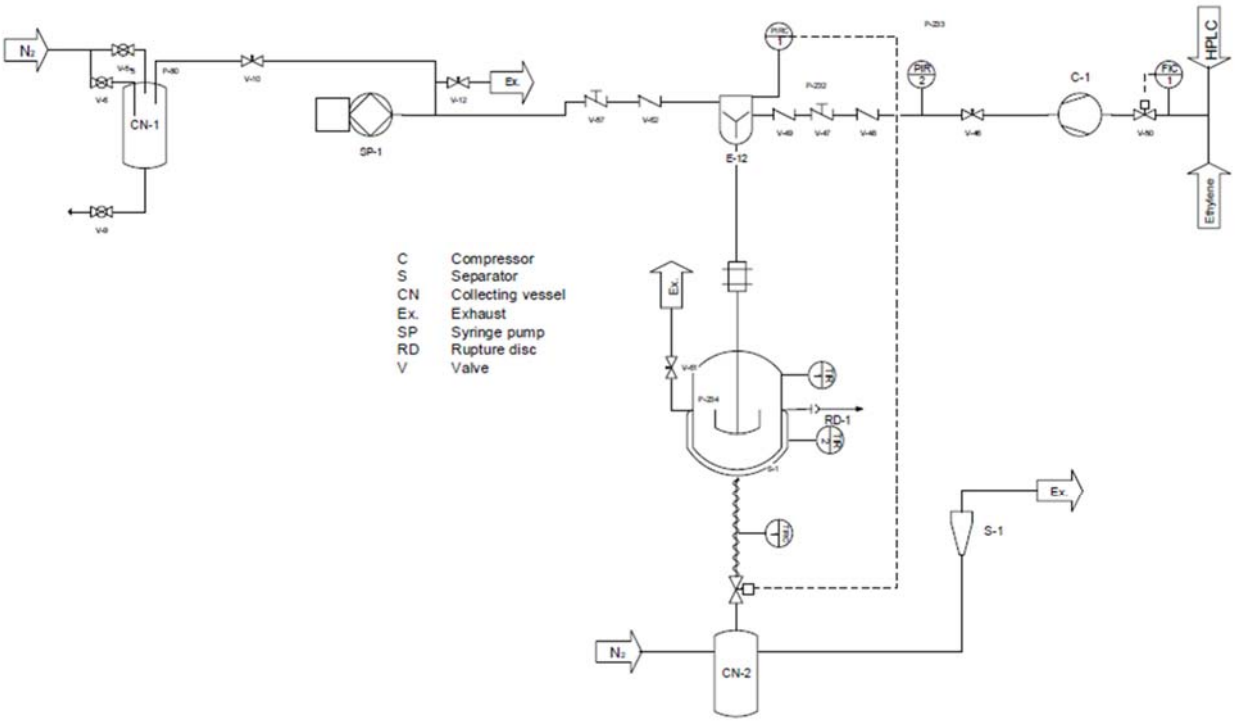


Figure 1: Experimental set-up.

For the investigation of methoxyphenole the first step is to perform a reference experiment with only initiator to have a starting point. Therefore, the conversion of ethylene with TBPPI under certain temperatures can be seen. The results of only ethylene and TBPPI and the influence by adding different amounts of stabilizer can be seen in Figure 2.

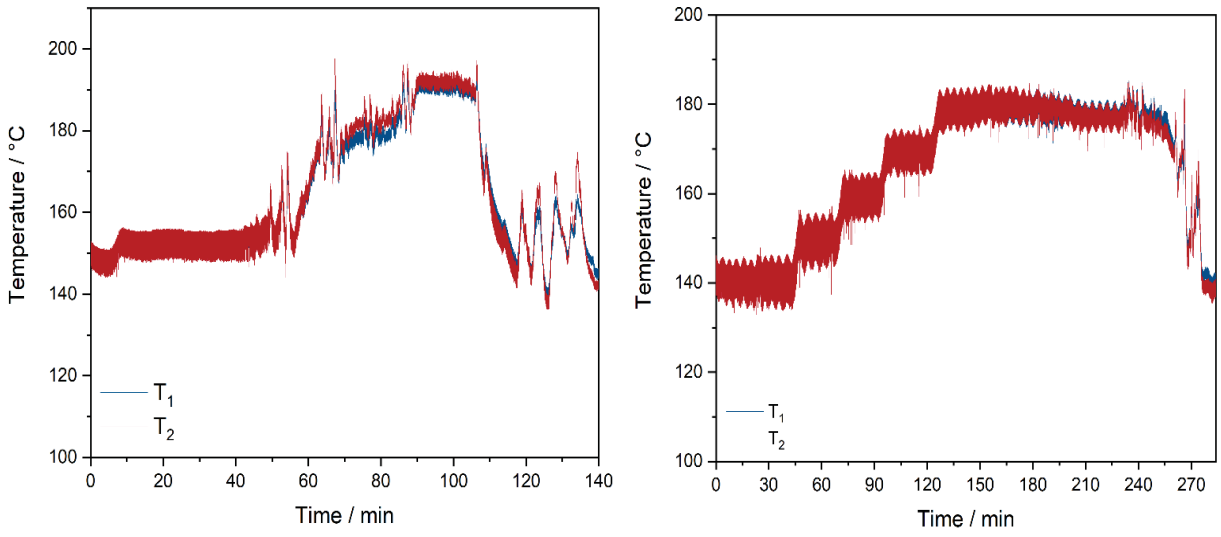


Figure 2: Temperature profiles without added stabilizer (left) and with stabilizer (right).

From both temperature profiles it can directly be seen that MeHQ leads to a smoother temperature profile without sharp temperature peaks. At the point where MeHQ is switched off at around 210 minutes, the temperature profile becomes sharper. Respective it can be seen how the temperature profile would look like without stabilizer.

## Summary

To summarize, the mini plant set up is shown which can be used for further investigations of several stabilizers. Also, the influence of certain stabilizers with different initiators can be investigated. Further the influence of different amounts of stabilizer in the polymer will be investigated.

## References

[1] Polymerisationsinhibierung von (Meth-)Acrylaten-Stabilisator und Sauerstoff-verbrauch, H. Becker; Dissertation, Technische Universität Darmstadt, **2003**.

[2] Acrylic reactor runaway and explosion accident analysis, Journal of Loss Prevention in the Process Industries, Chen-Shan Kao, Kwan-Hua Hu ,15, p. 213 – 222. **2002**.

# Application of Acoustic Levitation for the Investigation of Hydrogels

Joline Hansen

Chair of Process Technology, Ruhr-Universität Bochum, hansen@vtp.rub.de

## Introduction

Hydrogels can act as a precursor for aerogels, highly porous materials with low density and high specific surface area. Aerogels were first produced in the 1930s, but activity in that research field has increased over the last decades due to the extraordinary properties and the resulting high potential for applications in a variety of technical areas. The synthesis process of aerogels can be divided into the following steps: the sol preparation, the gelation, the aging, and the drying of the wet gel [11]. Gelation describes the transition from a sol to a wet gel, also called hydrogel. It consists of a porous, three-dimensional, continuous, solid network surrounded by a liquid phase. Regarding silica-based materials, which are usually used for the aerogel synthesis, the gelation can be induced by shifting the pH value into the acidic or the basic direction [7]. For this purpose, a pressurized $CO_2$ environment can be used, in which $CO_2$ dissolves into the sol and thus decreases the pH value [10]. However, the mechanism of the $CO_2$-induced gelation is not fully understood and needs further investigation, once it is essential to produce a particular gel structure. One commonly chosen parameter to characterize the sol-gel process is the gelation time. Since gelation can be detected by its effect on the system's viscosity, rheological measurement is one of the most feasible methods for a pressurized system. Katoueizadeh et al. and Ponton et al. performed experiments under ambient conditions to determine gelation time with rheological measurements of viscosity [4, 9]. An analysis performed by Smirnova et al. showed that increasing $CO_2$ concentration in the liquid phase accelerates the gelation process in general [10]. Nevertheless, in none of the studies viscosity measurements were carried out during $CO_2$-induced gelation to investigate the effect of pressure and temperature on the gelation time.

For such investigations during a $CO_2$-induced sol-gel process, one approach could be the use of acoustic levitation. At ambient pressure, acoustic levitation is a widely used technique in the research of crystallization, evaporation kinetics, and the measurement of thermophysical properties [8]. At elevated pressure, there have been investigations of thermophysical properties in pressurized $CO_2$ by Bear [1, 2], to determine phase equilibria with squalene, and by Borosa [3] and Kremer [5, 6] to determine the interfacial tension

and viscosity of different liquid material samples. For the viscosity measurements, shape oscillation was applied to levitated droplets.

This work presents some ideas for future investigations of the transition process from sol to gel using acoustic levitation. Therefore, the actual setup of the levitator for the measurement of viscosity in a pressurized environment is described and evaluated. Fields of optimization and adaption are discussed.

**Experimental**

For levitation under high pressure, a piezoelectric driven transducer and a reflector are installed in a high-pressure view cell, as shown in Figure 1, designed for pressures up to 200 bar and temperatures up to 180 °C.

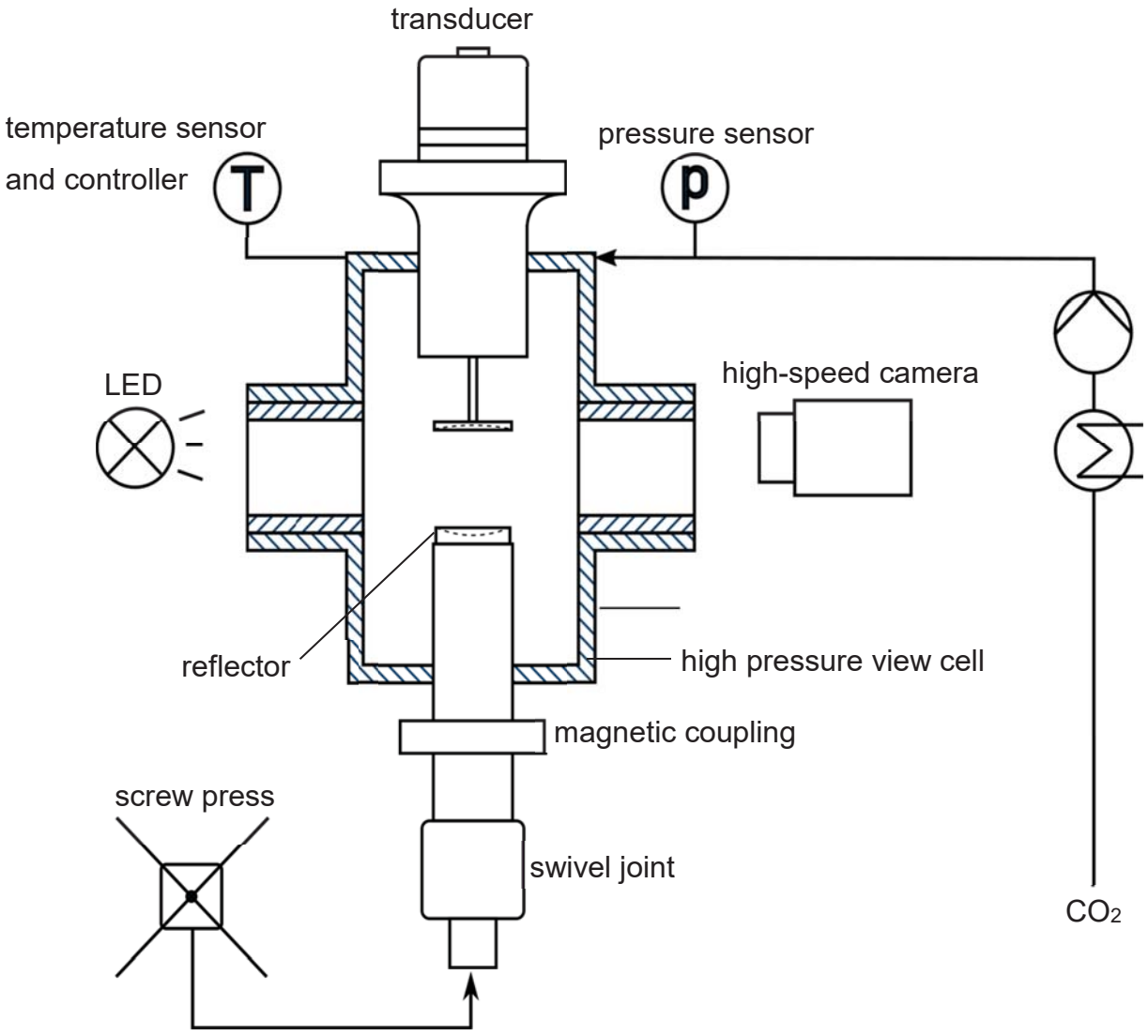


*Figure 1: Scheme of the high pressure acoustic levitation system. After [5]*

The transducer and reflector are aligned to each other along the cells vertical axis. The typical workflow is performed in the following steps:

- Filling the screw press with the liquid substance of interest
- Tempering and pressurizing the view cell
- Generating a standing sound field between transducer and reflector
- Inserting a liquid drop in the sound field
- Recording the oscillation of the drop and analyzing the recording afterward

The transducer in this setup is excited via piezo actors and is operated within frequencies between 30 kHz and 40 kHz. To create a standing sound field, the distance between reflector and transducer (Δz) has to be the integral multiple of the half wavelength. Therefore, it can be adjusted manually using the magnetic coupling shown in Figure 1. To insert a liquid drop in the sound field, a capillary connected with the screw press leads to a central bore in the reflector. It is moved along the axis of levitation using a swivel joint. Drop oscillation is induced by amplitude modulation (AM) of the standing sound wave. When the modulation is switched off, the friction-induced damped oscillation of the drop is recorded with a high-speed camera. The viscosity can then be calculated from the damping constant determined. Kremer achieved an average deviation of the calculated viscosity of 5,8 % to 10,3 % for the system squalane-$CO_2$ and 2,2 % to 7,2 % for PEG400-$CO_2$, proving the principle for these systems [5]. It has to be mentioned that no experiments have been carried out in this context with aqueous samples.

In order to enable gelation in the levitator, it is necessary to place a sol sample in the sound field within a pressurized environment. The reproduction of this procedure, and therefore a convenient way for the research objective, is not possible at this stage since gelation occurs in the upper end of the injection capillary after the first drop is inserted. Thus, the whole system needs to be demounted after the first sample injection to clean the capillary mechanically. Additionally, the investigation of pressure and temperature alternation in the gelation process is challenging since the changing pressure and temperature must not influence the stability of the levitation. The stability is not given for several design reasons: firstly, the $CO_2$ inlet is placed directly beside the sound field, so the drop is blown out of the field when varying the pressure. Secondly, the temperature control circuit and heating concept of the cell are not fast enough to guarantee a quick adaption without overheating after i.e. pressure variation. Third, the change of pressure and temperature significantly affects the density of the $CO_2$ environment and, subsequently, the needed Δz to ensure a stable standing sound field. The manually

performed adjustment with the magnetic coupling cannot meet this need. Hence, adaptions in design are needed to perform studies with changing pressure and temperature. The main challenge will be to enable the determination of the gelation time during levitation. Katoueizadeh et al. and Ponton et al. use a rotational rheometer, in which the elastic module G' and the loss module G" are measured continuously by frequency sweep tests during the gelation process. Comparing various approaches to determine the gel point from G' and G" Kathoueizadeh concluded that the dynamic moduli measurement method is the most accurate. It defines the gelation point when the ratio G’’/G' is independent of the excitation frequency [4]. At the current point, the utilization of this method for acoustic levitation is not feasible since it does not allow continuous measurements of the viscosity. This is due to the fact that the damping process after switching off the AM takes some seconds until the drop reaches its equilibrium shape again. Moreover, the determination of G’ and G’’ is not possible with the actual setup.

## Summary

Acoustic levitation is a promising approach for investigating the transition of the sol-gel process, which is inherent in aerogel production. The most important parameter is the gelation time, which can be determined via rheological measurements. Experiments with conventional methods like rotational rheometers have already been carried out under ambient conditions, but there is a lack of investigations of the sol-gel route under pressurized $CO_2$. The current setup of the high-pressure acoustic levitator enables the measurement of the viscosity of small samples in binary systems under high pressure and temperature. However, an optimization of the construction is necessary to meet the requirements for investigating the gelation time during a $CO_2$-induced sol-gel process.

## References

[1] Baer, S. 2015. *Entwicklung einer Ultraschall Levitations-Apparatur zur in-situ Phasengleichgewichtsmessung mittels Raman-Spektroskopie,* Ruhr-Universität Bochum.

[2] Baer, S., Esen, C., and Ostendorf, A. 2014. Phase equilibrium measurements of acoustically levitated squalane-CO 2 mixtures by Raman spectroscopy. *J. Raman Spectrosc.* 45, 8, 680–685.

[3] Boroša, D. J. 2013. *Entwicklung und Aufbau eines akustischen Levitators zur Untersuchung von Stofftransport- und Partikelbildungsmechanismen von Proben unter hohen Drücken*. Dissertation, Ruhr-Universität Bochum.

[4] Katoueizadeh, E., Rasouli, M., and Zebarjad, S. M. 2020. A comprehensive study on the gelation process of silica gels from sodium silicate. *Journal of Materials Research and Technology* 9, 5, 10157–10165.

[5] Kremer, J. 2018. *On the measurement of physical properties in high pressure systems using acoustic levitation,* Ruhr-Universität Bochum.

[6] Kremer, J., Bürk, V., Pollak, S., Kilzer, A., and Petermann, M. 2018. Viscosity of squalane under carbon dioxide pressure — Comparison of acoustic levitation with conventional methods. *The Journal of Supercritical Fluids* 141, 252–259.

[7] Levy, D. and Zayat, M., Eds. 2015. *The Sol-Gel Handbook*. *Synthesis, Characterization, and Applications*. Wiley Online Library. Wiley-VCH, Weinheim.

[8] Lierke, E. 1996. Akustische Positionierung-Ein unfassender Uberblick über Grundlagen und Anwendungen. *Acustica* 82, 2, 220–237.

[9] Ponton, A., Warlus, S., and Griesmar, P. 2002. Rheological study of the sol-gel transition in silica alkoxides. *Journal of Colloid and Interface Science* 249, 1, 209–216.

[10] Smirnova, I. and Arlt, W. 2003. Synthesis of Silica Aerogels: Influence of the Supercritical CO2 on the Sol-Gel Process. *Journal of Sol-Gel Science and Technology* 28, 2, 175–184.

[11] Soleimani Dorcheh, A. and Abbasi, M. H. 2008. Silica aerogel; synthesis, properties and characterization. *Journal of Materials Processing Technology* 199, 1-3, 10–26.

# Comparison of the Extracts of Albanian Sage and Lavender Gained Using Different Solvents and Techniques

Lorenci Gjurgjaj[1], Elva Duro[2], Jeta Lica[1], Mariza Andoni[1], Aurel Nuro[3], Altin Mele[1,3]

[1]Center of Techniques Studies, Ivodent Academy, 1016 Tirana, Albania, lorenci.gjurgjaj@ivodent.edu.al

[2]Department of Prosthesis, Ivodent Academy, 1016 Tirana, Albania

[3]Department of Chemistry, University of Tirana, 1001 Tirana, Albania

## Introduction

Sage and Lavander are commonly used herbs rich in bioactive compounds suitable for various applications. The actual studies compared the extracts obtained by supercritical fluid (SFE), water distillation, and alcoholic extractions. (Aprotosoaie et al., 2017; da Porto et al., 2009; Durling et al., 2007; Naziruddin et al., 2021). In the present study, we will compare the use of near-critical liquid $CO_2$ under liquid-vapor equilibrium conditions as a solvent for plant extraction.

## Experimental

Gas chromatographic analyses of plant extracts were realized with a Varian 450GC instrument equipped with a flame ionization detector and 1079 PTV injector. The temperature of the PTV injector was 553 K. One µl of each extract was diluted in Toluene and was injected manually in splitless mode. A temperature for FID was held at 553 K. Nitrogen was used as a carrier (1 ml/min) and make-up gas (25 ml/min). Hydrogen and air were flame detector gases with 30 ml/min and 300 ml/min, respectively. VF-1ms capillary column (30m x 0.33mm x 0.25µm) was used to separate the compounds. The oven temperature was programmed as follows: 313 K (held for 2 minutes) to 423 K (with 4K/min), and after that to 553 K with 10K/min and held for 2 minutes. The identification of the compounds was based on a comparison of their Kovats indices (KI), their retention times (RT), and literature (Adams, 2001; Dong et al., 2020; Porte et al., 2013; Scanlan et al., 2002). A mixture of n-alkanes (C6-C20) was used for the determination of retention indices.

The hydro distillation is performed through the Clevenger apparatus as recommendations by Pharmacopeia (EU, UK, USA, and Japan). In a 250 ml balloon, 50 g of the plant is added, 150 ml water, and 1 ml of toluene. Hydro distillation lasted from 4 to 6 hours. The

resulting essential oil is collected by dissolving in toluene and which is then evaporated with rotavapor.

The ultrasound-assisted ethanol extraction was performed in a 150 Erlenmeyer flask with 50 g of the plant and 50 ml of ethanol 70%. The extraction took place in a bathroom with an ultrasound for a duration of 30 minutes at a temperature 303 K. Upon completion of the extraction the plant material was separated from the extract by decantation and after the sample was evaporated to a volume of 2 ml.

The total reflux extraction was carried out in a 250 ml flask using 100 ml solvent water-ethanol solution 70% (v/v) and 50 g of plant. The extraction was done under stirring at boiling temperature for 3 hours. The extract was further dried in a thin film evaporator up to a volume of 2 ml. For the plant extraction with near-critical $CO_2$ under liquid-vapor equilibrium, an apparatus in which one can extract analogue to the Soxhlet method (Fig. 1). The only difference they have to a Soxhlet apparatus is the lack of vapor raising tube because here the extraction takes place inside the autoclave and this tube is not necessary. The autoclave is made out of stainless steel, especially resistant to chemically aggressive substances (DIN 17440, German material No. 1.4571), and had an outer diameter of 80 mm, a wall thickness of 8,5 mm, and a height of 430 mm. In the upper screw able cover were welded a capillary with a high-pressure valve for loading and discharging the solvent, a capillary with a pressure gauge, and a cooling finger. The 25 mm thick upper and down covers of the autoclave were sealed with O-rings (63x2 mm). In the upper cover of the autoclave, there is a window, made of synthetic sapphire (thickness 15 mm, diameter 30 mm), sealed with an O-ring (28x2 mm). Through the window, could be observed the drops of the condensed solvent on the cooling finger and the siphon of the glass apparatus inside the autoclave when it loads and empties. Afterward, the bottom of the autoclave was immersed in a thermostatic water bath at 313 K, and the cooling finger was circulated with colder water at 285 K. The pressure inside the vessel during extraction was in the range of 60-64 bar. The respective average temperature of the liquid $CO_2$ at equilibrium would be 295.5 to 297 K. Through the sapphire window, we could observe that the time for one filling and discharging of the siphon (one Soxhlet cycle) was 20 minutes. After 6 h of extraction, $CO_2$ gas was released from the autoclave, the bottom glass was weighted and the yield of the extraction against the dry mass of the plant material was determined (Mele et al., 2009).

Fig 1. Apparatus for the high-pressure extraction with compressed gases.

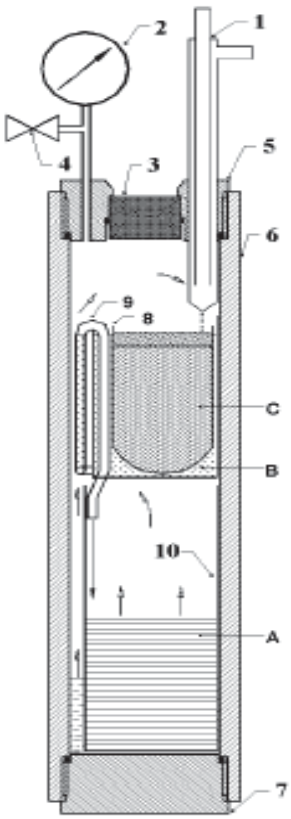


1. Cooling finger
2. Pressure gauge
3. Sapphire Window
4. Valve
5. Upper cover
6. Steel Cylinder
7. Bottom cover
8. Extracting thimble
9. Siphon
10. Product dropping glass

A. Product
B. Extract solution
C. Plant material.

A summarized table of results for the chromatographic analysis of the extracts of different solvents and techniques was realized with the purpose of comparing the chemical selectivity and yield of each method.

Table 1. GC-FID analysis of Sage extracts obtained by different techniques and solvents.

| **Salvia officinalis L.** | **Hydrodistillation** | **Ultrasound-assisted EtOH** | **Reflux EtOH** | **$CO_2$** |
|---|---|---|---|---|
| α-Pinene | 0.76 | n.d. | 0.75 | 0.13 |
| Camphene | 6.22 | 4.71 | 8.28 | 3.29 |
| β-Pinene | 7.22 | 5.86 | 9.53 | 4.14 |
| Myrcene | 0.78 | n.d. | 0.86 | 0.58 |
| Limonene | 0.09 | n.d. | n.d. | 0.55 |
| α-Terpinene | 1.30 | n.d. | 1.53 | 0.82 |
| 1.8-Cineole | 13.97 | 15.78 | 16.63 | 12.70 |
| para-Cymene | 0.03 | n.d. | n.d. | 0.04 |
| γ-Terpinene | 0.03 | n.d. | n.d. | 0.06 |
| Sabinene hydrate | 0.05 | n.d. | n.d. | 0.05 |
| Linalool | 0.09 | n.d. | n.d. | 0.07 |

| | | | | |
|---|---|---|---|---|
| α-Thujone | 25.50 | 27.11 | 23.56 | 27.06 |
| β-Thujone | 7.33 | 6.94 | 6.21 | 5.35 |
| Camphor | 21.73 | 23.79 | 18.99 | 21.70 |
| Borneol | 2.99 | 2.34 | 1.97 | 2.40 |
| Terpinen-4-ol | 0.44 | n.d. | 0.75 | 0.99 |
| α-Terpineol | 0.29 | n.d. | n.d. | 0.35 |
| Acetate Bornyl | 0.89 | n.d. | 1.86 | 1.02 |
| β-Caryophyllene | 0.85 | 3.20 | 2.49 | 3.77 |
| α-humulene | 1.23 | 3.54 | 4.90 | 4.43 |

Table 2. GC-FID analysis of Lavander extracts obtained by different techniques and solvents.

| **Lavandula angustifolia** | **Hydrodistillation** | **Ultrasound-assisted EtOH** | **Reflux EtOH** | **$CO_2$** |
|---|---|---|---|---|
| α-Pinene | 0.19 | 1.13 | n.d. | 0.22 |
| Camphene | 0.13 | 2.06 | n.d. | 0.09 |
| Sabinene | 0.38 | n.d. | n.d. | 0.44 |
| β-Pinene | 0.61 | 0.71 | n.d. | 0.64 |
| Myrcene | 0.80 | 0.73 | n.d. | 0.68 |
| α-Terpinene | 0.20 | 2.85 | n.d. | 0.69 |
| 1.8-Cineole | 14.25 | 6.07 | 18.75 | 11.58 |
| Limonene | 0.46 | n.d. | n.d. | 0.27 |
| cis-β-Ocimene | 2.05 | 2.17 | n.d. | 3.82 |
| trans-β-Ocimene | 1.54 | 5.56 | 2.62 | 3.36 |
| 3-Octanone | 0.17 | 0.68 | n.d. | n.d. |
| Linalool | 21.33 | 9.24 | 13.55 | 17.52 |
| Camphor | 14.14 | 5.95 | 16.28 | 13.97 |
| Linalyl Acetate | 4.62 | 7.43 | n.d. | 4.54 |
| Borneol | 1.29 | 1.95 | n.d. | 2.24 |
| Terpinen-4-ol | 2.57 | 4.63 | n.d. | 0.18 |
| α-Terpineol | 12.04 | 10.72 | 15.42 | 20.51 |
| β-Caryophyllene | 0.54 | 3.94 | n.d. | 1.14 |
| α-humulene | 1.11 | 2.93 | n.d. | 3.12 |

## Summary

In the present study, we investigated the use of near-critical liquid $CO_2$ as a suitable solvent for the extraction of Sage (Salvia officinalis L.), and Lavender (Lavandula angustifolia) via the Soxhlet-type process. The results were compared with those of their hydro distillation and ethanol-water extraction under total reflux and ultrasound-assisted. Gas-chromatographic analysis and internal standards were used for the identification of the main chemical constituents. A comparison of GC data for extracts showed that hydro distillate and $CO_2$ extract have similar chemical compositions. The extraction with ethanol-water mixture yields different results regarding the extract composition the reason for it could be the different temperatures of the selected processes. Heavier, non-polar compounds like caryophyllenes are more present in the $CO_2$ extract, compared to hydro distillate.

## References

1.) Adams, R. P. (2001). Identification of essential oil components by gas chromatography/quadrupole mass spectroscopy Allured Publishing Corporation. Carol Stream, IL, USA.
2.) Aprotosoaie, A. C., Gille, E., Trifan, A., Luca, V. S., & Miron, A. (2017). Essential oils of Lavandula genus: a systematic review of their chemistry. Phytochemistry Reviews 2017 16:4, 16(4), 761–799. https://doi.org/10.1007/S11101-017-9517-1
3.) da Porto, C., Decorti, D., & Kikic, I. (2009). Flavour compounds of Lavandula angustifolia L. to use in food manufacturing: Comparison of three different extraction methods. Food Chemistry, 112(4), 1072–1078. https://doi.org/10.1016/J.FOODCHEM.2008.07.015
4.) Dong, G., Bai, X., Aimila, A., Aisa, H. A., & Maiwulanjiang, M. (2020). Study on lavender essential oil chemical compositions by GC-MS and improved pGC. Molecules, 25(14). https://doi.org/10.3390/molecules25143166
5.) Durling, N. E., Catchpole, O. J., Grey, J. B., Webby, R. F., Mitchell, K. A., Foo, L. Y., & Perry, N. B. (2007). Extraction of phenolics and essential oil from dried sage (Salvia officinalis) using ethanol–water mixtures. Food Chemistry, 101(4), 1417–1424. https://doi.org/10.1016/J.FOODCHEM.2006.03.050
6.) Mele, A., Xhaxhiu, K., & Memo, A. (2009). High pressure soxhlet extraction process by liquid ammonia under its liquid-vapour equilibrium conditions. Albanian Journal of Natural and Technical Sciences, Vol. 3, 157-168, 2009.

7.) Naziruddin, M. A., Kian, L. K., Jawaid, M., Fouad, H., Sanny, M., & Braganca, R. M. (2021). Sage biomass powders by supercritical fluid extraction and hydro-distillation techniques: a comparative study of biological and chemical properties. Biomass Conversion and Biorefinery 2021, 1–11, https://doi.org/10.1007/S13399-021-02055-Y

8.) Porte, A., Godoy, & Maia-Porte, (2013). Chemical composition of sage (Salvia officinalis L.) essential oil from the Rio de Janeiro State (Brazil). In Rev. Bras. Pl. Med.

9.) Scanlan, F., Campari, G., & Sandra, P. (n.d.). Analysis of Essential Oil Compounds Using Retention Time Locked Methods and Retention Time Databases Application. https://www.researchgate.net/publication/266484789

# Investigation of the Packing Properties of Non-Spherical, Nanoporous Deformable Gel Particles During Supercritical Drying

Lara Gibowsky

Institute of Thermal Separation Processes, Hamburg University of Technology,
lara.gibowsky@tuhh.de

## Introduction

Presented research focuses on the production process of aerogels. In particular, the modelling and experimental investigation of aerogels’ behaviour during supercritical drying in a fixed bed will be conducted. Aerogels are nanostructured, highly porous materials and their pores (mainly in the mesoporous range) are filled with air (shown in Fig.1d). Due to their high mesoporous content, aerogels have specific properties like low thermal conductivities, very high surface areas (500 - 1200 $m^2/g$), low densities (0.003 - 0.15 $kg/m^3$) and high porosities. [1-3]

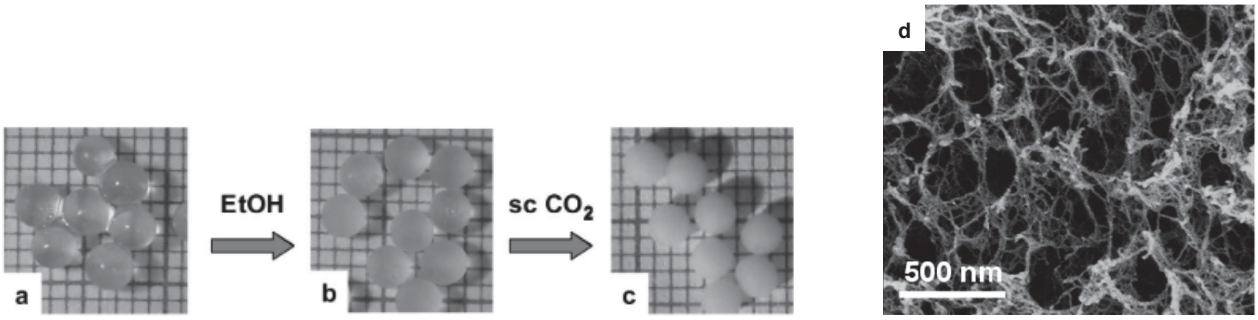


Fig. 1: Morphology of (a) Ca-alginate hydrogel, (b) alcogel, and (c) aerogel (smaller squares of the grids have 1 mm side length) and (d) SEM-picture of the Ca-alginate aerogel, adopted from [4].

The aerogel production process via supercritical drying allows the exchange of water in the pores of the hydrogel by air while preserving the macroscopic shape of the gel and the inner pore structure as well as shown in Fig.1a – 1c. The gelation of a dissolved substance (e.g. alginate or cellulose) is the first step in the aerogel production process and can be induced by heat, added ions or chance of pH. Afterwards the solvent used for the gelation is exchanged by an organic solvent like ethanol (Fig.2 step II.). The reasons for the solvent exchange are the lower critical temperature and pressure of ethanol compared to water and the good solubility in supercritical carbon dioxide ($CO_2$). [1, 2]

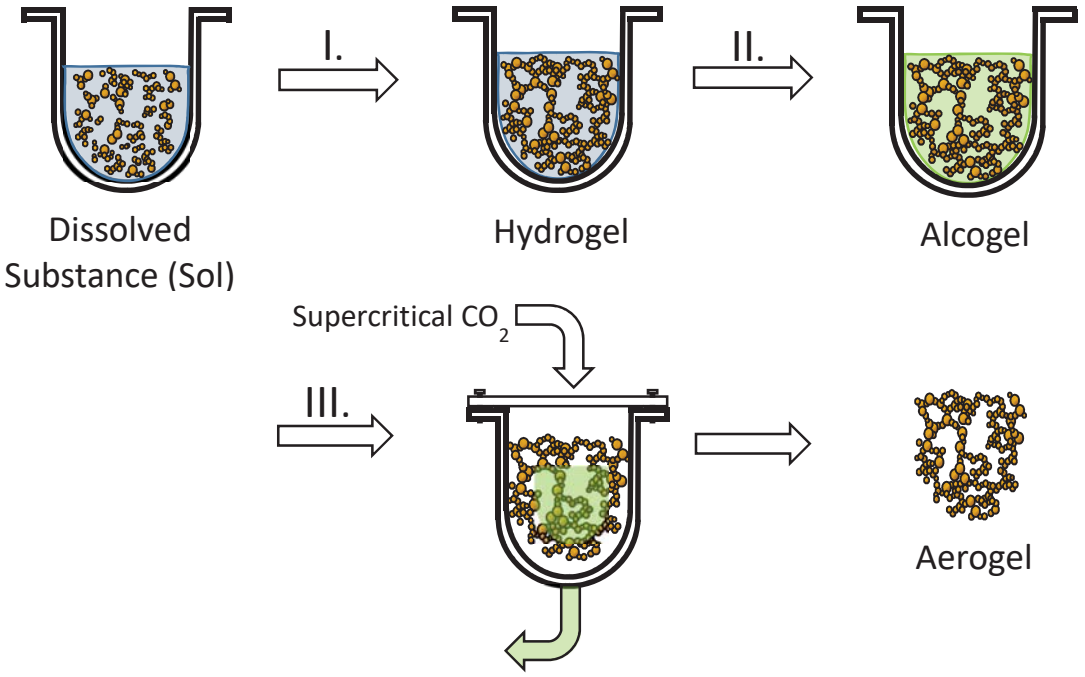


Fig. 2: Schematic steps of the aerogel production process:
I. gelation, II. solvent exchange and III. supercritical drying.

Supercritical drying is the last step in the aerogel production process (Fig. 2 step III.). It’s necessary to avoid capillary forces. Capillary forces occur within the pores, while liquid inside the pores evaporates (e.g. during ambient drying) and lead to destruction of the internal structure due to the resulting pore collapse. Supercritical $CO_2$ is used for the drying to extract the solvent from the wet gel. For this purpose, the alcogel is placed in a high-pressure autoclave at supercritical conditions of $CO_2$-ethanol mixture (approx. 40°C and 100 bar). Nevertheless, supercritical drying with $CO_2$ at elevated pressures and temperatures is the most expensive and time-consuming step in the production process of aerogels. Therefore, optimisation, further knowledge and the prediction of necessary drying conditions is highly required. [2, 4]

## Experimental

For the modelling of the aerogel particles in a fixed bed, a number of material and process data are required. These include mechanical properties of the particles, mass and heat transfer coefficients as well as material properties. The first part of the research project will focus on the mechanical properties during the supercritical drying. Spherical particles from calcium alginate with different G/M ratios and a size of 1 - 4 mm will be used. Mechanical stress can lead to deformation and in the worst case to destruction of these

aerogel particles. Therefore, various experimental studies are performed to investigate the compression behaviour, elasticity, brittleness and deformation of the material. The model is set up with the simulation program COMSOL Multiphysics® (COMSOL Multiphysics GmbH Göttingen, Germany), the goal is the description of supercritical drying in a fixed bed besides the prediction and optimisation of necessary parameters such as drying time and temperature.

## Summary

This research project aims the establishment of a model for the supercritical drying method of aerogel particles in a fixed bed. It is based on the experimentally determined mechanical properties. The next step will be the investigation of further parameters like mass and heat transfer coefficients and the implementation of these data into the model. This model can be used to make predictions about the optimal drying conditions for various aerogel particles.

Acknowledgment

This research project is supported by the German Research Foundation (DFG, GRK 2462: "Processes in Natural and Technical Particle Fluid Systems" (PintPFS).

## References

[1] The Chemistry and Physics of Aerogels: Synthesis, Processing and Properties, L. Ratke and P. Gurikov, Cambridge University Press, MRS (Materials Reasearch Society), 2021

[2] Prozessoptimierung der überkritischen Trocknung von Proteinaerogelen und deren Anwendung im Lebensmittelbereich, I. Selmer, Dissertation, 2020

[3] Aerogel production: Current status, research directions, and future opportunities, I. Smirnova and P. Gurikov, The Journal of Supercritical Fluids 134, pp. 228-233, 2018

[4] Nanostructure of Calcium Alginate Aerogels Obtained from Multistep Solvent Exchange Route, M. Robitzer, L. David, C. Rochas, F. Di Renzo and F. Quignard, Langmuir, Vol. 4, No. 21, 2008

[5] Mathematical modeling of simulation of gel drying with supercritical carbon dioxide, A. Orlovic, S. Petrovic and D. Skala, J. Serb. Chem. Soc. 70 (1), pp. 125-136, 2015

# Propargyl Methacrylate - A Bifunctional Comonomer in the High-Pressure Polymerization of Ethene

Laura Euler Bueno[1], Robin Dursun[1], Markus Busch[1], Jan Duchateau[2]
[1]Ernst-Berl-Institut, TU Darmstadt, markus.busch@pre.tu-darmstadt.de
[2]Saudi Basic Industries Corporation, Jan.Duchateau@SABIC.com

## Introduction

The production of low-density polyethylene (LDPE) is based on the mechanism of free radical polymerization, in which organic peroxides or oxygen are usually used to initiate the polymerization. [1] Due to the resulting long- and short-chain branching, the application of LDPE is very versatile. The benefits can be extended by adding suitable comonomers. Here, polarity, flexibility, solubility or thermal stability can be modified. Especially, polymers with polar functional groups are of great industrial importance because of their beneficial properties with respect to adhesion, printability and miscibility. [2]

The use of bifunctional comonomers enables subsequent reactions to extend the properties and thus the applications of the polymer. These subsequent reactions are referred to as polymeric analogous reactions. [3] A suitable bifunctional comonomer for the high-pressure ethene polymerization hereby is propargyl methacrylate (PMA). After the free radical polymerization with ethene, the triple bond is still present in the copolymer. This provides the possibility for grafting reactions on the triple bond, like click reactions.

Due to its flexibility, the combination of radical polymerization and subsequent grafting reactions offers many industrial advantages. No modifications of the polymerization process is required and the desired polymer properties can be achieved via post-modification with suitable grafting reagents. [4]

## Experimental

The polymerization is performed at 200°C and 2000 bar in a 100 mL and 15 mL high-pressure shrink autoclave. A membrane pump is used to feed a solution of PMA

solved in isopropanol into the reactor. The concentration of PMA in the reaction system can be varied during the experiments by increasing the mass flow rate of the pump and was between 0.02 mol% and 0.266 mol% referring to the overall monomer concentration.

Size exclusion chromatography (SEC) was conducted for all samples, to get the molecular weight distribution of the polymer. In order to identify the influence of PMA on the melting range, differential scanning calorimetry (DSC) measurements were performed.

The copolymer composition is obtained by nuclear magnetic resonance (NMR) and infrared (IR) spectroscopy. Figure 1 shows an example of a $^{1}$H-NMR spectrum and an IR spectrum of a copolymer sample.

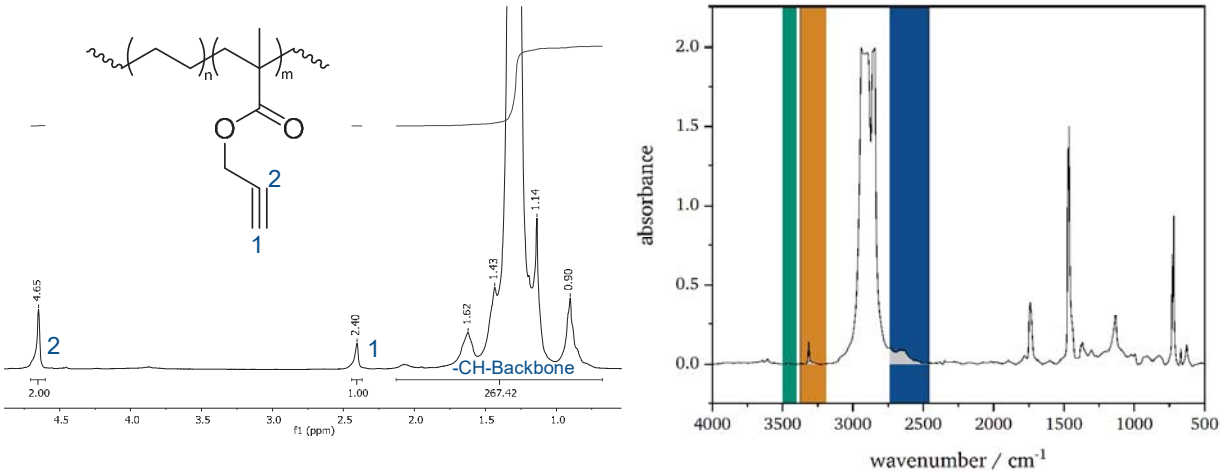


Figure 1: Exemplary $^{1}$H-NMR (400 MHz, TCE) spectrum of an ethene-PMA copolymer (left). Exemplary IR absorption spectrum of an ethene-PMA copolymer (right) with the integration ranges for the CH-groups (2460-2738 cm$^{-1}$), the C-H bond next to the triple bond (3189-3374 cm$^{-1}$) and the C=O ester bond (3400-3500 cm$^{-1}$).

For the quantitative evaluation by IR spectroscopy, a calibration from previous work by *Dursun* [5] is extended and used for the evaluation.

The reactivity ratios for ethene and PMA were determined and discussed by *Mayo-Lewis*, *Fineman-Ross* and the nonlinear fit. The obtained reactivity ratios over the three mentioned methods are shown in table 1.

Table 1: Summary of the determined reactivity ratios via *Mayo-Lewis*, *Fineman-Ross* and the nonlinear least-square fit at 200 °C.

| | ***Mayo-Lewis*** | | ***Fineman-Ross*** | | **Nonlinear fit** | |
|---|---|---|---|---|---|---|
| | **NMR** | **IR** | **NMR** | **IR** | **NMR** | **IR** |
| $r_{PMA}$ | 127.5 | 80 | 3.754 | 5.3704 | 261.84 (± 213.18) | 222.09(± 114.23) |
| $r_{ethene}$ | 0.08 | 0.1 | 0.0645 | 0.08258 | 0.0824 (± 0.016) | 0.0899 (± 0.015) |

The reactivity ratios obtained for ethene by the three methods are in good agreement, while those for PMA show large deviations from each other. This can be explained by the low concentration of PMA during the continuous experiments.

The feasibility of the click reaction using azidomethyl phenyl sulfide with the previously produced ethene-PMA copolymer is performed in an NMR tube, where trichloroethylene (TCE) is used as solvent. The NMR tube is placed in the spectrometer and the reaction is tracked hourly. The obtained NMR spectra with the characteristic signals are shown in figure 2. By integrating the NMR signals, the conversion of the click reaction with different azide to alkyne ratios can be represented.

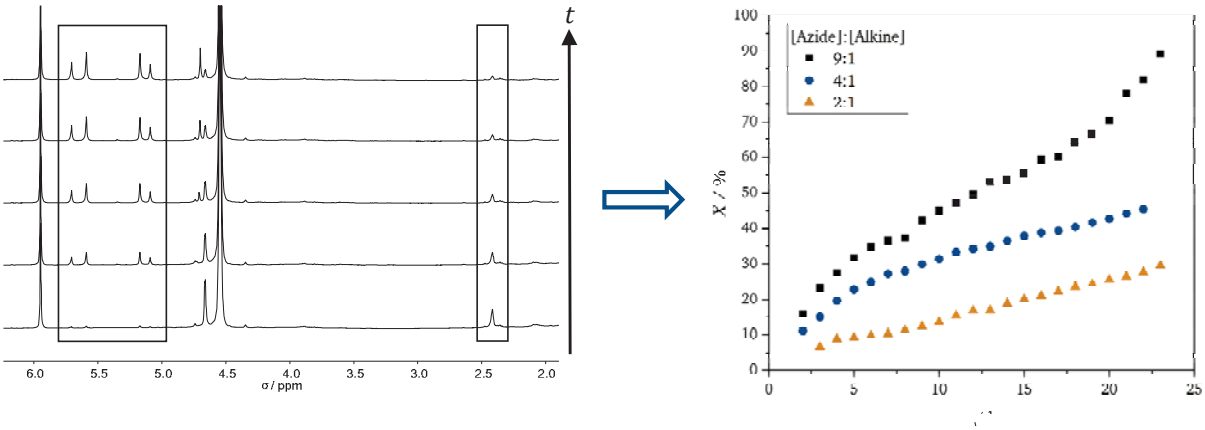


Figure 2: Characteristic signals in NMR spectra over time. Bottom spectrum after 2 h, increasing in 5 h-steps (left). This results in time-resolved conversion for the click reaction using different azide to alkyne ratios (right).

## Summary

The presented work deals with the kinetic investigation of the free radical copolymerization of ethene and PMA in a continuous high-pressure mini-plant and the subsequent click

reactions. Special focus was given to the determination of reactivity ratios in order to be able to compare them with those from previous work. [5] The obtained reactivity ratios for PMA with the three methods show large deviations from each other, which can be explained by the low concentration of PMA during the continuous experiments. For a more accurate estimation of the reactivity ratios of PMA, experiments with higher PMA concentrations should be performed. In addition, experimentally determined reactivity ratios can be verified by deterministic simulation using *Predici.*

## References

[1] G. Luft, *Chemie in unserer Zeit* **2000**, 34, 190.

[2] N. M. G. Franssen, K. Remerie, T. Macko, J. N. H. Reek, B. de Bruin, *Macromolecules* **2012**, 45, 3711.

[3] H.-G. Elias, *Makromoleküle. Band 1; Chemische Struktur und Synthesen*, Wiley-VCH, Weinheim, **1999**.

[4] D. M. Castaneda Zuniga, P. Neuteboom, J. N. E. Duchateau, M. Busch and S. B. Fries, US20170166668A1, **2017**.

[5] R. Dursun, *Master Thesis*, TU Darmstadt, **2018**.

# The Fatty Acid Analysis of Vitex Agnus Castus Extracts Obtained by Liquid $CO_2$

Jeta Lica [1], Lorenci Gjurgjaj[1], Iris Çaçani[2], Carla Ferreri[3], Altin Mele[1,4]

[1]Center of Techniques Study, Ivodent Academy, 1016 Tirana, Albania,
jeta.lica@ivodent.edu.al

[2]Department of Prosthetics, Ivodent Academy, 1016 Tirana, Albania,

3. Istituto per la Sintesi Organica e la Fotoreattività, Consiglio Nazionale delle Ricerche, Via P. Gobetti 101,40129 Bologna, Italy

[4] Department of Chemistry, University of Tirana, 1001 Tirana, Albania

## Introduction

Vitex Agnus Castus (chaste tree) is considered for its essential oil, containing several terpenic components (sabinene and 1,8- cineole) with antifungal, antimicrobial activity and other health effects. [1, 2]

Characterization of Vitex Agnus Castus components was previously reported also including fatty acid composition [3, 4, 5] and in one of them [5] there is the identification of a MG containing linoleic acid. In these reports no mention of branched or hydroxylated 18:2 derivatives is reported. The presence of branched fatty acids has been already reported in other plants [6-9].

The lipid part has to be evaluated for its value mainly for the presence of an essential fatty acid such as linoleic acid. This fatty acid must be taken as essential fat from the diet for humans, that cannot synthesize this fatty acid but need it for the constitution of all tissues. The plant and its fruits are used in traditional herbal medicine for menstrual problems, including depression and irritability, as well as for acne treatment. Some of the effects claimed for the plant can derive from the principal fatty acid components omega-6, well-known in dermatology and gynecology sectors.

Polar fraction of this plant is described in a recent report on LC/MS analysis of the hydro-alcoholic extracts [8].

Supercritical fluid extraction is used also and the recovery of diterpenes, triterpenes and casticin is evaluated [11, 15].

## Experimental

### Plant extraction

The grounded VAC (20 g) was placed into the extractor vessel. Extraction of the sample was collected at different times, respectively 3, 5, 7 and 24 hours. The extraction procedure and the high pressure apparatus used thereof are explained in detail in [15].

### Lipid identification and extraction

**Samples**: Identification of vials with the following marks: **3, 5, 7, 24, TOT**, using these marks to indicate the samples.

TLC (*n*-hexane: $Et_2O$ 7:3) (Figure 1A) of the crude samples before lipid extraction showed the presence of the following 3 main fractions by comparison with authentic samples:

**1)** a polar fraction ($R_f$:0.95),
**2)** triglyceride fraction ($R_f$:0.8)
**3)** Slow eluted fraction: mix of MG, DG and FFA, and no other lipid compounds were identified. ($R_f$ =0.3-0.5)

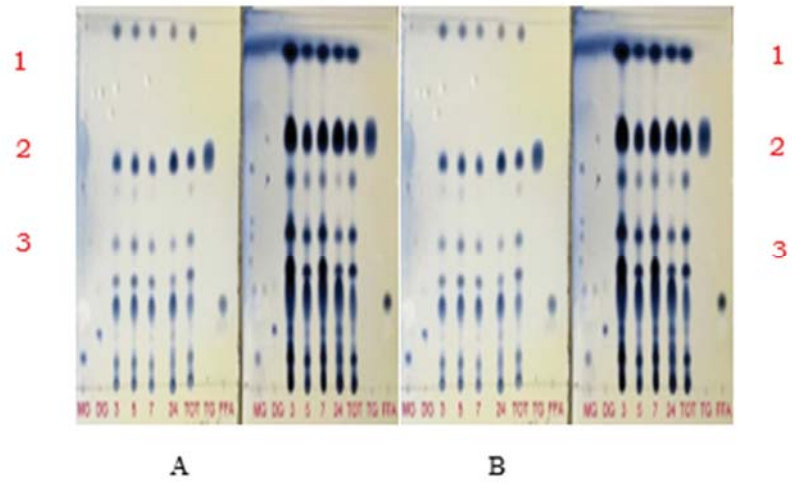


**Fig. 1.:** TLC of the composition (*n*-hexane:$Et_2O$ 7:3) of the five samples before (A) after (B) lipid extraction.

An aliquot from each fraction was taken, weight and extracted with 2:1 chloroform/methanol (4 × 4mL) after adding of tridistilled $H_20$ (1 mL) according to Folch

method (1) (see Table 1). After the extraction, TLC (*n*-hexane: $Et_2O$ 7:3) (Fig 1B) showed the following lipid composition (TG, DG, MG, FFA) and the presence of the slow eluted spot.

**Tab. 1.:** Weights of the samples before and after lipid extraction.

| *samples* | *extract weight* |
|---|---|
| TOT=18.7 mg | 12.2 mg |
| 24=19.2 mg | 14.8 mg |
| 7 =18.3 mg | 11.4 mg |
| 5 =19.1 mg | 13 mg |
| 3 =18.7 mg | 14.2 mg |

**Transesterification**

After the extraction two procedures were performed:

1) Total lipid transesterification in order to convert all lipids present in the samples to FAME by adding 0.5 M solution of KOH in MeOH (0.5 mL) and quenching the reaction after 30' by brine addition (0.5 mL). FAMEs were then extracted with *n*-hexane (3× 2mL), dried on anhydrous $Na_2SO_4$, evaporated to dryness and GC analyzed by comparison with standard references.
2) Separation of main extract components by preparative TLC (*n*-hexane:$Et_2O$ 7:3)
   1) apolar fraction for GC/MS and NMR characterization
   2) TG for selective transesterification using the method before described and GC analysis for fatty acid identification as FAME.
   3) slow eluting fraction for NMR characterization, transesterification for fatty acid identification as FAME (using the procedure before specified) and GC analysis.
   The weights of collected fractions are listed in Table 2.

**Tab. 2.:** Weights of the isolated fractions

| *samples* | *apolar spot* | *Tg* | *Down spot* |
|---|---|---|---|
| TOT= 5 mg | 0.48 | 2.2 mg | 1 mg |
| 24 = 6.2 mg | 0.6 | 1.8 mg | 0.7 mg |
| 7 = 3.8 mg | 0.25 | 1.5 mg | 0.8 mg |
| 5 = 5.5 mg | 0.45 | 1.8 mg | 0.8 mg |
| 3 = 5.8 mg | 0.5 | 1.4 mg | 0.5 mg |

## Results

1) The fatty acid content (as relative percentages) coming from the transesterification of *i*) total lipids *ii*) TG fraction and *iii*) DG and MG fractions (down spot) are listed in Table 3. See comments below.

2) Characterization of apolar fraction, performed by GC-MS analysis and $^{1}$HNMR, showed a mixture of compounds that could correspond to a mixture of cyclic terpenes, as monoterpene and sesquiterpenes [19], and in particular the NMR spectrum did not show the presence of aromatic compound in this fraction.

3) The NMR of slow eluting fraction before transesterification showed, in addition to the peaks of lipids, the characteristics peaks in the aromatic hydrogen area.

**Tab. 3**.: Fatty acid content of the samples expressed as relative percentages.

| | Total lipids | | | | | TG fraction | | | | | Down fraction | | | | |
|---|---|---|---|---|---|---|---|---|---|---|---|---|---|---|---|
| | 3 | 5 | 7 | 24 | TOT | 3 | 5 | 7 | 24 | TOT | 3 | 5 | 7 | 24 | TOT |
| 16:0 (palmitic) | 5.4 | 5.7 | 5.9 | 5.8 | 6.5 | 6.2 | 6.2 | 7.8 | 5.8 | 7.8 | 11.7 | 10.6 | 8.1 | 11.9 | 6.3 |
| 16:1 (Δ6 + D7) | 1.8 | 2.0 | 1.6 | 0.7 | 1.6 | 0.1 | 0.6 | 0.7 | 0.1 | 1.3 | 0.4 | 0.5 | 0.1 | 0.1 | 1.3 |
| 16:1 Δ9 c (palmitoleic) | 0.3 | 0.4 | 0.3 | 0.2 | 0.3 | 0.1 | 0.1 | 0.1 | 0.1 | 0.4 | 0.4 | 0.5 | 0.1 | 0.2 | 0.3 |
| 18:0 (stearic) | 3.0 | 3.3 | 3.5 | 3.5 | 3.4 | 3.4 | 3.2 | 4.6 | 3.3 | 4.5 | 5.2 | 5.1 | 3.0 | 4.0 | 3.5 |
| 18:1 Δ9 t (trans oleic) | 0.5 | 0.4 | 0.3 | 0.3 | 0.3 | 0.0 | 0.0 | 0.0 | 0.0 | 0.1 | 0.0 | 1.6 | 0.0 | 0.0 | 0.0 |
| 18:1 Δ9 c (oleic) | 11.6 | 11.8 | 11.9 | 12.3 | 12.0 | 11.8 | 11.9 | 15.4 | 12.2 | 15.4 | 17.6 | 13.6 | 0.7 | 13.4 | 12.8 |
| 18:1 Δ11 c (vaccenic) | 0.7 | 0.5 | 0.7 | 0.7 | 0.8 | 0.8 | 0.7 | 0.9 | 1.0 | 1.4 | 1.4 | 1.2 | 13.3 | 1.8 | 1.1 |
| t 18:2 ω6 | 0.4 | 0.3 | 0.4 | 0.2 | 0.0 | 0.2 | 0.1 | 0.1 | 0.2 | 0.1 | 0.0 | 0.0 | 0.1 | 0.2 | 0.1 |
| 18:2 ω6 (linoleic) | 67.7 | 66.8 | 68.9 | 73.4 | 68.8 | 71.6 | 75.3 | 67.0 | 73.9 | 67.4 | 15.7 | 33.9 | 37.2 | 43.9 | 66.8 |
| 18:2 ω6 branched isomers | 7.5 | 7.4 | 5.7 | 2.0 | 5.6 | 5.0 | 1.5 | 2.0 | 3.0 | 0.8 | 44.0 | 29.3 | 35.9 | 22.8 | 6.6 |
| 18:3 ω6 | 0.7 | 0.7 | 0.3 | 0.2 | 0.7 | 0.0 | 0.0 | 0.9 | 0.0 | 0.3 | 3.1 | 3.0 | 0.0 | 1.1 | 0.7 |
| 18:3 ω3 | 0.5 | 0.7 | 0.6 | 0.6 | 0.1 | 0.9 | 0.4 | 0.3 | 0.4 | 0.6 | 0.5 | 0.8 | 0.6 | 0.7 | 0.7 |

## Summary

The FAME analysis of the extracts showed that the main fatty acid of the lipid fractions is linoleic acid (66-70%), an essential fatty acid of the omega-6 family. The second fatty acid

is oleic acid (ca 10%), and saturated fatty acids are ca. 8% of the total fatty acid composition. Using the GC analysis a peak was evidenced, very concentrated in the slow eluting fraction, not corresponding to the reference fatty acid mixture of saturated, mono- and poly-unsaturated components. Through the chemical approach of DMDS derivatization and GC-MS analysis we could identify the structure of a fatty acid where the carbon atom chain contains 18 carbon atoms with methyl or OH groups as substituents along the chain.

## References

1. Duymus, H. G. et al. Ind. Crops Prod. (2014) 55, 33-42.
2. Stiokovic, D. et al. Food Chem. (2011) 128, 1017-1022.
3. Asdadi A. et al. J. Mycologie Medicale (2015), 25, e118-e127.
4. Ozkaya et al. J. of Chem. (2013*)* Article ID 845743.
5. Chen, S.-N. et al, Fitoterapia (2011), 82, 528-533.
6. Hierro MTG et al., J. Am Oil Chem Soc (1996) 73, 575
7. http://lipidlibrary.aocs.org/content.cfm?ItemNumber=40259
8. Thiele R et al., J Agric Food Chem (2008) 56, 4219
9. review: Velisek J, Cejpek K. Czech J.Food Sci (2006) 24, 193-216
10. Mari A. et al. J Pharm. Biomed. Anal. (2015) 102, 215-221.
11. Cossuta, D. et al J. Supercritical Fluids (2008) 47, 188-194.
12. Stela Jokić, et al., J. of Supercritical Fluids, Volume 123, 2017, Pages 50-57,
13. Mele et al., (2015) IV International Congress: "Engineering, Environment and Materials in Processing Industry"
14. Mele et al. (2011), International Conference Biotechnological Developments, Book of Abstracts, Page 53.
15. Mele et al. (2013), The Journal of Supercritical Fluids, 79(), 123–126.
16. Folch et al., J Biol Chem 1957, 226, 497
17. Nichols, P.D., Volkman, J.K.,and Everitt, D.A..Oceanol. Acta (1989), *12*, 393-403.
18. Yamamoto, K., Shibahare, A., Nakayama, T., and Kajimoto, G., Chem Phys Lipids (1991), *60*, 39-50.
19. Artz B. M. Evening Primrose, In *Herbal products. Toxicology and clinical pharmacology*, 2nd ed., Tracy T. S. & Kingston, R. L. Eds., 2007, Humana Press, Totowa, pp. 211-232.

# Understanding the Role of Sub/Supercritical Water in the Hydrolysis of the Ester Link in Polyesters

Enkeledo Menalla, Maria Jose Cocero

BioecoUva Research Institute, PressTech research group. EII sede Mergelina.

University of Valladolid, 47011 Valladolid, Spain

enkeledo.menalla@uva.es

## Indroduction

Water above its critical point (Tc 374ºC, 22 MPa) is an alternative solvent for dissolution/ hydrolysis of biomass. Its low viscosity and high diffusivity facilitate water penetration into the complex structure of biomass, and its low dielectric constant, similar to non-polar organic solvents, allows it to have the behavior of a non-polar solvent able to dissolve organic compounds[12]. The development of the sudden expansion reactor by our research group, has allow to operate with residence time below one second. This technology has given excellent results for the fractionation of lignocellulosic biomass as defatted grape seed[3] pulp beet[4], inulin[2], and for lignin depolymerization because minimize the polymerization that takes place by more conventional procedures[5]

Other biomasses with industrial interest valorization are biomasses with high concentration of natural biopolyesters, as cutin and suberin. The main problem associated with its characterization is the total hydrolysis of the esters link to acids, so its ester structure is not known[67]. Considering the change of water properties with pressure and temperature, it is possible to move the ionic product of the water from ionic media at subcritical operation conditions to non-ionic media at supercritical conditions. So, the sub/supercritical water could be suitable depolymerization medium to get partial hydrolysis of cutin to ester monomers that will allow to improve the knowledge of the ester structure of the cutin.

The aim of this thesis is to improve the knowledge of the ester structure of the cutin, by study the ester group hydrolysis in sub/supercritical water. Identify the partial hydrolysis products, it will be determined its kinetics, reaction rate and hydrolyzation mechanism. As starting point, simple compound with ester link will be use to study its partial hydrolysis, as it is triacetin. The goal of this research is to learn more about the process of producing ester from sub/SCW

hydrolysis, by following DA (diacetin), MA (monoacetin), glycerol and acetic acid reaction products

## Experimental

Figure 1 shows the continuous pilot plant used in this study. Using a sudden expansion reactor, the hydrolysis pilot plan was design to function at 400°C and 30 MPa (SMRE). The key benefit of this reactor is the immediate cooling of the products, which effectively stops hydrolysis processes in very short time. In a similar way, the heating of the triglyceride stream is achieved instantaneously by a supercritical water injection at the reactor inlet. With this heating method, it is possible to change the temperature of a triglyceride stream from room temperature up to 400 °C in a mixer which is placed at the reactor. This plant is developed by our group and more information about the design of the plant we can find [8,9].

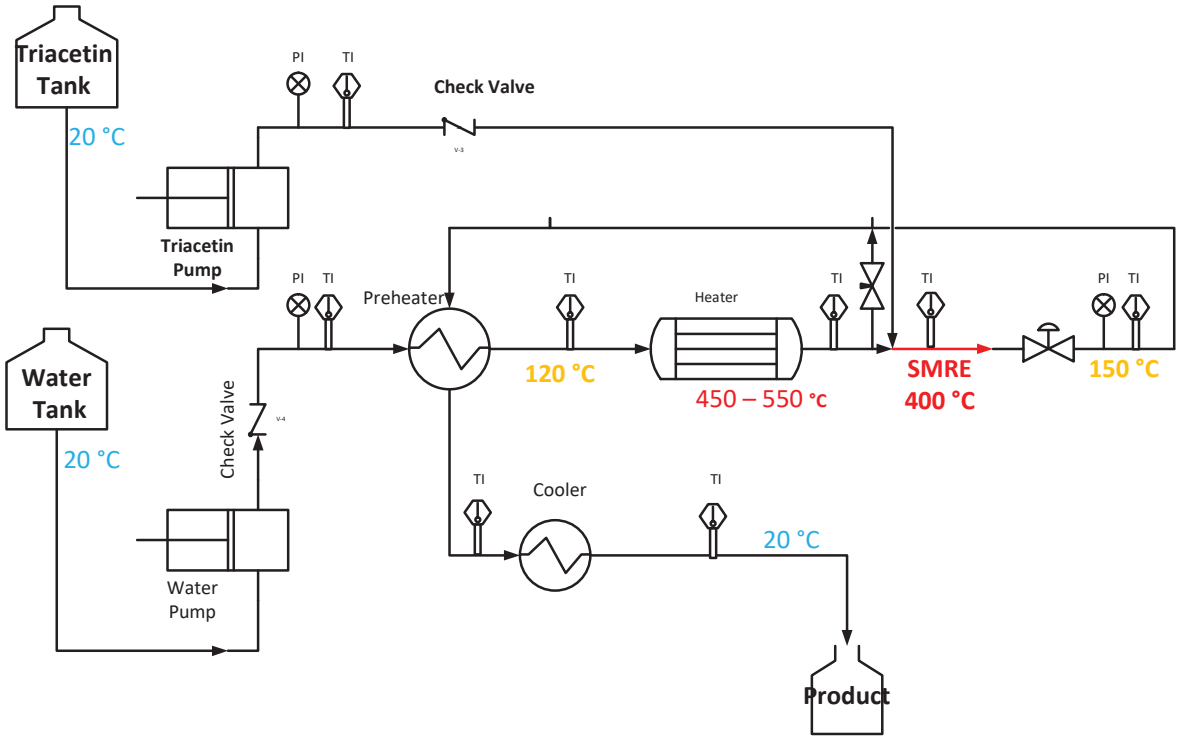


Figure 1. PFD diagram of SCW plant

The triacetin solution is continually compressed and pumped up to operating pressure, remaining at room temperature until it reaches the reactor's inlet. In the mixing point, the compressed triacetin solution is mixed with a stream of hot pressured water. After T pipe the triacetin reacts with water and depending the length of the reactor is the residence time. After

reaction the product is depressurized using a high-temperature needle valve (high-T valve), which instantly cools the effluent to around 150 °C and therefore stops the reaction. By using this technology, the production of hydrolysis product is fast, continues and by the flow and reactor volume we control the reaction time. The next step is to reduce the temperature after the reactor; with this heat, we can raise the temperature of water that will reach supercritical conditions, and with the temperature of cold water, we can lower the temperature of the reactor's stream until 20 °C. In my talk I will present preliminary results about partial hydrolysis of triacetin.

## Acknowledgements

Projects funded by FEDER, Ministry of Science and Innovation project PID2019-105975GB-100 and Junta de Castilla y Leon CLU-2019-04.

## References

1. Cocero, M. J. *et al.* Understanding biomass fractionation in subcritical & supercritical water. *J. Supercrit. Fluids* **133**, 550–565 (2018).
2. Martínez, C. M., Adamovic, T., Cantero, D. A. & Cocero, M. J. Industrial Crops & Products Ultrafast hydrolysis of inulin in supercritical water : Fructooligosaccharides reaction pathway and Jerusalem artichoke valorization. *Ind. Crop. Prod.* **133**, 72–78 (2019).
3. Adamovic, T., Tarasov, D., Demirkaya, E., Balakshin, M. & Cocero, M. J. A feasibility study on green biorefinery of high lignin content agro-food industry waste through supercritical water treatment. *J. Clean. Prod.* **323**, (2021).
4. Martínez, C. M., Cantero, D. A. & Cocero, M. J. Production of saccharides from sugar beet pulp by ultrafast hydrolysis in supercritical water. *J. Clean. Prod.* **204**, 888–895 (2018).
5. Saisu, M., Sato, T., Watanabe, M. & Adschiri, T. Conversion of Lignin with Supercritical Water - Phenol Mixtures. 3124–3130 (2003).
6. Domínguez, E., Heredia-Guerrero, J. A. & Heredia, A. Plant cutin genesis: Unanswered questions. *Trends Plant Sci.* **20**, 551–558 (2015).
7. Gringel, W. *et al.* Biopolyester Membranes of Plants : Cutin and Suberin. **208**, (1980).
8. Cantero, D. A., Dolores Bermejo, M. & José Cocero, M. High glucose selectivity in pressurized water hydrolysis of cellulose using ultra-fast reactors. *Bioresour. Technol.* **135**, 697–703 (2013).
9. Cantero, D. A., Bermejo, M. D. & Cocero, M. J. Kinetic analysis of cellulose depolymerization reactions in near critical water. *J. Supercrit. Fluids* **75**, 48–57 (2013).

# Influence of Mixing on the Initiator Efficiency in High-Pressure Polymerization Reactors

Lena Gockel, Markus Busch*

TU Darmstadt, Darmstadt/Germany

*markus.busch@pre.tu-darmstadt.de

## Introduction

LDPE (low-density polyethylene) production takes place under extreme process conditions with temperatures up to 300 °C and pressures up to 3000 bar. Laboratory plants are expensive to operate and require high safety standards. Relevant information, such as the concentration of the reactive radical species, can hardly be determined experimentally. Therefore, reactor models are an important tool to get a better understanding of the process.

LDPE is formed by free-radical polymerization of ethylene. The polymerization is started by an initiator e.g., an organic peroxide that decomposes into radicals. The initiator decomposition is temperature dependent and for each peroxide an optimum polymerization temperature with a minimum in initiator consumption exists. This connectivity was experimentally investigated by Luft[1] and van der Molen[2]. Simple reactor models, that are based on the concept of a perfectly mixed tank fail to describe the experimental data. At temperatures above the optimum polymerization temperature, the initiator consumption increases due to inefficient mixing. Therefore, a model must capture the mixing in the reactor to be able to describe the increase in initiator consumption at high temperatures.

Furthermore, in many models the initiator efficiency is used as a fit parameter to describe experimental data. In this case, the efficiency factor includes the reduction of the initiator efficiency due to side reactions and the higher initiator consumption due to inefficient mixing. Thus, the efficiency factor is not only dependent on the type of initiator, but also on the process conditions and the reactor geometry. The aim of this work is to describe the mixing in an LDPE reactor by using CFD (computational fluid dynamics). A better understanding of the influence of mixing on the initiator efficiency should be gained to go one step further in reducing fit parameters and increasing the predictability of LDPE reactor models.

## Modeling

The geometry of the CFD simulation is orientated to a continuous high-pressure mini-plant with a volume of 100 mL as shown in Figure 1. Typical experiments are carried out at 200 °C, 2000 bar and a stirrer speed of 800 rpm. Ethylene, propene as a CTA and a peroxide(mixture) e.g. TBPA (*tert*-butyl peroxyacetate) and TBPPI (*tert*-butyl peroxy-pivalate) are fed through a small ring gap around the stirrer shaft. Those conditions are adapted in the CFD model. Additionally, the reactor is assumed to be adiabatic. The thermo-physical properties like density, viscosity, thermal conductivity, and heat capacity depend on temperature, pressure, and polymer content in the reactor.

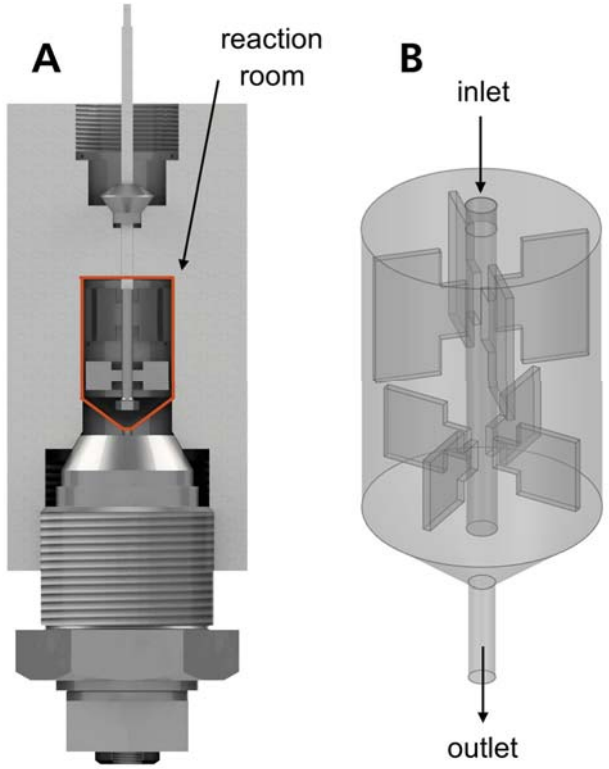


Fig. 1.: A) CAD drawing of the 100 mL high-pressure reactor and B) reactor geometry of the CFD model.

During the simulation the mass, heat and momentum balance is solved. The mass balance includes a detailed kinetic mechanism of the radical polymerization. It considers the basic reactions initiation, propagation, and termination, as well as the transfer reactions to monomer and CTA (chain transfer agent). The characteristic long- and short chain branches of LDPE are built via transfer to polymer and back-biting (intramolecular transfer) respect-tively. In addition, the β-scission and the terminal double bond propagation are taken into account.[3]

To get information on average polymer properties, the method of moments is applied. Based on those, the number- and weight-average molecular weight, as well as the PDI (polydispersity index) are calculated. Therefore, six additional balance equations for the zeroth, first and second moment of the primary radical, the secondary radical and the dead polymer distribution are implemented.

## Summary

The CFD model is applied to analyze different reactor setups regarding their impact on the initiator efficiency. Especially the position of the feed point, the feed composition and the feed rate are investigated. The results show that a locally high radical concentration has the consequence that the ratio between termination and propagation reaction rate increases. That leads to a lower conversion and a lower reactor temperature what again results in a decrease in transfer to low molecular species. Regarding the polymer properties it is found that the molecular weight is increased while short- and long-chain branching densities are reduced.

This work is funded by the Federal Ministry of Education and Research (BMBF) and the state of Hesse as part of the NHR Program.

## References

[1] G. Luft, H. Bitsch, H. Seidl, Journal of Macromolecular Science: Part A - Chemistry 1977, 11, 1089–1112.

[2] T. van der Molen, A. Koenen, H. Oosterwijk, H. van der Bend, Ing. Chim. Ital. 1982, 18, 7–15.

[3] M. Busch, Macromol. Theory Simul., 2001, 10, 408-429.

# Inverse Molecular Docking of Cannabinoids

Vid Ravnik[1*], Marko Jukić[1,2], Urban Bren[1,2]

[1] *Faculty of Chemistry and Chemical Engineering, University of Maribor (UM FKKT), Smetanova Ulica 17, 2000 Maribor, Slovenia*

[2] *Faculty of Mathematics, Natural Sciences and Information Technologies; University of Primorska (UP FAMNIT), Glagoljaška 8, SI–6000 Koper, Slovenia.*

* vid.ravnik2@um.si

## Introduction

*Cannabis sativa* is a widely used plant that has found many uses over the millennia. Today it is well known for its psychotropic effects and recreational use. However, anecdotal evidence and, more recently, more concrete medical studies have highlighted the therapeutic potential of the plant's chemical constituents. These unique metabolites found only in *Cannabis* are known as cannabinoids. The exact number of cannabinoids is not known; two of the most notable are receiving the most attention, namely: delta-9-tetrahydrocannabinol (THC) and cannabidiol (CBD). THC has been identified as the major psychotropic component of cannabis, while the other cannabinoids have little or no psychotropic effects [1-3].

Using radiolabelled THC analogue researchers identified THC-binding sites with high affinity in the brain, which were later identified as cannabinoid receptor 1 (CB1), a G protein-coupled receptor (GPCR). Cannabinoid receptor 2 (CB2) was later identified by homology cloning and is highly expressed in the immune system. Researchers have also discovered several endogenous ligands that activate CB1 and CB2 with high affinity and potency; these are known as endocannabinoids. Many neurological disorders are associated with alterations in the endocannabinoid system, suggesting that targeting these pathways is a potential therapeutic strategy. The endocannabinoid system is complicated by numerous mediators and overlaps with other signalling pathways and metabolic processes. Therefore, modulation of its components affects a broader endocannabinoid system known as the endocannabinoidome [4].

Such a broad system offers significant opportunities for therapeutic studies of non-THC cannabinoids, which often modulate multiple proteins of the endocannabinoidome. In this study, we aim to identify potential target proteins for several cannabinoids using an inverse molecular docking approach.

Inverse molecular docking is a relatively new approach that focuses on finding an enriched subset of potential protein targets for a given ligand. Recent studies suggest that existing drugs bind to multiple proteins. Therefore, identifying the target proteins of a potential drug can be crucial to avoid unexpected side effects in late-stage clinical trials [5]. An inverse docking approach has been successfully used to repurpose existing drugs [6], to gain new insights into the side effects of existing drugs [7], or to discover new potential targets for a natural drug candidate [9].

Inverse molecular docking uses a molecular docking approach to predict the binding affinity of a ligand of interest to an extensive database of protein targets, resulting in a subset of promising candidates with high predicted binding affinity. It is based on molecular docking, a method for predicting the binding mode and assessing the affinity of a ligand to a receptor. In general, docking methods consist of two main components, a sampling algorithm and a scoring function. The sampling algorithm generates putative binding modes, while the scoring function assigns a score to the predicted binding modes. In general, the accuracy of the binding energy prediction is limited by the scoring function [5].

## Experimental

In this study, our goal is to identify potential new targets for cannabinoids. We focus on a set of 16 cannabinoid ligands.

First, we docked these 16 ligands to a set of 21 receptor structures known to be associated with cannabinoids. These include CB1 and CB2, as well as several ion channels and nuclear receptors that contribute to the extended endocannabinoid system.

We used human structures of the proteins from the Protein Data Bank (RSCB PDB). For some receptors, there were no human representatives in the PDB; these were modelled from similar structures using the YASARA software package. Protein binding sites were created using the web server Proteins Plus [9]. We defined the binding site as a centroid at the cavity with the largest drug score found by DoGSiteScorer of Proteins Plus.

We used the docking algorithm PROTEUS that reconstructs small ligands at the binding site of the receptor from fragments and outputs multiple poses of the ligand at the binding site with different docking scores. These are given in arbitrary units and represent approximations of the relative free energy of binding of the receptor and ligand in the

specific pose. The binding site is defined in PROTEUS as a union of centroids, i.e., the total space occupied by multiple spheres.

To validate the method, we used a redocking procedure. From our set of receptors from the PDB, we selected the structures with small ligands that were co-crystallised in the cavities we examined using our inverse docking procedure. We ended up with 5 structures for validation of the method. We removed the co-crystallised ligands from the binding site and then re-docked the ligand to the binding site. We compared the docked and native co-crystallised positions of the ligands and calculated the root-mean-square-deviation (RMSD) of their atomic positions. Using the redocking method, we showed that our docking method can yield similar positions of the ligands as the native ones. An example of a native and a redocking position is shown in Figure 1. Of the 5 redocking examples, 2 were found to be a good fit (RMSD < 2 Å).

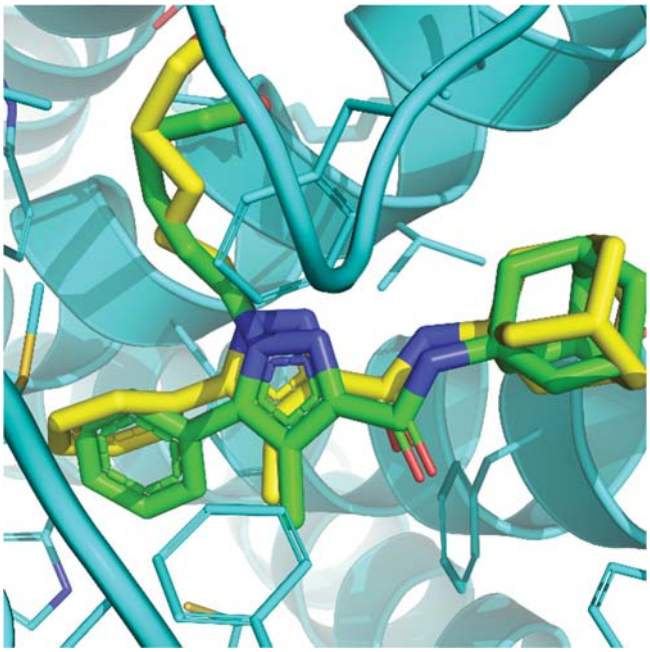

**Figure 1**: An example of the redocking procedure: Native (yellow) and redocked (green) poses of the ligand (9JU) in Cannabinoid receptor 2 (PDB ID 5zty, chain A), RSMD: 1.58 Å.

The inverse docking results for this small group of targets show us a clear trend for which cannabinoids give the best docking results on average. Based on the encouraging results, we applied a similar inverse docking procedure to protein structures from the entire human genome. We used protein structures based on the human subset of the ProBiS docking database [10]. Our database included about 55000 receptor structures. Our docking

software failed on about 15% of the structures in the database. The results of the successful runs can provide us with potential new targets for our cannabinoid ligands. The same ligand has the highest average docking scores as with our small group of ligands previously. We also analysed the results by categorising the receptors according to their function as classified in the PDB.

## Summary

Using an inverse docking approach, we sought to identify new potential targets for a series of 16 cannabinoid ligands. First, we performed a smaller study on 21 receptors known to be associated with cannabinoids. The results of the study were encouraging, and we also performed their validation using redocking procedures. After the study with the small group of receptors, we used inverse molecular docking on proteins from the entire human genome. We identified a cannabinoid that exhibited the highest average docking scores. It represents a promising candidate for further studies, and the proteins to which it binds most strongly are also worthy of a closer investigation.

## Acknowledgment

This work was financial supported from the Slovenian Research Agency (ARRS) through project (J1-2471) and programme (P1-0403) grants. Additionally, I would like to thank Prof. Dr. Urban Bren and Dr. Marko Jukić for their supervision and advice.

## References

[1] Abyadeh, M., Gupta, V., Paulo, J., Gupta, V., Chitranshi, N., & Godinez, A. et al. (2021). A Proteomic View of Cellular and Molecular Effects of Cannabis. *Biomolecules*, *11*(10), 1411. doi: 10.3390/biom11101411

[2] Alexander, S. (2016). Therapeutic potential of cannabis-related drugs. *Progress In Neuro-Psychopharmacology And Biological Psychiatry*, *64*, 157-166. doi: 10.1016/j.pnpbp.2015.07.001

[3] Grotenhermen, F. (2005). Cannabinoids. *Current Drug Target -CNS &Amp; Neurological Disorders*, *4*(5), 507-530. doi: 10.2174/156800705774322111

[4] Cristino, L., Bisogno, T., & Di Marzo, V. (2019). Cannabinoids and the expanded endocannabinoid system in neurological disorders. *Nature Reviews Neurology*, *16*(1), 9-29. doi: 10.1038/s41582-019-0284-z

[5] Xu, X., Huang, M., & Zou, X. (2018). Docking-based inverse virtual screening: methods, applications, and challenges. *Biophysics Reports*, *4*(1), 1-16. doi: 10.1007/s41048-017-0045-8

[6] Jukič, M., Kores, K., Janežič, D., & Bren, U. (2021). Repurposing of Drugs for SARS-CoV-2 Using Inverse Docking Fingerprints. *Frontiers In Chemistry*, *9*. doi: 10.3389/fchem.2021.757826

[7] Kores, K., Konc, J., & Bren, U. (2021). Mechanistic Insights into Side Effects of Troglitazone and Rosiglitazone Using a Novel Inverse Molecular Docking Protocol. *Pharmaceutics*, *13*(3), 315. doi: 10.3390/pharmaceutics13030315

[8] Kores, K., Lešnik, S., Bren, U., Janežič, D., & Konc, J. (2019). Discovery of Novel Potential Human Targets of Resveratrol by Inverse Molecular Docking. *Journal of Chemical Information And Modeling*, *59*(5), 2467-2478. doi: 10.1021/acs.jcim.8b00981

[9] Xu, X., Huang, M., & Zou, X. (2018). Docking-based inverse virtual screening: methods, applications, and challenges. Biophysics Reports, 4(1), 1-16. doi: 10.1007/s41048-017-0045-8

[10] Konc, J., Lešnik, S., Škrlj, B., & Janežič, D. (2021). ProBiS-Dock Database: A Web Server and Interactive Web Repository of Small Ligand–Protein Binding Sites for Drug Design. Journal of Chemical Information And Modeling, 61(8), 4097-4107. doi: 10.1021/acs.jcim.1c00454

# Ventilated Deflagrations of Polymerization Mixtures

Moritz Imhoff, Markus Busch*

Ernst-Berl-Institut, Technische Universität Darmstadt,

*markus.busch@pre.tu-darmstadt.de

## Introduction

The design of pressure relief systems for high-pressure applications such as the high-pressure polymerization process can be calculated via the API 520 [1]. The DuPont method [2] was further developed to include the decomposition reaction of ethene into the design of relief valve especially for high pressure separator units operating at 200 to 500 bar. The depressurization trough the safety valve and pressure rise due to the decomposition is calculated via the density of ethene for the given process conditions. Different physical properties of an unburned and burned phase in the case of a ventilated deflagration are not considered. The objective of the presented work is to generate a more in-depth understanding of ventilated deflagrations. This is achieved by systematic analysis of the pressure relief and the deflagration reaction. Here the safety related key numbers are determined, like the discharge coefficient $K_d$, the adiabatic flame temperature, and the laminar flame front velocity. The pressure and temperature dependent burning velocity of ethene was determined within the work of DELIBALTA[3]. The general method is illustrated in figure 1. Various types of fast measurement techniques, like high-pressure piezo sensors and custom thermocouples are employed to depict the rapid and transient process of ventilation and deflagration.

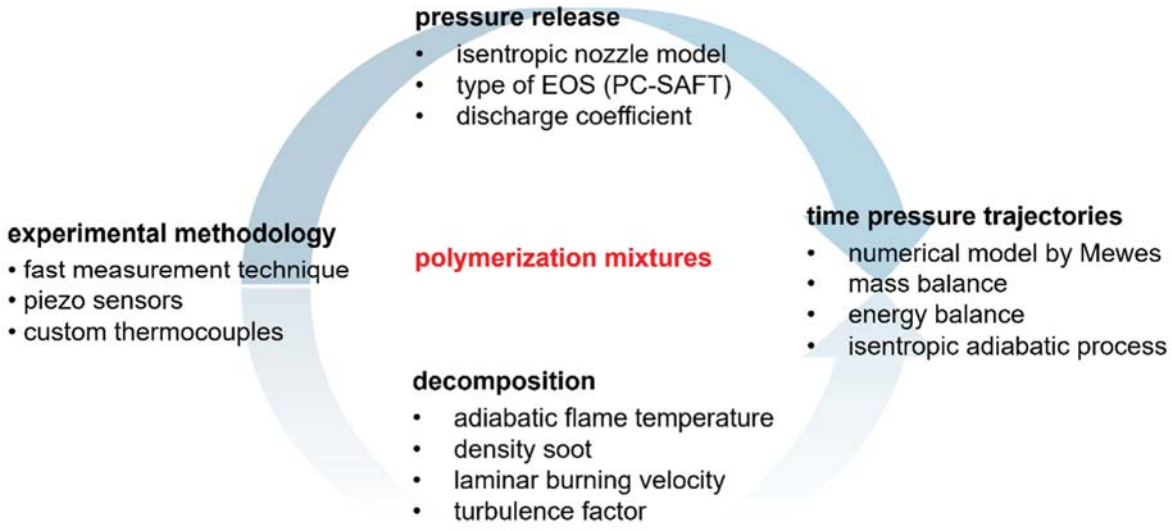


Fig. 1.: Representation of the methodic approach for the investigation of safety related events within the high-pressure polymerization process.

## Experimental

Ventilated decomposition reactions are carried out in a high-pressure vessel with a diameter of 50 mm and a length of 105 mm. The vessel is designed for 4000 bar at 300 °C. Experimental pressure and temperature profiles are recalculated via a numeric reactor model developed by ZINK[4]. The calculations consist of an isentropic nozzle model according to SCHMIDT[5] and a decomposition model adapted from MEWES[6]. Figure 2 shows the decomposition reactor and illustrates the calculation considering the mass and energy balance of the burned and unburned phase during a ventilated deflagration.

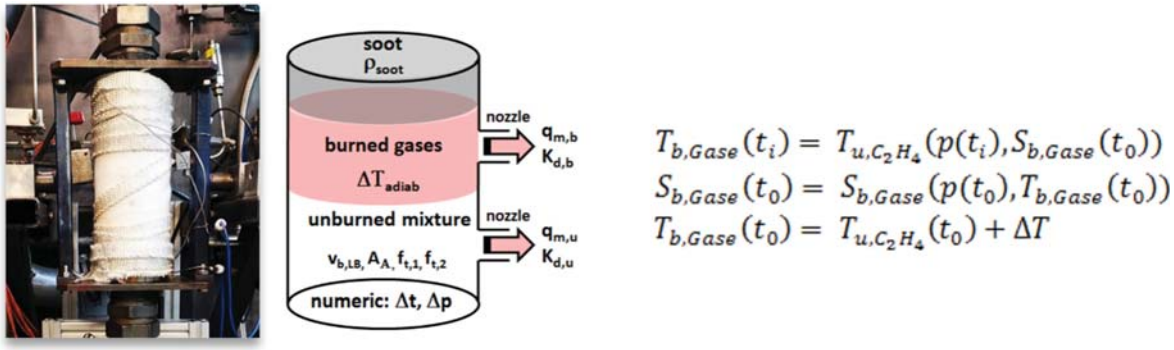


Fig. 2.: The 200 mL pressure vessel is shown on the left side. The schematic reactor geometry on the right depicts the numeric approach of the decomposition and pressure relief calculation with the soot, the burned and unburned phase as separate and transient balance rooms.

Here, this model is used as a simulative analytic tool to depict effects like an accelerated deflagration reaction by the expansion of the gas phase during ventilation. This effect can be described by a turbulence factor $f_t$.

A laminar flame front is created by igniting ethene with a tungsten wire at the top of the reactor vessel. A pneumatic relief valve with varying nozzle diameters is installed at the bottom of the reactor. In one experimental series, the initial pressure is increased whereby ventilation takes place with a constant nozzle diameter of 1 mm at 250 °C starting temperature. The pressure relief is triggered by a programmable logic controller. Further, the nozzle diameter is changed at a constant initial pressure of 2000 bar and a ventilation pressure of 2400 bar. The experimental pressure profiles are plotted as pressure change rate against the reactor pressure and are fitted via the turbulence factor. The resulting curves are shown in figure 3.

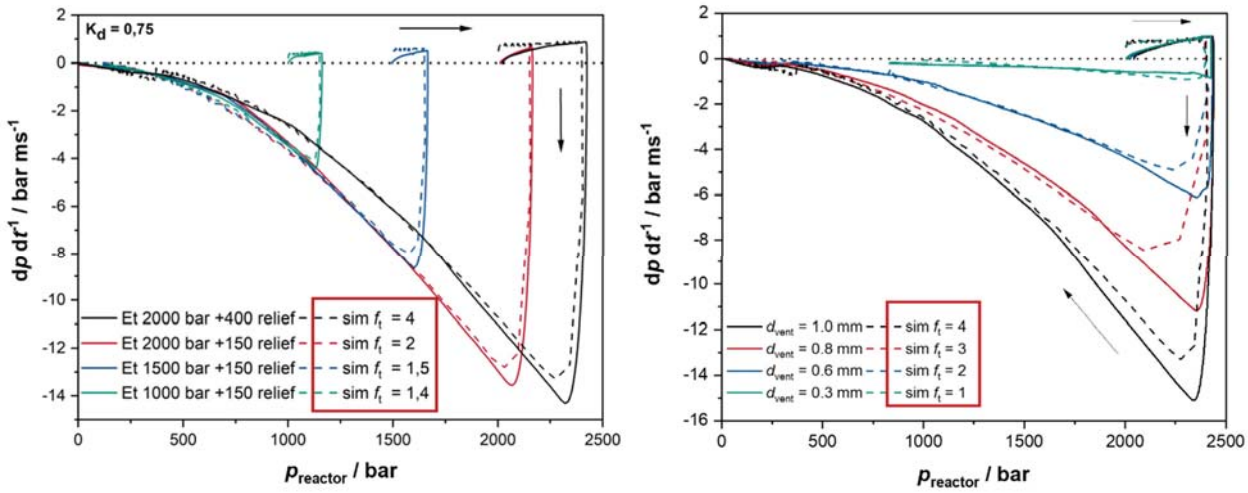


Fig. 3.: Experimental and recalculated pressure change rates. The turbulence factors highlighted in red boxes are dependent on the initial and vent pressure as well as the discharge nozzle diameter $d_{vent}$. The pressure is changed in the left and the nozzle in the right graph at a starting temperature of 250 °C.

In all cases, the pressure drops after the relief is triggered. The necessary turbulence factor after the relief varies with the initial and relief pressure as well as the nozzle diameter. When increasing the pressure, an acceleration of the decomposition reaction can be recalculated. The largest effect is seen, when the relief pressure is set from 2150 to 2400 bar, at an initial pressure of 2000 bar whereby $f_t$ is 4. Here, the more advanced flame front and the stronger expansion during the relief process leads to the induction of more violent turbulences. The acceleration of the burning process is correlated to the

expansion and flow velocity of the gas phase. The turbulence factor is successively reduced by smaller nozzle diameters. No turbulences are induced by pressure relief via the 0.3 mm nozzle.

## Summary

The presented work depicts the simulative and experimental method used to investigate pressure relief, decomposition, and ventilated deflagration reaction. Here, the effect of ventilation on an “ideal” laminar flame front is shown. Many safety related questions were and are ongoing to be addressed in further studies. Some of those are:

- impact of a polymer component on the relief process
- relief of pyrolysis gas from ethene decomposition
- transient pyrolysis gas composition at process conditions
- impact of the ignition position on ventilated deflagrations
- impact of pyrolysis soot on the relief process

The in-depth understanding of the decomposition and ventilation of polymerization mixtures can be used for a retrospective evaluation of safety events. Phenomenological findings may help to design safety equipment in the future.

## References

[1] G. Luft et al., *Chemical Engineering Technology 30*, **2007**, 695-70.
[2] D. Shannon, *Process Safety Progress 27*, **2008**, 35-40.
[3] Ö. Delibalta, *unpublished dissertatio*n, Technical University Darmstadt, **2022**.
[4] D. Zink, *dissertation*, Technical University Darmstadt, **2022**.
[5] J. Schmidt; W. Peschel, *Process and Plant Safety*, **2012**, 71-77.
[6] U. Grubber; D. Mewes, *Chem.-Ing.-Tech. 59*, **1987**, 12, 917-926.

# Optimization of $scCO_2$ Drying of Tuna Fillets

Elisa Mialich

Department of Industrial Engineering, University of Padova,

elisa.mialich@studenti.unipd.it

## Introduction

Food drying is an effective and well-known food preservation technique that ensures a prolonged shelf life of food by reducing the amount of moisture in the product. However, the drying techniques commonly used in the food industry, like sun drying, convective air drying and freeze drying, present some limitations. Among them there are the poor nutrient retention after the process, the alteration of organoleptic and sensorial properties of the fresh food, a limited inactivation power against microorganisms, together with high production costs and energy consumption (Bourdoux *et al.*, 2016). Moreover, due to the increasing demand from legislation and consumers for better quality and safer products, new drying methodologies have been developed. Among all the various alternatives to conventional processes, the use of supercritical carbon dioxide ($scCO_2$) has been recently recognized as an alternative low-temperature drying technique able to simultaneously dry and inactivate microorganisms in the food.

Since the critical temperature and pressure of $CO_2$ are 31°C and 73.8 bar respectively, mild conditions can be used in the process. These allow better retention of the nutritional and sensory properties of the fresh food, avoids thermal degradation and make the process more economic and green in comparison with conventional drying. Moreover, thanks to the high solvating power of supercritical fluids, water is removed without the presence of a vapour-liquid interphase, preserving the product's internal structure (Bourdoux *et al.*, 2016). Thanks to the bactericidal effect of $scCO_2$ the process also guarantees a good microbial inactivation. My research work explores the feasibility to apply supercritical carbon dioxide to dry and increase the microbial safety of fish fillets of Yellowfin tuna (*Thunnus albacares*), coming from the oriental Pacific Ocean. In particular, the present work consists on the optimization of the process parameters, such as $CO_2$ flowrate, temperature and drying time, in function of the $scCO_2$ drying efficiency and the safety and quality aspects of the final product.

Fish has been selected because of the high protein and low fats content that makes it essential in a mixed human diet, increasing its consumption in recent years.

## Experimental

A total of 20 experimental trials were carried out with a lab-scale batch reactor equipped with $CO_2$ recirculation. The plant is divided into two main parts. The feed part includes a $CO_2$ tank (Messer, carbon dioxide 4.0, purity 99.990%), a chiller reservoir (M418-BC MPM Instruments, Milan, Italy) with the refrigeration cycle and a high-pressure diaphragm pump (Lewa, type EK01, serial no. 425574/P200). In the second section, a centrifugal pump (Separex, serial no. 4448/P300) allows the recycling of $CO_2$ through a heater, the drying reactor (Separex S.A.S., Champigneulles, France) and finally the regeneration reactor filled with absorbent material (zeolites). For each experiment, 9 samples of 2 cm x 1 cm x 1 cm dimension and 2.0 ± 0.2 g were treated, after being thawed for 16 h at 4 °C from a storage temperature of -80°C.

The central composite rotatable design was used as experimental design first to design the experimental trials and then to investigate the impact of temperature (25-45°C), treatment time (2-6 h) and $CO_2$ flowrate (15-25 kg/h) on the drying performance and pH, colour, rehydration capacity and microbial count of the treated sample. The pressure was maintained unchanged at 100 bar since higher values do not enhance significantly $CO_2$ solubilization in the liquid phase (Ferrentino *et al.*, 2013).

After each experimental test, both the drying efficiency, the microbiological stability and the physical-chemical properties of the dried product were monitored. The drying efficiency was evaluated in terms of final moisture content, weight loss and moisture ratio by measuring the weight of each sample before and after the treatment with a precision balance (Radwag, PS 6000 R2). The microbial inactivation was determined for the naturally present microflora (total mesophilic bacteria). The quantification was performed through the standard plate count technique using a Plate Count Agar medium (PCA, Sacco, Italy) after serial dilution of the sample (1:10 dilution) in Ringer solution (Merck KGaA, Germany). As regards the physical-chemical properties, the water activity, colour loss and pH were evaluated. Water activity was measured using the instrument Hygropalm HP-23-A (Rotronic), made of a $a_w$ and temperature probe HC2-AW-(USB), a sample holder (WP-40S ) and a disposable sample cups (PS-14/PS-40). A digital pHmeter

(pH 1100 L of VWR) was used for the pH measurement while a colourimeter (3nh - NR100) allowed the calculation of the 3 colour coordinates of the CIEL*a*b* colour space. In addition, the rehydration capacity analysis was performed to quantify the capacity of a dried product to absorb moisture when it is immersed in a liquid medium. For this purpose, the dried sample was placed in a beaker with distilled water at 30°C in the incubator (Memmert, Vetrotecnica) for 24 h.

## Summary

The results of the preliminary test demonstrated the capability of the drying to reduce the moisture content from 74.1 % to 27.6 % with a treatment at 35°C,15 kg/h $CO_2$ flowrate for 6 h, reaching a final water activity of 0.69. Even higher dehydration was achieved with higher temperature and flow rate, decreasing moisture content and water activity down to 25.7 % and 0.679 respectively. Moreover, the treatment was able to completely inactivate the mesophilic bacteria under the detection limit ( < 10 CFU/g) for long time treatment (6 h or more), and the same bactericidal effect was reached for lower drying time at high-temperature. As expected, the inactivation rate increased with temperature and drying time (Bourdoux *et al.*, 2016), as previously demonstrated in the case of chicken breast (Morbiato *et al.*, 2019) where a higher inactivation capacity of total mesophilic bacteria was observed at the higher drying time. However, $scCO_2$ inactivation is highly matrix dependent. A recent study of Zambon *et al.*, 2022 on strawberry slices (100 bar and 40°C for 6 h) showed a limited inactivation power towards the total mesophilic bacteria, while up to 3 Log CFU/g reduction was reached on coriander treated at 40°C and 100 bar just after the pressurization and depressurization steps (Zambon *et al.*, 2018). The preliminary results achieved on tuna highlighted the capability of $scCO_2$ drying to obtain simultaneously a dried and microbiologically safe product also in the seafood matrix.

Considering the physical-chemical properties of the treated samples, pH was not affected by the process since a very small increase was observed for only some process conditions. The main defect of the dried tuna was related to the loss of colour varying with the process conditions, confirming the evidence of $scCO_2$ drying of red bell pepper (Zambon *et al.*, 2020). Limited rehydration capacity was achieved for the dried samples, up to a maximum value for the most dried one ( 441 min, 40°C and 20 kg/h).

In conclusion, the results achieved in the present work confirm the potentiality of $scCO_2$ drying technique as an alternative to the conventional processes to produce stable, safe and high quality dried products without the use of high temperatures.

Nevertheless, additional information on organoleptic properties and the nutritional quality of the treated product should be collected to make it attractive for large scale industrial applications.

## Acknowledgment

Elisa Mialich thanks Prof. Spilimbergo and Dr Alessandro Zambon for the opportunity to work with the Superunit research team, the COST Association for the GEHPT experience, Yago Alves de Aguiar Bernardo and Carlos Adam Conte Junior from the Federal University of Rio de Janeiro (UFRJ) and Mr Riccardo Zulli, Mr Pietro Andrigo and Mr Fabio Santi for the support in the experimental work.

## References

Bourdoux, S., Li, D., Rajkovic, A., Devlieghere, F., & Uyttendaele, M. (2016). Performance of Drying Technologies to Ensure Microbial Safety of Dried Fruits and Vegetables. *Comprehensive Reviews in Food Science and Food Safety*, *15*(6), 1056–1066. https://doi.org/10.1111/1541-4337.12224

Ferrentino, G., Balzan, S., & Spilimbergo, S. (2013). Optimization of supercritical carbon dioxide treatment for the inactivation of the natural microbial flora in cubed cooked ham. *International Journal of Food Microbiology*, *161*(3), 189–196. https://doi.org/10.1016/j.ijfoodmicro.2012.12.004

Garcia-Gonzalez, L., Geeraerd, A. H., Spilimbergo, S., Elst, K., van Ginneken, L., Debevere, J., van Impe, J. F., & Devlieghere, F. (2007). High pressure carbon dioxide inactivation of microorganisms in foods: The past, the present and the future. In *International Journal of Food Microbiology* (Vol. 117, Issue 1, pp. 1–28). https://doi.org/10.1016/j.ijfoodmicro.2007.02.018

Morbiato, G., Zambon, A., Toffoletto, M., Poloniato, G., Dall’Acqua, S., de Bernard, M., & Spilimbergo, S. (2019). Supercritical carbon dioxide combined with high power ultrasound as innovate drying process for chicken breast. *Journal of Supercritical Fluids*, *147*, 24–32. https://doi.org/10.1016/j.supflu.2019.02.004

Zambon, A., Michelino, F., Bourdoux, S., Devlieghere, F., Sut, S., Dall'Acqua, S., Rajkovic, A., & Spilimbergo, S. (2018). Microbial inactivation efficiency of supercritical $CO_2$ drying process. *Drying Technology*, *36*(16), 2016–2021. https://doi.org/10.1080/07373937.2018.1433683

Zambon, A., Tomic, N., Djekic, I., Hofland, G., Rajkovic, A., & Spilimbergo, S. (2020). Supercritical $CO_2$ Drying of Red Bell Pepper. *Food and Bioprocess Technology*, *13*(5), 753–763. https://doi.org/10.1007/s11947-020-02432-x

Zambon, A., Zulli, R., Boldrin, F., & Spilimbergo, S. (2022). Microbial inactivation and drying of strawberry slices by supercritical $CO_2$. *Journal of Supercritical Fluids*, *180*. https://doi.org/10.1016/j.supflu.2021.105430

# Group Contribution Method for Transfer Activity in the LDPE Process

Alexander Klimeck, Markus Busch

Ernst-Berl-Institut, TU Darmstadt, markus.busch@pre.tu-darmstadt.de

## Introduction

The high-pressure LDPE process is characterized not only by its harsh conditions in which ethene is polymerized at pressures up to 3000 bar and temperatures up to 300 °C in a free-radical polymerization to LDPE. Another important aspect of the process derives from the free-radical polymerization process character. Thus, behind the process of LDPE synthesis is a complex reaction network with numerous different reaction steps, which can be roughly divided into the categories of initiation, growth, transfer reactions and termination. The subgroup of transfer reactions can be roughly subdivided again into transfer reactions to the polymer and transfer reactions to low molecular weight species. In addition to the monomer ethene, low-molecular-weight species also include other substances that were added to the process either as solvents or as chain transfer agents (CTAs). In the case of solvents, this addition of substances can be done for more process-related reasons, for example to dilute initiator. CTAs are used from a product-specific point of view, influencing the molecular weight distribution of the product and thus also to control the product properties.

Therefore, a better and comprehensive understanding of the kinetics of transfer to CTAs is essential to make processes as efficient as possible and to better assess the impact of choosing a CTA and the quantity of it. Numerous transfer constants determined on a laboratory scale can already be found in the literature.[1] The existing data are mainly limited to literature values at conditions differing from the process (130 °C, 1360 atm).[1] Furthermore, the methods for determining the parameters have also been adapted over time to make the determination of an isolated kinetic step in this complex network as accurate as possible.[2] In the work of Wilhelm[2] a homologues series of alkanes was investigated and a linear relationship between the transfer constant and the sequence in the homologous series was established (Figure 1).

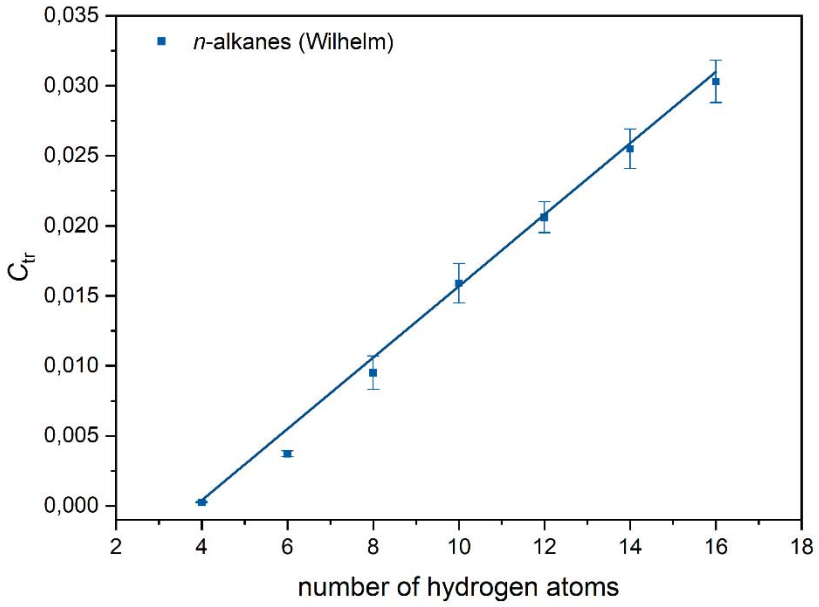


Fig. 1.: Plot of the transfer constant of a homologous series of *n*-alkanes. [2]

This allowed to formulate a transfer constant for a single increment in this homologous series and to predict further components in this series.

## Experimental

This influence is investigated experimentally on a continuously operating mini-plant. In addition to the harsh conditions of pressures at 2000 bar and temperatures at 180 °C, which are applied to the process conditions of the LDPE process, the entire reaction network must be taken into account when considering one reaction step in isolation. The method for the experimental determination of the transfer constants in this system is based on Wilhelm [2]. Here, the large and complex reaction network of free-radical polymerization is simplified via assumptions and the experimental design. Thus, the experimental determination of the transfer constants is based on an avoidance of interfering side reactions and on the formation of long polymer chains. This can be approximated experimentally by a low conversion and no addition of initiator, solvents, or other substances. In order to meet the requirements of the evaluation methods, the Mayo [3] and CLD [4] method, stationary process conditions are also required, which are made possible by the continuous mode of polymerization. Using this experimental

method, different organic substances are investigated for their transfer activity in a homologous series in a 100 ml high-pressure autoclave at a constant ethene flow rate of 2000 g $h^{-1}$.

## Summary

This work deals with the influence of functional groups in a homologous series regarding the transfer constant. Different functional groups were investigated in homologous series to examine whether a similar relationship to the findings of Wilhelm can be formulated and to which extent the influence of the functional group can be described. The aim of these investigations would be to attribute the transfer activity of a molecule to the transfer activities of the individual molecular increments and thus make predictions about the transfer behavior of a substance.

## Acknowledgment

We acknowledge the generous support of SK Innovation.

## References

[1] G. A. Mortimer, *Journal of Polymer Science Part A-1: Polymer Chemistry* **1966**, *4*, 881-900.

[2] S. Wilhelm, *PhD Thesis*, Darmstadt **2021**.

[3] F. R. Mayo, *Journal of the American Chemical Society* **1943**, *65*, 2324-2329

[4] P. A. Clay, R. G. Gilbert, *Macromolecules* **1995**, *28*, 552-569

# Presentation of P,V,T,x Phase Equilibria on Mole Volume – Composition Diagram in the Example of the $CO_2$ – $C_2H_5OH$ System

Altin Mele[1, 2], Jeta Lica[1], Lorenci Gjurgjaj[1], Dorina Mele[3], Ardita Mele[1]

1. Center of Techniques Studies, Ivodent Academy, Tirana, Albania
2. Department of Chemistry, University of Tirana, Tirana, Albania
3. Department of Prosthetics, Ivodent Academy, Tirana, Albania

altin.mele@ivodent.edu.al

## Introduction

The phase boundaries of mixtures are usually given in P-x (isotherms), T-x (isobars) or P-T (isopleths) representations. The densities or the molar volumes of the phases are very rarely measured and even if they are, the volume-concentration diagram is not the selected type of representation. The coexisting phases of a system usually differ in terms of molar volume and composition, but not in terms of pressure and temperature. Therefore the $V_m$-x diagram, although very rarely used, is an informative representation.

The phase behaviour of carbon dioxide + ethanol system has been investigated mainly in terms of the variables pressure, temperature and composition. Earlier publications related to VLE data of this system have been reviewed by Suzuki et. al. [1] and Dohrn and Brunner [2]. Data are also reported in recent articles ([3], [4], [5], [6], [7], [8], [9], [10], [11], [12], [13], [14]). These studies are all limited to temperatures below 373,15 K. With few exceptions ([3], [4], [5], [7], [8], [12], [13]) the densities of the coexisting phases are neglected and even when measured, they range in temperatures between 291,15 K to 313,15 K. For a complete description of the phase equilibrium in this system further measurements should be made, up to temperatures in the neighbourhood of the critical temperature of ethanol.

## Experimental

The high pressure apparatus used in this work for measuring the densities of the coexisting phases at equilibrium for a settled pressure and temperature, is described in detail in an earlier publication [15].

Temperature and pressure were measured with an accuracy of 0,15 K and 0,01 MPa respectively. The repeated measurements under the same conditions showed a

reproducibility of > 0,0015 in the mole fraction and > 0,003 × ρ in the density determination. This is in good agreement with error analysis, taking into consideration the inaccuracies of all measuring instruments [16].

Carbon dioxide used was of mole-fraction purity 99,996 % from Messer-Griesheim and Ethanol > 99,5 % from Merck-Schuchardt. A gas-chromatography analysis of ethanol resulted to a concentration of > 99,8 %.

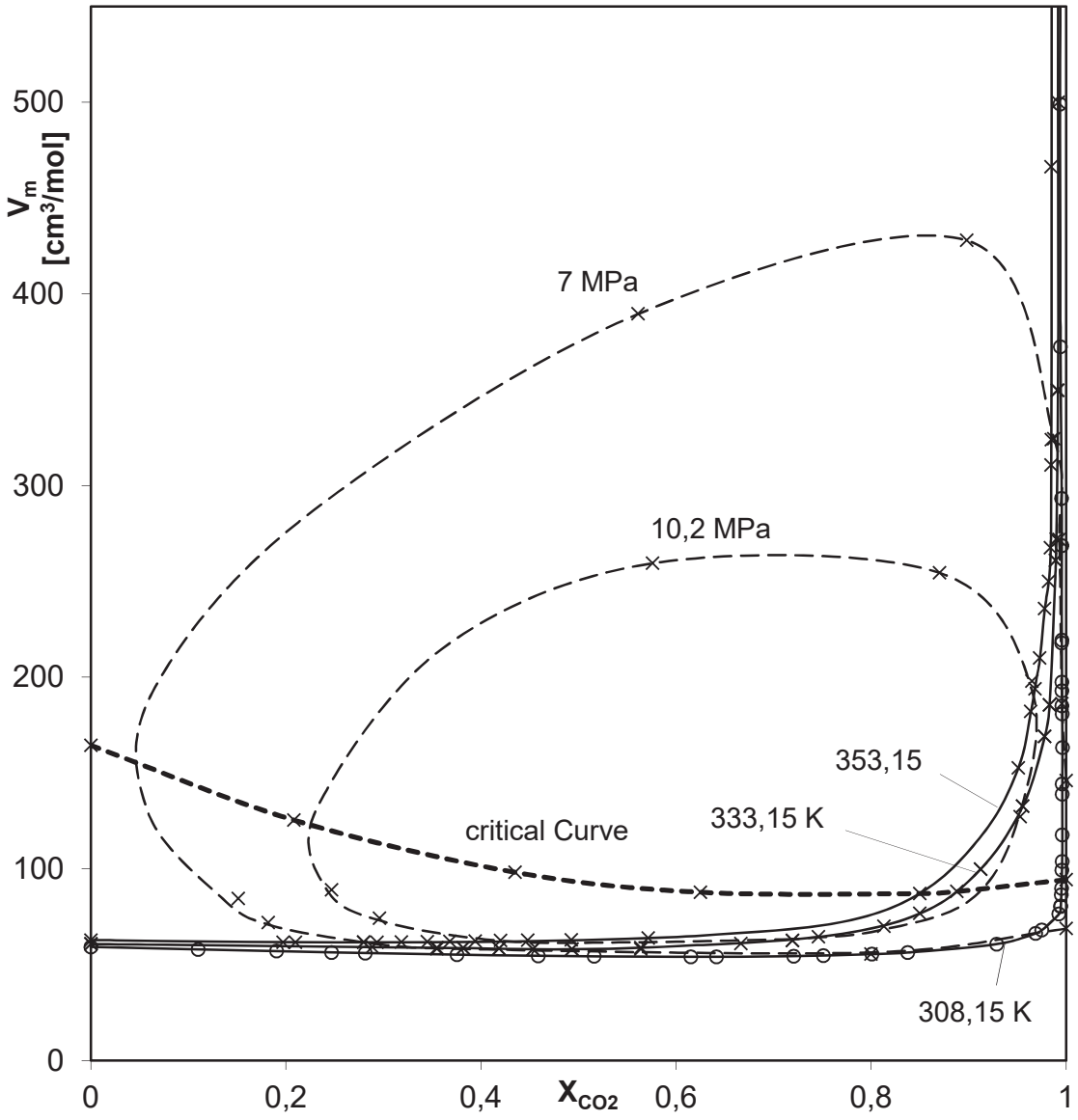


**Fig 1**: V-x Diagram in the $CO_2$ - $C_2H_5OH$ System with Isobars ( ----- ), Isotherms ( —— ), critical curve ( ▪▪▪▪ ), this work measured points (x) and points from Kato [44] (o).

The isothermal phase boundary (also with regard to the molar volumes) is determined at 308.15 K from the measurement data from Kato [3].

To complete and set up a $V_m$-x diagram for the $CO_2$-$C_2H_5OH$ system, the coexisting phase densities and compositions are measured, and the respective molar volumes are calculated, at 333.15 K and 353.15 K, for pressures between 5 MPa and 12 MPa. Results are shown in the table 1 and figure 1.

**Tab. 1**: Molar volumes and composition of the coexisting phases in the liquid-gas equilibrium of the $CO_2$ - $C_2H_5OH$ system at 333.15 K and 353.15 K and pressures between 5 MPa and 12 MPa

| P [MPa] | $x_{CO_2}$ | $V_m$ liq. [cm$^3$/mol] | $y_{CO_2}$ | $V_m$ gas [cm$^3$/mol] |
|---|---|---|---|---|
| T = 333,15 K | | | | |
| 7,5 | 0,3817 | 58,80 | 0,9910 | 349,66 |
| 8,0 | 0,4183 | 58,50 | 0,9890 | 272,00 |
| 8,5 | 0,4533 | 58,19 | 0,9920 | 260,90 |
| 9,0 | 0,4931 | 58,20 | 0,9830 | 185,53 |
| 9,5 | 0,5667 | 58,20 | 0,9780 | 169,12 |
| 10,0 | 0,6664 | 61,10 | 0,9555 | 132,79 |
| 10,5 | 0,8131 | 70,00 | 0,9122 | 99,94 |
| T = 353,15 K | | | | |
| 5,0 | 0,1969 | 61,69 | 0,9848 | 559,67 |
| 5,5 | 0,2097 | 61,74 | 0,9825 | 466,28 |
| 7,0 | 0,2798 | 61,70 | 0,9850 | 323,99 |
| 7,5 | 0,2933 | 61,65 | 0,9846 | 310,73 |
| 8,0 | 0,3184 | 61,89 | 0,9840 | 267,58 |
| 8,5 | 0,3450 | 62,00 | 0,9820 | 250,05 |
| 9,0 | 0,3682 | 62,17 | 0,9780 | 235,79 |
| 9,5 | 0,3942 | 62,41 | 0,9730 | 210,00 |
| 10,5 | 0,4480 | 62,80 | 0,9720 | 198,00 |
| 11,0 | 0,4926 | 62,90 | 0,9637 | 182,16 |
| 12,0 | 0,5714 | 63,96 | 0,9510 | 152,79 |

The P-T-x on the critical curve of the $CO_2$-$C_2H_5OH$ system, are known from the literature ([17], [18], [19], [20], [21]), showing a continuous line connecting the critical points of $CO_2$ and $C_2H_5OH$. The critical pressure at 308,15 K is comparable to the critical pressure of $CO_2$. It increases in the beginning with the temperature, exhibits a maximum (P = 15,4 MPa; $x_{CO_2}$ = 0,66; T = 403 K) and falls again with increasing temperature to the critical pressure of pure ethanol ([20], [21]).

Using the data of [3] and our own measurements the critical densities of the studied isotherms has been determined by a method from Mathis, graphically, in the ρ-P diagram. The critical molar volumes for the isotherms examined here are presented in the figure 1. The critical densities curve will pass through a minimum at $x_{CO_2}$ = 0,88; P = 12,2 MPa and T = 340 K, as could be graphically estimated.

At 10,2 MPa the system exhibits an upper critical temperature (482 K; $x_{CO_2}$ = 0,3) and a lower one (338 K; $x_{CO_2}$ = 0,91) as shown in the figure 1. Such an isotherm shows a closed loop with a minimum in gas phase density and a maximum in the liquid phase density, without touching either of pure component axes.

## Summary

Densities and mutual solubility of carbon dioxide and ethanol were determined at the temperatures 333,15 K, and 353,15 K, and pressures from 5 MPa to 12 MPa. The phase behaviour is presented in molar volume – composition diagram.

## References

[1]. Suzuki T, Tsuse N, Nagahama K. (1991).
*Fluid Phase Equilibria* 67, 213-226.

[2]. Dohrn R, Brunner G. (1995).
*Fluid Phase Equilibria,* 106, 213-282.

[3]. Kato T. (1995). *J. Chem. Eng. Japan,* 28(3), 263-266.

[4]. Kordikowski A, Schenk AP, van Nielen RM, Peters CJ. (1995).
*The Journal of Supercritical Fluids,* 8, 205-216.

[5]. Chang C, Ching Y. (1997). *Fluid Phase Equilibria,* 131, 243-258.

[6]. Pfohl O, Pgel A, Brunner G. (1999). *Fluid Phase Equilibria,* 157, 205-216.

[7]. Stievano M, Elvassore N. (2005). *The Journal of Supercritical Fluids*, 33 (1), 7-14.

[8]. I. Tsivintzelis, D. Missopolinou, K. Kalogiannis, C. Panayiotou. (2004).

*Fluid Phase Equilibria*, 224, pp. 89-96.

[9]. Durling NE, Catchpole OJ, Tallon SJ, Grey JB. (2007).

*Fluid Phase Equilibria*, 252 (1–2), 103-113.

[10]. Knez Ž, Škerget M, Ilič L, Lütge C. (2008).

*The Journal of Supercritical Fluids*, 43 (3), 383-389.

[11]. M. Kato, D. Kodama, T. Ono, M. Kokubo.

*J. Chem. Eng. Data*, 54 (2009), pp. 2953-2956.

[12]. B. Seifried, F. Temelli. *J. Chem. Eng. Data*, 55 (2010), pp. 2410-2415

[13]. M. Kariznovi, H. Nourozieh, J. Abedi, (2013).

*J. Chem. Thermodyn.,* 57, pp. 408-415

[14]. L.P. Cunico, C. Turner, (2017).

*J. Chem. Eng. Data*, 62, pp. 3525-3533.

[15]. Lentz H, Zeuner V. (1995).

*J. Chem. Thermodynamics,* 27, 997-1015.

[16]. Nünnerich P. (1999). Aachen: Shaker Verlag.

[17]. B. Guan, Z. Liu, B. Han, H. Yan. (1999).

*Journal of Supercritical Fluids*, 14, 213–218.

[18]. A.G. Badalyan, G.T. Wilkinson, B.S. Chun. (1998).

*Journal of Supercritical Fluids*, 13, 319–324.

[19]. L. Montanari, P. Fantozzi, J.M. Snyder, J.W. King. (1999).

*Journal of Supercritical Fluids*, 14, 87–93.

[20]. Ziegler JV, Chester TL, Innis D. (1996). *ACS Symposium Series* 608, 93-110.

[21]. Pöhler H, Kiran E. 1997. *J. Chem. Eng. Data* 42, 384-388.

# Solvent Absorption Study of Cross-Linked Polymers

Julija Strunčnik

Institute of Chemical Engineering and Environmental Technology, Graz University of Technology, julija.struncnik@student.tugraz.at

## Introduction

Cross-linking relates to the formation of intermolecular interactions through chemical bonds, which among others affects chains mobility. [1] With the number of cross-links the rigidity of polymer increases and it cannot stretch as much. [2] Due to the solvent uptake chains are stretched and as a consequence, forces that inhibit further solvent uptake are activated. Highly cross-linked polymers offer many applications such as electronics encapsulation and protective coating, where high stability and minimum moisture uptake are desirable. [3]

The glass transition temperature is among the most important factors to consider when processing polymers. Together with the melting temperature it determines process parameters and the physical, mechanical and chemical properties of the end-product are related to these temperatures. [4] Adding cross-links increase glass transition temperature [2], which is described as a temperature at which the molecular structure exhibits macromolecular mobility. It comes to the transition from rigid state to more flexible state. At this temperature the free volume, which represents the gap between the molecular chains, is increased. [5]

## Experimental

Within our study we are focusing on highly cross-linked polymer solvent absorption at different temperatures, using solvents with different polarities.

Experimental procedure starts with samples preparation and drying. Before starting solvent absorption experiment, samples should be as dry as possible, otherwise the results are not accurate since the moisture is still inside the polymer. Therefore, we have to measure the weight during the drying process – constant weight indicates dry sample. When samples are completely dry, we put them into the bottles, filled with a solvent. Bottles are then placed into thermostatic vessels, which should provide constant

temperature over a long time. However, long-time solvent absorption experiments require reliable and accurate equipment. The quality of a scale also plays an important role due to daily measurements of polymer samples weight change. Furthermore, there are also some polymers that have to be measured hourly due to the large solvent uptake and consequently quickly achieved equilibrium state. Use of anti-static equipment during weighing is recommended, because we have observed a significant effect of static charges on measured weight.

Besides polymer solvent absorption experiments, we are using differential scanning calorimetry to determine glass transition temperature. Differential scanning calorimetry apparatus determines the temperature and heat flow associated with material transitions as a function of time and temperature. [6]

## Summary

Solvent absorption study of highly cross-linked polymers consists of absorption experiments at different temperatures in solvents with different polarities. These experiments will be supplemented by DSC method, where glass transition temperature will be investigated.

The results are intended to be used to adjust and validate a rigorous thermodynamic model for solvent absorption in polymers based on the PC-SAFT equation of state.

## References

[1] R.O.Ebewele, “Polymer science and technology,” New York, 2000. ISBN 0-8493-8939-9.

[2] J. Maitra and V. Kumar Shukla,“ Cross-linking in Hydrogels - A Review,” American Journal of Polymer Science 2014, doi:10.5923/j.ajps.20140402.01

[3] P. Krenn, P. Zimmermann, M. Fischlschweiger and T. Zeiner, “Modeling Highly Cross-Linked Epoxy Resins in Solvents of Different Polarities with PCSAFT”, Ind. Eng. Chem. Res. 59 (2020) 5133–5141 https://doi.org/10.1021/acs.iecr.9b06499.

[4] Riza, S. H., Masood, S. H., Rashid, R. A. R., & Chandra, S. (2020). Selective laser sintering in biomedical manufacturing. Metallic Biomaterials Processing and Medical Device Manufacturing, 193–233. doi:10.1016/b978-0-08-102965-7.00006-0

[5] Shrivastava, A. (2018). Introduction to Plastics Engineering. Introduction to Plastics Engineering, 1–16. doi:10.1016/b978-0-323-39500-7.00001-0

[6] Gill P, Moghadam TT, Ranjbar B. Differential scanning calorimetry techniques: applications in biology and nanoscience. J Biomol Tech. 2010 Dec;21(4):167-93. PMID: 21119929; PMCID: PMC2977967.

# A Mini-Plant as a Tool for Understanding the Solution Polymerisation Process

Isabel M. Kronshorst, Laura Ständecke, Julia Eigenseer, Markus Busch*

TU Darmstadt, Darmstadt/Germany

*e-mail: *markus.busch@pre.tu-darmstadt.de*

## Introduction

Our modern world is highly reliant on plastics that can be used in various applications such as packing, construction, or high-performance materials like *Teflon*®. Given today’s environmental challenges, intelligent material design is a key to sustainability. Here, both preparation of polymers with targeted material properties and their life cycle can serve as a lever. By understanding the underlying effects, the production process can be optimized to reduce the environmental impact. Through this, polymers with tailor-made properties can be prepared with the lowest possible energy and material input. This concept is described by the polymer reaction engineering approach. The basic process is shown in Figure1.

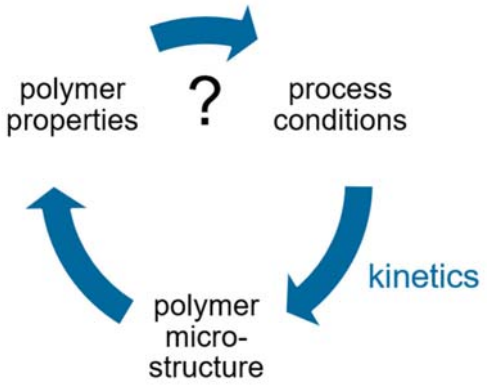


Fig. 1.: General approach of polymer reaction engineering.

Combined with the process conditions, the kinetics of polymerisation determine the resulting microstructure of the obtained polymers which then defines the polymer properties. To obtain targeted properties by reverse engineering, the underlying principles must be identified and understood.

The process of interest is a catalytic solution polymerisation of ethylene either in a homo-polymerisation or in a co-polymerisation with α-olefins. A mini-plant is a promising tool for this. A semi-batch operation mode is suitable for estimating the polymerisation kinetics, as it makes time-dependent parameters accessible in the form of monomer uptake profiles. For the determination of microstructural aspects such as reactivity profile or molecular weight control, it is necessary to avoid gradients in the reactor composition. This can be achieved by using the continuous operation mode. Both approaches can be pursued using the same mini-plant.

## Experimental

As part of this work, the mini-plant is expanded with a semi-batch operation mode added to the existing continuous operation mode. For the conceptual design of the plant, the requirements for the data acquisition are key. Here, especially the injection of catalytically active substances with high precision and good reproducibility is of major concern. For this, a system of sample loop valves is chosen that can be operated via the plant control. The setup of the semi-batch approach of the mini-plant is depicted in Figure 2.

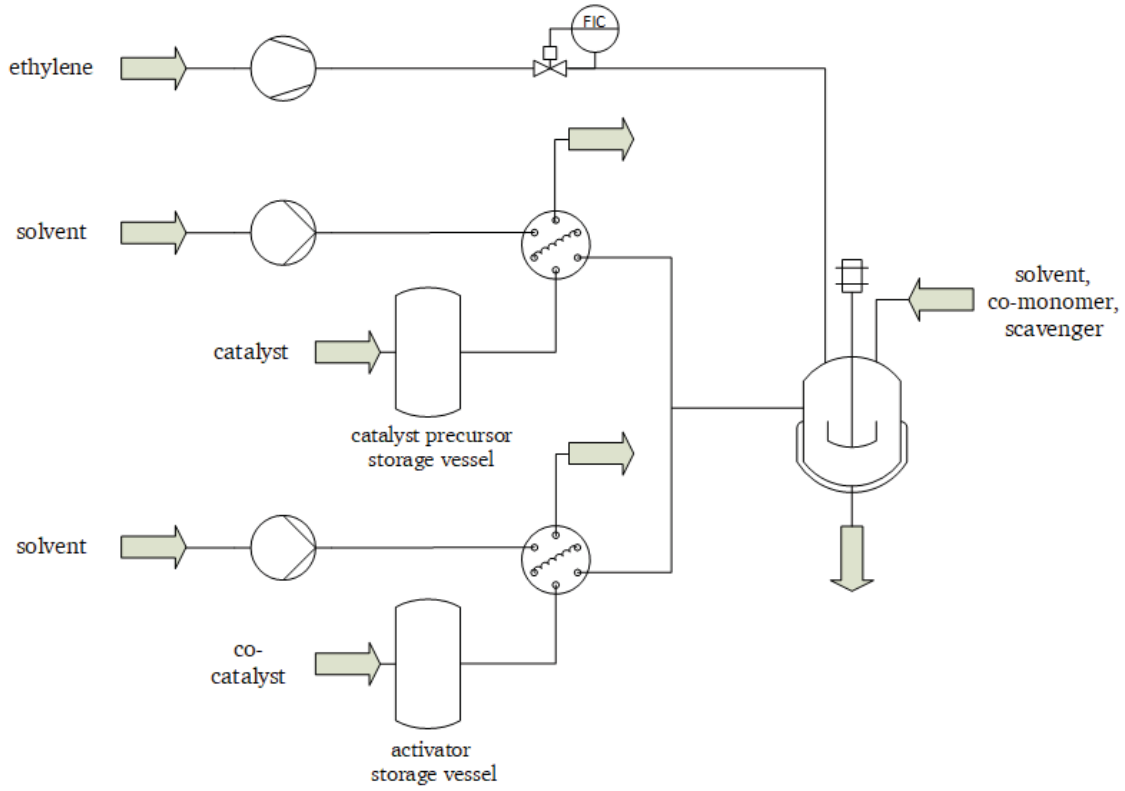


Figure 2: Simplified flowsheet of the set up semi-batch polymerization mini-plant.

The setup has been assembled, optimised, and benchmarked against literature.[1] It was possible to show that the designed plant operates with high precision and is suitable for the determination of kinetic parameters similar to those in literature.

Furthermore, the investigation of microstructural parameters is part of this work. Obtaining polymers with target polymer properties is especially complicated for co-polymers. Here, it is known that different microstructural properties interfere with each other. These aspects include short-chain branching length (determined by the used co-monomer), the short-chain branching density (reactivity ratios of the co-polymerisation) and molecular weight. Furthermore, the conversion and temperature in the reactor play a major role. Therefore, the system’s complexity is reduced to one co-monomer and temperature and the reactivity ratios for this system are determined. By this, the polymer properties given these conditions can be controlled using the obtained reactivity ratios.

## Summary

To summarize, the mini-plant as presented in this work is a valuable tool for the determination of kinetic and microstructural parameters. By this, the polymerisation process can be controlled better and more efficiently also on larger scales. The determined parameters are expected to be catalyst-specific quantities and thus, independent of the plant.

## Acknowledgment

We acknowledge the generous support of Borealis AG.

## References

[1] S. Mehdiabadi, J. B. P. Soares, D. Bilbao (2013), Macromolecules, 46, 1312–1324.

# Development and Optimization of an Electrochemical-Impedimetric Biosensor Based on Whole Cells for the Detection of Active Compounds

Zala Štukovnik, Urban Bren

Faculty of Chemistry and Chemical Engineering, University of Maribor,
zala.stukovnik1@um.si

## Introduction

The demand for biosensors based on living cells has increased significantly due to the need for specific sensors that enable rapid and reliable measurements in various research areas, including monitoring of isolation of active compounds, the determination of active compounds, and the effect of active compounds on whole cells. The development of biosensors is also of interest for different applications ranging from biochemical profiling of normal and pathologic cells, over clinical diagnostics and drug discovery to more straightforward analyses such as fermentation process monitoring, environmental testing, and food and beverages quality control [1-3].

Biosensors are small and inexpensive analytical devices that convert a biological response into an electrical signal and provide us with information about the concentration of the target analyte [4, 5]. The quality of this information depends on the type of the analyte components, the type of active biological component, the design of the biosensor, and the physical properties of the transducer [6]. Biosensors can be classified according to the method of physical-chemical conversion or according to the type of biorecognition element. Based on the transducer, biosensors can be classified into electrochemical, optical, and mechanical biosensors [7]. Active biological components can generally be enzymes, antibodies, whole cells, organelles, or tissues [8].

Living cells have been used as biorecognition elements in biosensors since the early 1970s. They are an interesting choice of biorecognition element since they are cheaper than purified enzymes and antibodies, allow flexibility in determining the sensing strategy, and are relatively easy and inexpensive to manufacture [9-11]. However, despite these advantages, there are challenges such as cell adhesion to the surface, regeneration of cells on the surface, and storage life [12].

In recent years, many biosensors have been developed that utilize whole cells for active compound detection, environmental monitoring, detection of pathological biomarkers, and cell culture monitoring. Our research focuses on developing and optimizing biosensors based on the whole cells to detect various toxins and active compounds.

## Experimental

We developed an electrochemical cell that serves as a model biosensor. In the assembling of the electrochemical cell, stainless steel type SS316 (manufacturer TBJ Industries, Germany) was used. *Saccharomyces cerevisiae* cells were applied to the working electrode (WE) as a biological component. Model electrochemical devices that used different WE and utilized different dimensions were assembled and tested with electrochemical impedance spectroscopy (EIS), where the response of the yeast to a 10%v/v $CH_3OH$ solution when changing various parameters was monitored. The electrodes were manufactured in two different dimensions: the dimension of electrode 20 mm × 2 mm, where the active component was applied to 5 mm × 2 mm, and the dimension of electrode 20 mm × 5 mm, where the active component was applied to 5 mm x 5 mm. The position of the electrodes was RCW-side-by-side (Fig.1.): the reference electrode (RE), the counter electrode (CE), and the working electrode (WE).

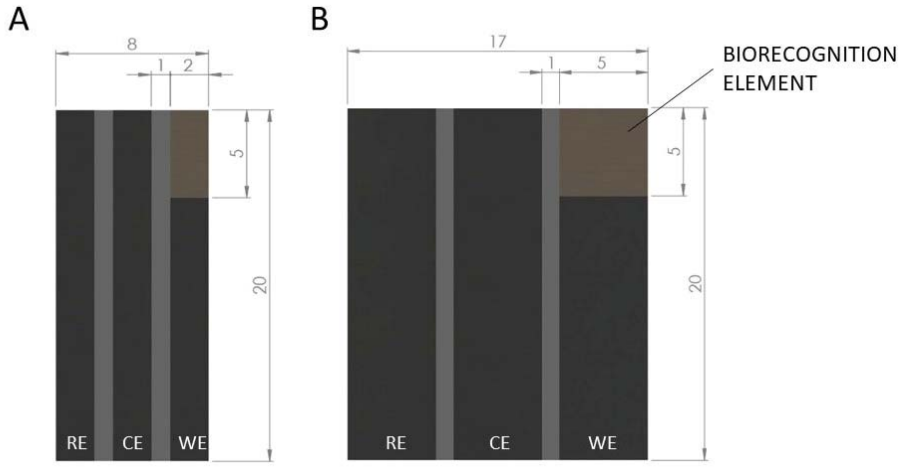


Fig. 1.: Representation of a small (Fig.1.A) and of a large electrochemical cell (Fig.1.B)

The developed model electrochemical cells served as a case study for the development of more complex biosensors that utilize living cells as the active layer.

Furthermore, based on the developed large model electrochemical cell, an electrochemical-impedimetric biosensor using *Saccharomyces cerevisiae* was designed

to detect caffeine. The electrochemical stability of the sensing electrode was evaluated by measuring the open circuit potential (OCP), and electrochemical impedance spectroscopy (EIS) was applied to determine the impedimetric response of the biosensor with *Saccharomyces cerevisiae* cells attached to WE in the absence (0.9% NaCl) and presence (10 mg·mL$^{-1}$ in 0.9% NaCl) of caffeine. Nyquist diagrams were interpreted as the results.

Fig.2. represents the Nyquist diagram, where the change in the impedance of the system is observed. When caffeine was added to the system, the *Saccharomyces cerevisiae* cells detached from the stainless steel surface, and consequently, the electrode surface was released. Therefore, the resistance of the system dropped, and the capacitance and the impedance of diffusion increased.

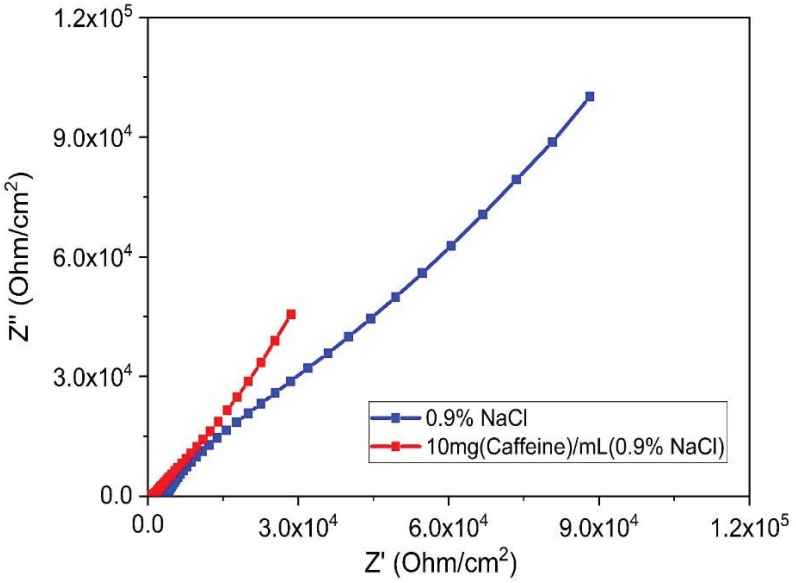


Fig. 2.: Nyquist diagram

Moreover, the system's linearity was obtained in the concentration range from 0.1 mg·mL$^{-1}$ to 5 mg·mL$^{-1}$ with $R^2$ of 0.997 (Fig.3.A). Based on the 3-Sigma criteria, the LOD was determined at 0.728 mg·mL$^{-1}$, and based on the 10-sigma criteria, the LOQ was determined at a concentration of 0.382 mg·mL$^{-1}$.

The impedance decrease with increasing concentrations is represented as a box plot (Fig.3.B). The data were obtained at a frequency of 125 mHz. The box plot shows the mean values as a dot, the upper whiskers represent the maximum, the lower whiskers

represent the minimum, and the box represents the interquartile range. The distinct decrease in the impedance is observed at 0.1 mg/mL concentration.

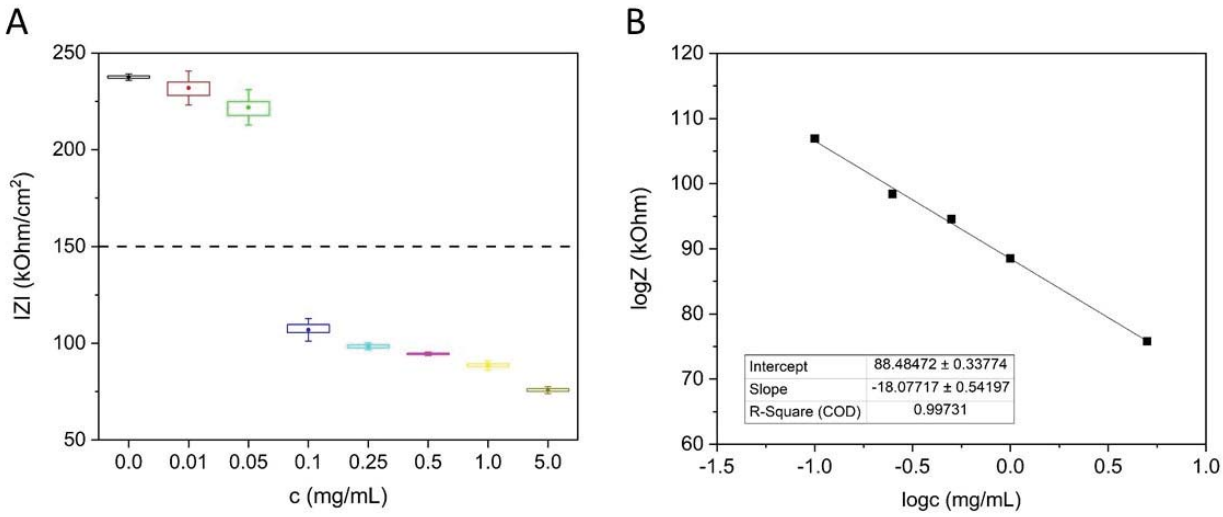


Fig. 3.: Box plot representing the impedance (log|Z|) decrease with the increasing concentrations (c) of caffeine (Fig.3.A) and the calibration curve between the impedance (log|Z|) and the caffeine concentrations (log c) (Fig.3.B).

It was observed that the impedance decreased with the increasing concentration of the caffeine in the solution. Thus, it was concluded that the biosensor could sense the presence of caffeine in the solution.

**Summary**

Our research focused on developing and optimizing whole cell-based biosensors using *Saccharomyces cerevisiae*. The developed biosensor represents a good candidate for detecting caffeine in beverages, foods, and drugs with the merits of time-saving, robustness, low cost, and low detection limit. It can be concluded that yeasts, although very resistant to adverse environmental conditions, can sense and respond to caffeine as stimuli and could also be utilized to detect various active compounds.

Our study established a new approach to biosensor development that involves assembling a low-cost and disposable electrochemical system to detect active compounds such as caffeine. Based on the presented approach, biosensors that use simplified potentiostat/galvanostat could be applied on a large scale to monitor or determine active compounds.

## Acknowledgment

Financial support from the Slovenian Research Agency through a project (J1-2471) and programme (P2-0046) grants is gratefully acknowledged. Additionally, I would like to thank Prof. Dr. U. Bren and Prof. Dr. R. Fuchs Godec for their supervision.

## References

[1] V.R.S. Babu, S. Patra, N.G. Karanth, M.A. Kumar, M.S. Thakur, Development of a biosensor for caffeine, Analytica Chimica Acta 582(2) (2007) 329-334.

[2] H. Kaur, A. Bhosale, S. Shrivastav, Biosensors: classification, fundamental characterization and new trends: a review, Int J Health Sci Res 8(6) (2018) 315-333.

[3] P. Mehrotra, Biosensors and their applications – A review, Journal of Oral Biology and Craniofacial Research 6(2) (2016) 153-159.

[4] I.E. Tothill, A.P.F. Turner, BIOSENSORS, in: B. Caballero (Ed.), Encyclopedia of Food Sciences and Nutrition (Second Edition), Academic Press, Oxford, 2003, pp. 489-499.

[5] B. Caballero, L.C. Trugo, P.M. Finglas, Encyclopedia of food sciences and nutrition, Academic2003.

[6] N. Bhalla, P. Jolly, N. Formisano, P. Estrela, Introduction to biosensors, Essays Biochem 60(1) (2016) 1-8.

[7] S. Malhotra, A. Verma, N.K. Tyagi, V. Kumar, Biosensors: Principle, types and applications, International Journal of Advance Research and Innovative Ideas in Education 3 (2017) 3639-3644.

[8] F. Karim, A.N.M. Fakhruddin, Recent advances in the development of biosensor for phenol: a review, Reviews in Environmental Science and Bio/Technology 11(3) (2012) 261-274.

[9] F. Amaro, A.P. Turkewitz, A. MartĂ-n-GonzĂĄlez, J.C. GutiĂŠrrez, Functional GFP-metallothionein fusion protein from Tetrahymena therm ophila: a potential whole-cell biosensor for monitoring heavy metal pollution and a cell model to study metallothionein overproduction effects, BioMetals 27(1) (2014) 195-205.

[10] A. Courbet, D. Endy, E. Renard, F. Molina, J. Bonnet, Detection of pathological biomarkers in human clinical samples via amplifying genetic switches and logic gates, Science translational medicine 7(289) (2015) 289ra83-289ra83.

[11] L. Goers, C. Ainsworth, C.H. Goey, C. Kontoravdi, P.S. Freemont, K.M. Polizzi, Whole-cell Escherichia coli lactate biosensor for monitoring mammalian cell cultures during biopharmaceutical production, Biotechnology and Bioengineering 114(6) (2017) 1290-1300.

[12] N. Gupta, V. Renugopalakrishnan, D. Liepmann, R. Paulmurugan, B.D. Malhotra, Cell-based biosensors: Recent trends, challenges and future perspectives, Biosensors and Bioelectronics 141 (2019) 111435.

# $CO_2$ and Biomass as Feedstock for the Production of Chemical Intermediates

Ka Loi Lin,[#] Thomas Ernst Müller*

Carbon Sources and Conversion, Faculty of Mechanical Engineering,

Ruhr-University Bochum, [#] lin@ls-csc.rub.de

## Introduction

At present, fossil resources constitute the primary feedstock for the production of organic base chemicals.[1] Yet, renewable carbon sources and green and economic catalytic processes for converting these to the target molecules are at the base of long-term sustainable industrial value-chains of the chemical industry. During the last decades, the utilization of carbon dioxide ($CO_2$) as C1-building block in chemical reactions gained much attention. Carbon dioxide is an interesting renewable feedstock, as it is abundant, inexpensive and non-toxic.[2] One of the reactions that would be of great interest is the selective conversion of lower alkenes to the corresponding epoxides thereby utilizing $CO_2$ as oxidant. Epoxides are important intermediates for the production of various commodity chemicals, such as ethylene glycols, ethanolamines, ethoxylates, glycol ethers and polyols. Carbon monoxide is generated as by-product that in combination with hydrogen can be utilized as synthesis gas for the Fischer-Tropsch process to build up hydrocarbons, such as linear alkanes, alkenes and oxygenates. The oxidation of alkenes with $CO_2$ would give rise to a novel process combination that would provide access to bulk intermediates, where the entire carbon originates from sustainable sources. The aim of this project is to identify suitable catalysts that are active for activating $CO_2$ as oxidant and test them in the epoxidation of lower olefins.

## Experimental

Catalysts were prepared by conventional synthetic methods, as, for instance, hydrothermal synthesis, incipient wetness impregnation and co-precipitation. The chemical and morphological properties of the resulting solids were characterized by standard analytics such as powder X-ray diffraction (XRD), X-ray photoelectron spectroscopy (XPS), Fourier transform infrared spectroscopy (FT-IR), $N_2$ adsorption-desorption isotherm analysis, transmission electron microscopy (TEM), and scanning electron microscopy (SEM). The adsorption and desorption ability of the catalysts for $CO_2$

was tested in a tubular reactor by directing a $CO_2$-gas stream through a bed of the catalyst particles for a specific time. The outgoing gas stream was then analysed by mass spectrometry to give a breakthrough curve.

In the next stage, the solid catalysts were screened in a 4-fold multi-batch-reactor (Fig. 1, left) to study their catalytic activities in the epoxidation of alkenes. Alkenes with high reactivities were used as model substrates for initial exploratory experiments. The product mixture was evaluated by gas chromatography and NMR spectroscopy and the catalyst’s activity was compared based on conversion, selectivity, and product yield.

***Figure 1:*** *4-Fold multi-batch-reactor for catalyst screening (left) and fixed-bed reactor equipped with online gas chromatograph (right).*

Once the catalyst screening was completed, suitable catalysts were studied in a fixed-bed reactor equipped with an online gas chromatograph (Fig. 1, right) for their activity in the epoxidation of lower alkenes. Experimental conditions such as temperature, pressure, time and concentration were adjusted to optimize the conversion and the selectivity towards the epoxide.

## Results and Discussion

In an initial set of experiments the epoxidation catalysts were used in the oxidation of propene with oxygen (synthetic air) as the oxidant and acetonitrile (ACN) as the solvent. *i*-Butyraldehyde was used as a sacrificial reductant. Formation of styrene oxide and benzaldehyde was observed. Oxidative carboxylation of the intermediate epoxide to propylene carbonate was observed as side reaction.

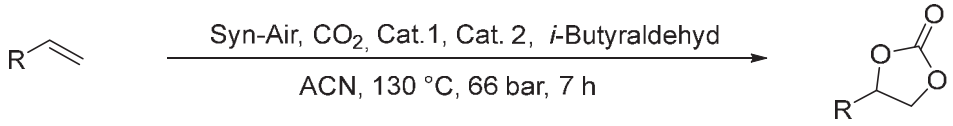

***Table 1.*** *Oxidation of styrene in the presence of carbon dioxide with $O_2$ in synthetic air as the oxidizing agent and i-butyraldehyde as sacrificial reducing agent. Also, the effect of a carboxylation catalyst was explored.*

| Cat.1 | Cat. 2 | Conversion [%] | Yield [%] | | |
|---|---|---|---|---|---|
| | | | Benzaldehyde | Styrene oxide | Styrene carbonate |
| None | None | Full | 14 | 27 | 0 |
| None | $Bu_4NBr$ | Full | 11 | 0 | 61 |

## Summary

Compared to the well-known $CO_2$-insertion reactions, the utilization of $CO_2$ as soft oxidant opens an attractive alternative path for the production of industrially important commodity and fine chemicals. In this work, promising catalysts for the epoxidation of olefins with $CO_2$ to the corresponding epoxides have been synthesized and characterized. The next stages of this project comprise measuring the performance of the catalysts and applying the most promising catalysts to the epoxidation of less reactive alkenes.

## Acknowledgment

K.L.L. is highly grateful to funding of his first year as PhD student by the endowed chair Carbon Sources and Conversion. The support by the benefactors of the endowed chair Carbon Sources and Conversion, the State of North Rhine-Westphalia (contract number IRR-2018-1), RWE Power AG, and the Faculty of Mechanical Engineering of Ruhr-Universität Bochum is acknowledged.

We are grateful to the *Indo-German Science & Technology Centre and the Federal Ministry of Education and Research (BMBF)* for funding of the project $CO_2$BioFeed. The Indian cooperation partners Prof. Asim Bhaumik, Indian Association for the Cultivation of Science, Kolkata, Prof. Biswajit Chowdhury, Indian Institute of Technology (Indian School of Mines), Dhanbad, Dr. Praveen Chinthala, Reliance Industries Limited, Jamnagar are acknowledged for stimulating scientific discussions within of the project $CO_2$BioFeed.

## References

[1] M. Hermesmann, K. Grübel, L. Scherotzki, T. E. Müller, *Renewable and Sustainable Energy Reviews* **2021**, *138*, 110644.

[2] E. Alper, O. Yuksel Orhan, *Petroleum* **2017**, *3*, 109.

# Nano-Silica Grafting with Aminosilanes in Supercritical Carbon Dioxide for Polymer Nanocomposites Preparation

Patience Nnenna Abugu

Department of Chemistry, Wroclaw University of Science and Technology

259204@student.pwr.edu.pl

## Introduction

Polymer nanocomposites (PNCs) are multi-component systems consisting of one or more nanoscale fillers dispersed in a polymeric matrix (*1)*, (*2)*. Their impressive properties are due to the dramatic increase in the interface area between the organic polymer phase and the high-aspect ratio nanoparticles (*2)*. Silicon dioxide nanoparticles ($SiO_2$ NPs) are used to make PNCs for various applications, including films for packaging applications using various polymer matrices, and among them, biopolymers such as starch (*3)*,(*4),* and chitosan (*5)*,(*6)*. However, due to their hydrophilic surface, $SiO_2$ NPs suffer from aggregation and weak interactions with the polymer phase. These challenges can be overcome by grafting small organic molecules on the surface of $SiO_2$ NPs to reduce surface hydrophilicity, prevent aggregation, provide better cohesion and strengthen the interactions between the phases, thereby improving the properties of PNCs of $SiO_2$ NPs (*1)*.

Silane coupling agents (with general formula $R'SiR_3$, where R is a hydrolysable group and R' is an organo-functionality) are widely used for post-synthesis modification of the surface of $SiO_2$ NPs as they can act as a bridge between silica and organic polymer (*7)*, (*8)*. For the highly reactive aminosilane molecules (where R' contains an amine group), grafting is done in a non-aqueous or anhydrous medium to prevent the uncontrollable hydrolysis and polycondensation reactions of aminosilanes (*8)*. In the past, high volumes of organic solvents such as toluene have been used for this purpose. Still, recently, unconventional and green processing techniques employing supercritical carbon dioxide ($scCO_2$) have demonstrated great potential as an alternative non-aqueous medium for the modification of the surface of $SiO_2$ NPs with silanes (*9–11)*. Carbon dioxide is one of the most used supercritical fluids due to its moderate critical points (31.1$^oC$ and 7.38 MPa), non-flammability, availability, and innocuousness. It is considered an energy-efficient green solvent that can replace many harmful organic solvents used in conventional processing (*7)*. Furthermore, it has some superior properties as a solvent: (i) the solubility of a solute

in it can be tuned simply by changing the pressure and temperature in the supercritical region, (ii) the reaction kinetics are greatly enhanced due to its gas-like diffusivity, (iii) it provides good wetting for materials with irregular and/or porous surfaces and (iv) it easily separates from the processed material after decompression without leaving any by-products (*12)*.

Therefore, the first objective of this research project was to achieve covalent grafting of aminosilane molecules on the surface of $SiO_2$ NPs using $scCO_2$ as solvent and reaction medium. Two impregnation methods, namely, supercritical assisted impregnation and supercritical solvent impregnation, and three aminosilane types were investigated for their efficiency in the grafting reactions while adjusting the reaction pressure and time. Finally, to investigate the modification impact, the neat and modified $SiO_2$ NPs were used in the production of starch-chitosan blend films for packaging applications.

## 1.0 Experimental

### 1.1 Materials

Spherical and porous silicon dioxide nanoparticles with particle size 5-20 nm were purchased from Sigma Aldrich (Steinheim, Germany) and used in the experiments as received. For the grafting to $SiO_2$ NPs, APDEMS or 3-aminopropyldiethoxymethyl silane (silane 1) purchased from Sigma Aldrich (Steinheim, Germany), AEAPTMS or N-2-aminoethyl-2-aminopropyltrimethoxysilane (silane 2) and APTES or 3-aminopropyl-triethoxysilane (silane 3) both sourced from UniSil Co. Ltd. (Tarnow, Poland) were used. Ethanol (99.9% purity) from Stanlab (Lubin, Poland) and toluene (≥99.5% purity) from Sigma Aldrich (Steinheim, Germany) were employed as co-solvents.

Food grade potato starch (bought at the local market), chitosan (high molecular weight, ≥75% deacetylated) supplied by Sigma Aldrich (Steinheim, Germany), acetic acid (99.5-99.9% purity) and anhydrous glycerol both supplied by Poch, (Gliwice Poland) were used to produce the starch-chitosan blend films.

### 1.2 Methods

#### 1.2.1 $SiO_2$ NPs Grafting with Aminosilanes in $scCO_2$

The experimental set-up consisted of a $CO_2$ cylinder connected to an air-driven gas booster and a 280 mL high-pressure vessel fitted with temperature and pressure control panels. A uniform temperature was maintained by hot water circulated from a bath circulator to the heating jacket surrounding the vessel. Two positions were possible for the

vessel during impregnation: a vertical and a horizontal position, allowing for two methods of supercritical impregnation.

**A. Supercritical Assisted Impregnation (SAI)**

This process allows for contact between the solid phase ($SiO_2$ NPs) and liquid phase (grafting solution) before the introduction of $CO_2$ into the system. First, 8.0 mL of the grafting solution (a 1:1 solution of aminosilane in co-solvent – toluene or ethanol) was prepared and added to 0.60 g of $SiO_2$ NPs in a test tube. This mixture was stirred properly and placed in the high-pressure vessel arranged in the vertical position. Then the vessel was sealed, $CO_2$ was compressed and introduced into the system, and the impregnation reaction was allowed to proceed at 50 °C and 12 MPa for 1 or 2 hours. Afterwards, decompression was done at the average rate of 0.3 MPa/minute, the vessel was opened, and the test tube was removed. The content of the test tube was washed in the co-solvent and centrifugated at 3600 rpm for 10 minutes (twice). The washed product was then taken for curing in the oven at 110 °C for 2 hours. This process was performed only for silane 1.

**B. Supercritical Solvent Impregnation (SSI)**

In SSI, the solid phase ($SiO_2$ NPs) was kept separate from the liquid phase in the vessel which was arranged in the horizontal position. 0.60g of $SiO_2$ NPs was measured, placed into two glass containers, and wrapped in cellulose paper to prevent loss and splashing during the decompression. Then 8.0 mL of the grafting solution (silane to ethanol in 1:1 wt. ratio) was placed in three glass vessels surrounding the $SiO_2$ NPs. Stainless steel support containing the above mentioned glass containers was inserted into the high-pressure vessel, which was then sealed, and the remaining volume was filled with compressed $CO_2$. The reaction was carried out at a temperature of 50 °C, the pressure of 12, 20 and 25 MPa for 4, 8 and 12 hours. After the impregnation reaction, decompression was done at an average rate of 0.3 MPa/minute, the vessel was opened, and the resulting dry product was taken for curing at 110 °C for 2 hours. This process was performed and optimized for grafting of $SiO_2$ NPs with silane 1 and the optimized parameters were employed for grafting of $SiO_2$ NPs with silane 2 and silane 3. Table 1 presents the reaction parameters for each sample of grafted $SiO_2$ NPs. The yield of the grafting reaction in $scCO_2$ was calculated as: $Y(\%) = \frac{W-W_0}{W_0} \times 100$; where $W_0$ and W are the weights of the $SiO_2$ NPs before the reaction and after the curing step, respectively. Y is expressed as percentages in table 1.

Tab. 1.: Experimental conditions used to prepare aminosilane grafted $SiO_2$ NPs in $scCO_2$ and yield of grafting reaction

| Sample | Aminosilane | Method | Co-solvent | Pressure MPa | Time hr | Yield, % |
|---|---|---|---|---|---|---|
| s1-A | 1 | SAI | Toluene | 12 | 2 | 129.55 |
| s1-B | 1 | SAI | Ethanol | 12 | 1 | 16.55 |
| s1-C | 1 | SSI | Toluene | 12 | 12 | n.a. |
| s1-D | 1 | SSI | Ethanol | 12 | 4 | n.a. |
| s1-E | 1 | SSI | Ethanol | 20 | 8 | 10.79 |
| s1-F | 1 | SSI | Ethanol | 20 | 12 | 22.43 |
| s1-G | 1 | SSI | Ethanol | 25 | 8 | 8.81 |
| s2-A | 2 | SSI | Ethanol | 20 | 12 | n.a. |
| s3-A | 3 | SSI | Ethanol | 20 | 12 | 11.66 |

### 1.2.2 Production of Starch-Chitosan Blends Reinforced with $SiO_2$ NPs

The films were prepared by the solvent casting method as illustrated in figure 1.

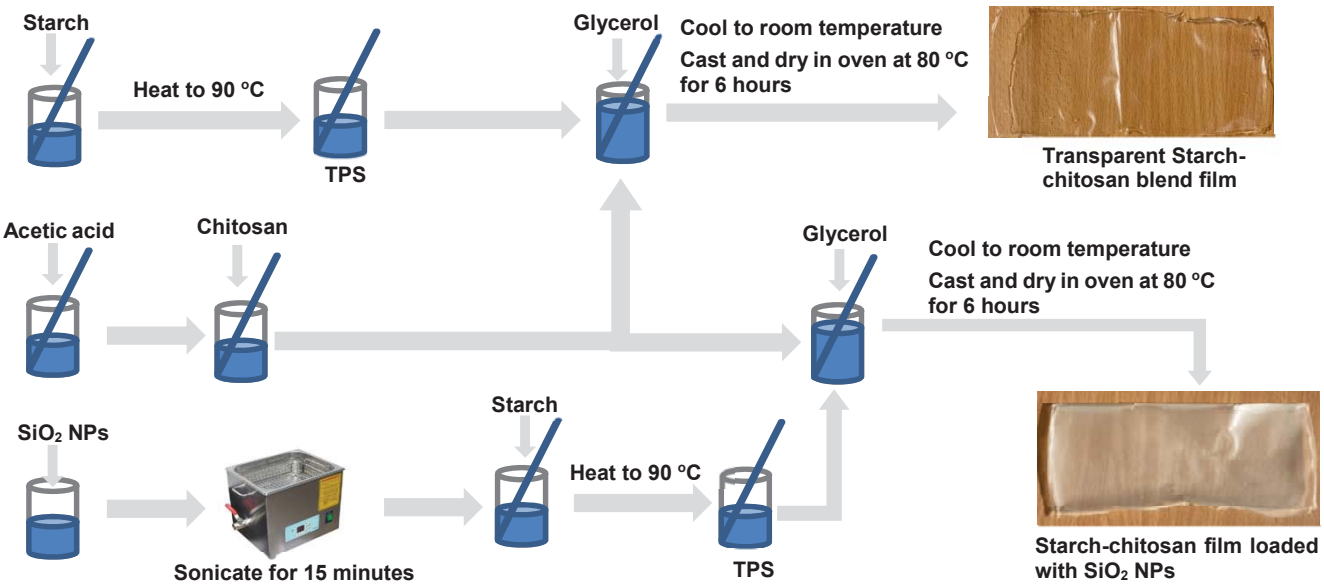


Fig. 1.: Schematic representation of method of film production

### 1.2.3 Material Characterization

Fourier-Transform Infra-red Spectroscopy (FTIR) was used to confirm covalent bonding between $SiO_2$ NPs and the aminosilane molecules. The spectra were recorded in the ATR mode using Nicolet iS50 Spectrometer (Thermo Fisher SCIENTIFIC) with a resolution of 4 $cm^{-1}$ in the wavenumber range between 500-4000 $cm^{-1}$.

## Summary

The use of supercritical $CO_2$ in surface modification of $SiO_2$ NPs was successful. Calculations of reaction yield and results of FTIR (disappearance of the hydroxyl group band) confirm the covalent bonding of aminosilane molecules on $SiO_2$ NPs. Supercritical assisted techniques (SAI), though requiring a shorter reaction time and lower $CO_2$ pressure, proved tedious in the post-modification process. Furthermore, SAI processes require a large amount of solvent for washing and recovering $SiO_2$ NPs from the solution. However, the supercritical solvent impregnation process (SSI) featured all the advantages of material processing in the supercritical phase combined with ease of NP recovery and comparable yields with the SAI techniques. In the next stage of experiments, thermogravimetric analysis, scanning electron microscopy and X-ray diffraction measurements will be used to deduce the grafting degree and visualize $SiO_2$ NPs deagglomeration in the polymer matrix.

Acknowledgment

The financial support of National Science Center (Poland), grant number 2018/31/B/ ST8/01826 is gratefully acknowledged.

## References

1. S. Mallakpour, M. Naghdi, Polymer/SiO 2 nanocomposites: Production and applications. *Prog. Mater. Sci.* **97**, 409–447 (2018).

2. J. Huang, J. Zhou, M. Liu, Interphase in polymer nanocomposites. *JACS Au* (2022), doi:10.1021/jacsau.1c00430.

3. R. Zhang, X. Wang, M. Cheng, Preparation and Characterization of Potato Starch Film with Various Size of Nano-SiO□. *Polymers (Basel)*. **10** (2018), doi:10.3390/polym10101172.

4. O. O. Oluwasina, B. P. Akinyele, S. J. Olusegun, O. O. Oluwasina, N. D. S. Mohallem, Evaluation of the effects of additives on the properties of starch-based bioplastic film. *SN Appl. Sci.* **3**, 421 (2021).

5. Y. Liu, Z. Cai, L. Sheng, M. Ma, Q. Xu, Influence of nanosilica on inner structure and performance of chitosan based films. *Carbohydr. Polym.* **212**, 421–429 (2019).

6. B. Tian, D. Xu, J. Cheng, Y. Liu, Chitosan-silica with hops β-acids added films as prospective food packaging materials: Preparation, characterization, and properties. *Carbohydr. Polym.* **272**, 118457 (2021).

7. Y. Haldorai, J.-J. Shim, K. T. Lim, Synthesis of polymer–inorganic filler nanocomposites in supercritical CO2. *J. Supercrit. Fluids*. **71**, 45–63 (2012).

8. I. A. Rahman, V. Padavettan, Synthesis of Silica Nanoparticles by Sol-Gel: Size-Dependent Properties, Surface Modification, and Applications in Silica-Polymer Nanocomposites—A Review. *J. Nanomater.* **2012**, 1–15 (2012).

9. D. Stojanovic, A. Orlovic, S. Markovic, V. Radmilovic, P. S. Uskokovic, R. Aleksic, Nanosilica/PMMA composites obtained by the modification of silica nanoparticles in a supercritical carbon dioxide–ethanol mixture. *J. Mater. Sci.* **44**, 6223–6232 (2009).

10. D. Stojanovic, A. Orlovic, S. B. Glisic, S. Markovic, V. Radmilovic, P. S. Uskokovic, R. Aleksic, Preparation of MEMO silane-coated SiO2 nanoparticles under high pressure of carbon dioxide and ethanol. *J. Supercrit. Fluids*. **52**, 276–284 (2010).

11. C. Fedosse Zornio, S. Livi, J. Jestin, J. Duchet, J.-F. Gérard, Ionic PMMA/nanosilica interfaces from grafting ionic liquids under supercritical CO2 conditions. *Eur. Polym. J.* **109**, 82–92 (2018).

12. X. Zhang, S. Heinonen, E. Levänen, Applications of supercritical carbon dioxide in materials processing and synthesis. *RSC Adv.* **4**, 61137–61152 (2014).

# Conversion of Lignin to Phenolic Base Chemicals

Dennis Panke#, Thomas E. Müller*

Carbon Sources and Conversion, Faculty of Mechanical Engineering,

Ruhr-University Bochum, # panke@ls-csc.rub.de

## Introduction

The chemical industry is searching urgently for replacements of fossil carbon sources that are the base of the current value chains. For substituting fossil fuels as feedstock, new starting materials and intermediates for the chemical industry based on renewable feedstock are required. Aromatic compounds, such as benzene, toluene and xylene, summarized as BTX and phenolic base chemicals have a important share of the base chemical market. However, there are no established large-scale processes for producing aromatic compounds from renewable resources. One of the most promising renewable feedstocks for producing aromatics may be lignin, as it contains a large number of aromatic units in its polymeric structure (Figure 1). It is one of the main constituents of lignocellulosic bio mass and contained, e.g., in wood. Lignin is available worldwide in sufficiently large quantities to replace fossil-based aromatics (*Figure 1*). Large quantities of lignin are separated as by-product in the production of the pulp and paper industry and, at present, mostly

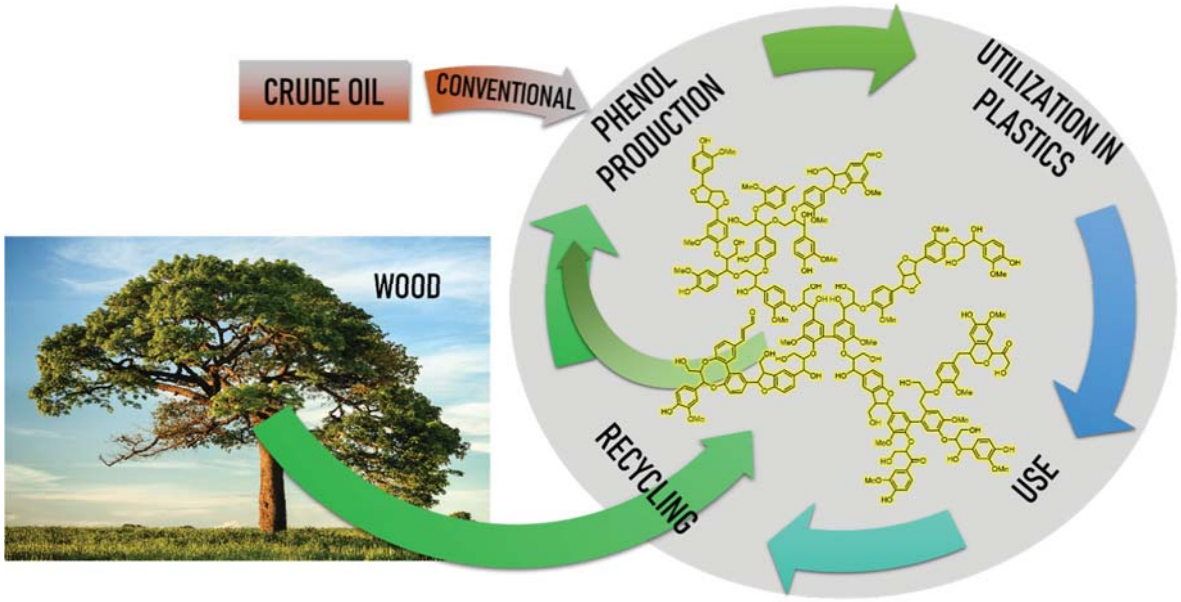


*Figure 1: Envisioned circular economy for phenolic compounds based on the renewable resource wood.*

burnt for energy generation.[1] So far, there is hardly any chemical utilization of the lignin, except for the production of small amounts of vanillin from lignosulphonates, e.g., in a production site based in Norway.[2] The aim of this work is to selectively depolymerize lignin towards phenolic compounds that are useful for polymer applications. For this purpose, the use of selective catalysts was explored and the optimal reaction conditions for the depolymerisation of lignin were investigated.

## Experimental

Depolymerisation reactions were carried out in a 300 mL stainless steel batch reactor (Parr Instruments). The reactor was equipped with a gas entrainment stirrer, a thermocouple for temperature control, a riser pipe to withdraw liquid samples during the reaction and a pressure transducer (Figure 2). The product composition was analysed by gas chromatography (GC), infrared spectroscopy (IR) and nuclear magnetic resonance spectroscopy (NMR).

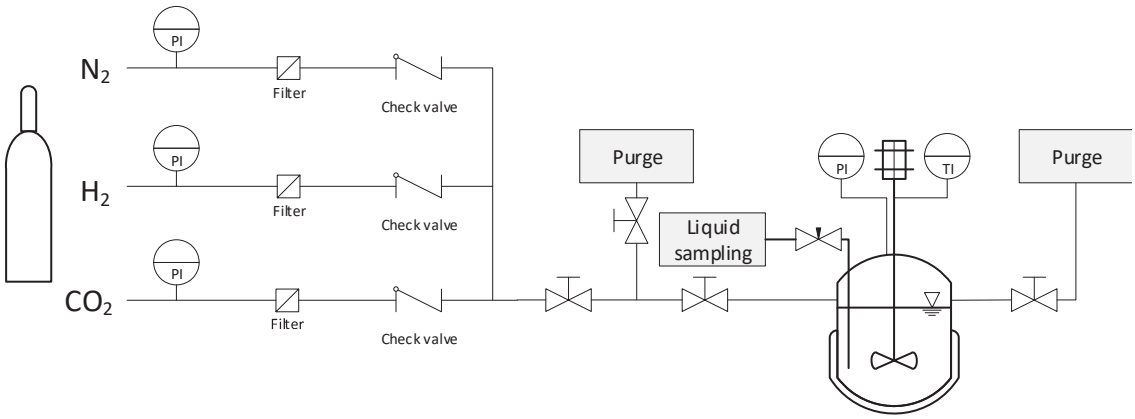


*Figure 2: Schematic illustration of the reactor setup comprising gas supply for $H_2$, $CO_2$ and $N_2$, and a stirred tank reactor with liquid sampling.*

## Results and Discussion

Commercially available Kraft lignin was depolymerized in the presence of a homogeneous ruthenium catalyst.[3] The reaction was performed in a mixture of lignin and the catalyst in a solvent (*vide infra*). The mixture was pressurized with hydrogen and heated to temperatures near the critical point of the solvent. Noteworthy, yields of soluble products higher than 90% were obtained in methanol. Also, the influence of reaction parameters such as temperature and solvent on the activity of the catalyst and the product selectivity were studied (Figure 3).

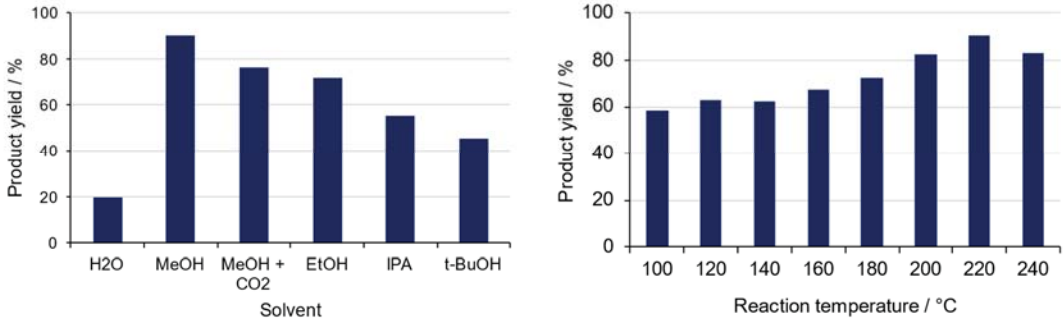


*Figure 3: Influence of the solvent on the depolymerization of Kraft lignin in the presence of a homogeneous Ru-catalyst (left) and temperature dependence of the depolymerization of Kraft lignin in methanol (right).*

Methanol provided the highest yield in soluble products (Figure 3, left). Significantly lower yields were obtained with other alcohols, such as ethanol (EtOH), isopropanol (IPA), or *tert*-butanol (*t*-BuOH), water, or a mixture of methanol with $CO_2$. Most likely, the lower yield is related to a lower solubility of lignin as well as a reduced solubility of hydrogen in the later solvents compared to methanol.[4] Thus, methanol was the most suitable solvent for the depolymerisation of lignin under our reaction conditions.

The product yield in methanolic solution increased with increasing temperature up to a temperature of 220 °C (Figure 3, right). At higher temperatures, the yield in soluble products decreased. Most likely, repolymerization of the lignin fragments was more pronounced leading to decreasing yields in soluble products.

## Summary

In this work, the high-pressure depolymerization of Kraft lignin was carried out utilizing a homogeneous ruthenium catalyst for cleaving specific bonds in lignin. The influence of the reaction parameters on the performance of the catalyst was analysed and the reaction conditions were optimised. Under the best conditions, near quantitative conversion of lignin towards soluble products was obtained. Future research will include the detailed analysis of the products as well as optimising the catalyst regarding selectivity to specific target products.

## Acknowledgments

The support of the State of North Rhine-Westphalia (contract number IRR-2018-1), RWE Power AG, and the Faculty of Mechanical Engineering of Ruhr-Universität Bochum is acknowledged.

## References

1 D. S. Bajwa, G. Pourhashem, A. H. Ullah and S. G. Bajwa, *Industrial Crops and Products*, 2019, **139**, 111526, DOI: 10.1016/j.indcrop.2019.111526.

2 M. Zirbes, L. L. Quadri, M. Breiner, A. Stenglein, A. Bomm, W. Schade and S. R. Waldvogel, *ACS Sustainable Chem. Eng.*, 2020, **8**, 7300–7307, DOI: 10.1021/acssuschemeng.0c00162..

3 T. E. Müller, Hydrogenation and Hydrogenolysis with Ruthenium Catalysts and Application to Biomass Conversion, in *Ruthenium - an Element Loved by Researchers*, IntechOpen, 2021, DOI: 10.5772/intechopen.97034.

4 T. Katayama and T. Nitta, *J. Chem. Eng. Data*, 1976, **21**, 194–196, DOI: 10.1021/je60069a018.

# Visualization of Relief and Decomposition Phenomena in High-Pressure Systems

Aaron Röblitz, Markus Busch*

Ernst-Berl-Institut, Technische Universität Darmstadt,

*markus.busch@pre.tu-darmstadt.de

## Introduction

The prevention of decomposition during polymerization processes is an essential part of the safe operation of production plants. Nevertheless, they can occur due to inadmissible temperature rises or the formation of a hotspot, which is why analyzing the decomposition process and thus reducing the consequences that occur is of great importance. Important parameters here are the maximum decomposition temperature and pressure, as well as the velocity of the flame front. This is often determined using several thermocouples, whereby the detected temperature rises at the respective measuring points can provide information about the geometry of the flame front. For a detailed representation of the flame front movement and formation, however, visual observations are necessary. In this context, the investigation of the influence of a subsequent discharge on the decomposition process can also help to optimize safety devices in technical plants.

## Experimental

A view cell with a volume of 34 ml was used for the experimental investigation. The visual recording was performed with a high-speed camera, and analysis was performed with the aid of a tracking program. In addition, pressure and temperature were measured using a strain gauge sensor and a thermocouple, respectively.

When considering relief processes, the so-called discharge coefficient (the $K_d$-value) plays a decisive role. This describes the ratio between the experimentally determined and the calculated ventilated mass flow. Factors such as the mixture composition or the valve geometry have a considerable influence on the $K_d$-value. For this reason, experiments were carried out with ethene and vinyl acetate in which the composition of the system was varied. The results were evaluated with the aid of pressure and temperature data and by analyzing a video sequence created with a high-speed camera. From this, information can be obtained about the phase behavior during the relief process. Further experiments

investigated the influence of the relief position and the length of the relief line. This made it possible to describe the dependence of the $K_d$-value concerning the parameters mentioned. The results are shown in Figure 1.

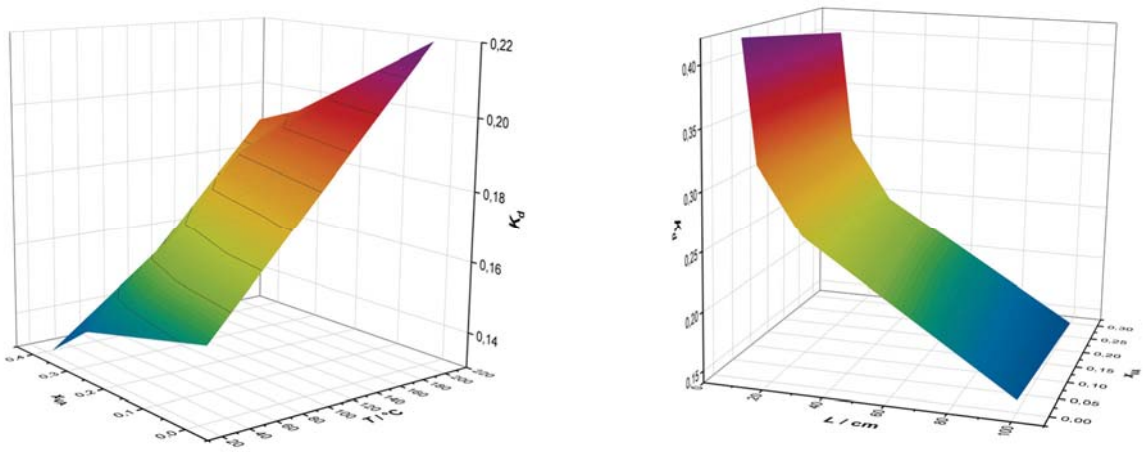


Figure 1: Overview of the $K_d$-values determined. Left: the $K_d$-value as a function of VA-content and temperature. Right: the $K_d$-value as a function of VA-content and nozzle length.

To investigate decomposition processes, a hotspot is generated in the view cell by annealing a tungsten filament, which induces decomposition of the reaction mixture. By using the high-speed camera, the propagation of the flame front can be analyzed and the burning velocity can be determined. The recording of the pressure and temperature data provides information about the rate of pressure increase and the maximum pressure resulting from the decomposition. Various parameters were varied, such as the mixture composition, the initial conditions and the ignition position. Figures 2 to 4 show the corresponding results.

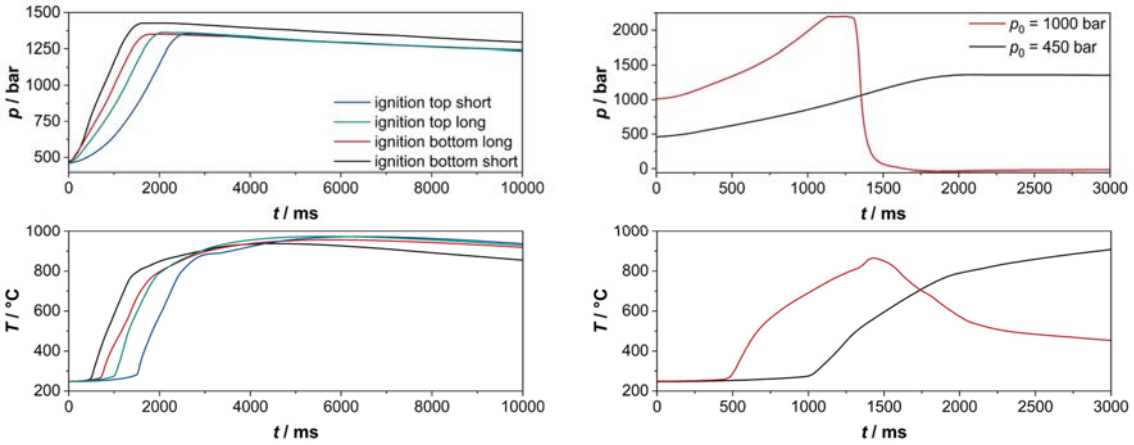


Figure 2: Reactor pressure and temperature plotted against experimental time. $p_0$ = 450 bar; $T_0$ = 250 °C; $x_{LDPE}$ = 0.2. Left: investigation of the influence of the ignition position. Right: investigation of the influence of the initial pressure. [2]

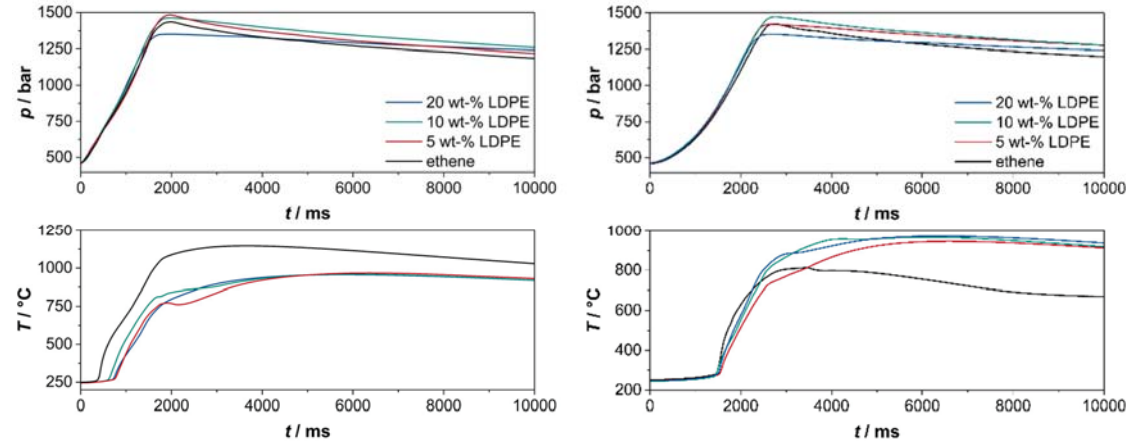


Figure 3: Reactor pressure and temperature plotted against experimental time. $p_0$ = 450 bar; $T_0$ = 250 °C. Left: ignition top short. Right: ignition bottom long. [2]

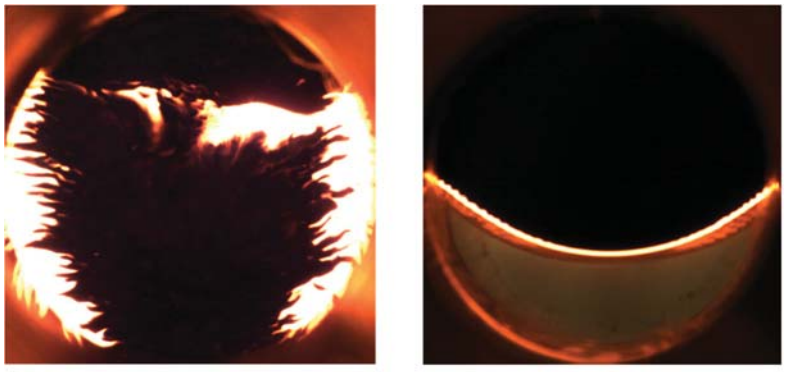

Figure 4: Investigation of flame front propagation as a function of ignition position. $p_0$ = 450 bar; $T_0$ = 250 °C; $x_{Et}$ = 1. Left: ignition bottom short. Right: ignition top long.

## Summary

To better understand relief and decomposition processes, experiments were carried out in a view cell in which decomposition is induced by an artificially generated hotspot. It is shown that the flame front geometry strongly depends on the ignition position. Thus, hotspot formation in the lower reactor region causes the flame front to move turbulently through the reactor, while ignition in the upper reactor region results in a laminar flame front. Increasing the starting pressure causes the rate of pressure to rise and the maximum pressure to increase significantly. A change in the composition of the reaction mixture due to the addition of LDPE has an influence on the temperature curve, whereby the dependence on the ignition position is again evident there.

To investigate the relief process, the $K_d$-value was used as a comparative value. By evaluating the visual results and using Multiflash, the phase behavior during the relief process and thus the influence on the $K_d$-value could be determined. The dependence on the nozzle length as well as the starting conditions and the composition of the reaction mixture was investigated. It was found that an increasing VA-content as well as longer nozzles lead to a stronger boiling delay and thus to two-phase formation.[1] This results in a reduction of the $K_d$-value, so the non-ideality of the investigated system increases.

## References

[1] J. Schmidt, *Forsch Ingenieurwes*, 71, 47-58 (2007).

[2] A. Konopka, *Masterthesis*, TU Darmstadt (2022).

# Evaluation of Chemical Reaction of Biomass under Partial Oxidation in Supercritical Water

Alina Satpayeva, Juan Garcia-Serna, Danilo Cantero

Institute of Bioeconomy, Department of Chemical Engineering and Environmental Technology, University of Valladolid, alina.satpayeva@uva.es

## Introduction

Nowadays a lot of attention is paid to biomass recycling products as a source of renewable energy, food, health products, and industrial chemical products. Well-supported and centralized plant is needed to be developed to achieve the optimal and eco-friendly conditions of the biomass conversion to those products. Hence, the innovation may start from the efficient handling of energy and reducing the equipment costs. Also, the complexity of the process can be reduced by using easily accessed solvents and reducing reaction time we can achieve high yield process with cost effective benefits.

The main components of various types of biomass are cellulose (34–50%), hemicellulose (16–34%) and lignin (11–29%) [1]. Hydrolysis is the process that converts biomass to the simpler components while cleaving of ether and ester bonds by the addition of one molecule of water for every broken linkage [2]. In previous studies it was concluded that supercritical water can be used as an excellent solvent for environmentally safe and clean biomass decomposition process [2–6]. Main limitations which can be overcame by using hydrothermal media are: (1) water content, biomass can be used directly and in this way energy profile is in saving mode; (2) biomass solvent, there is no need for finding another media; (3) mass transfer limitations can be reduced or avoided due to homogeneous phase of biomass and high diffusion rate; thus, reaction rates are faster [7–11]. Moreover, supercritical water has ability to disinfect the biomass from bacteria, viruses and harmful proteins since the process is operated at relatively high temperatures (≥374°C).

The aim of this work is to understand the hydrolysis of biomass when oxidative compounds are present in the medium. It is known that oxidation process is an exothermic reaction that can produce different products to hydrolysis. Hydrogen peroxide ($H_2O_2$) is used as and oxidation agent and its content effect is investigated. One more parameter which impact is examined is temperature, sub- and supercritical conditions are checked. Moreover, studies are conducted to analyze biomass decomposition by changing dimensions of the reactor and reaching different reaction times.

## Experimental

A Pressurized Hydrolysis Unit (PHUN 1) plant is designed and build according to the previous studies (Fig. 1) [12]. The biomass suspension with different $H_2O_2$ content was fed to the reactor at a flow rate of 5 kg/h. To supply same and constant concentration of biomass (3.75 % w/w) in the reactor, suspension was kept at constant mixing rate. The reactor was thermally isolated. The pressure of the system was controlled manually using the high temperature valve. To achieve fully controlled reactions without producing byproducts, the installation was created based on rapidly changing temperature profiles. A hot pressurized stream of water is mixed with a biomass suspension to achieve desired high temperature in the reactor. The reaction time was changed by modifying the reactor volumes (length and inner diameter in tubular reactors). Finally, after the desired reaction time and temperature are achieved, the products should be rapidly cooled to stop the hydrolysis reactions. A high temperature valve with ability to perform sudden decompression was used to cool the system in a very short time.

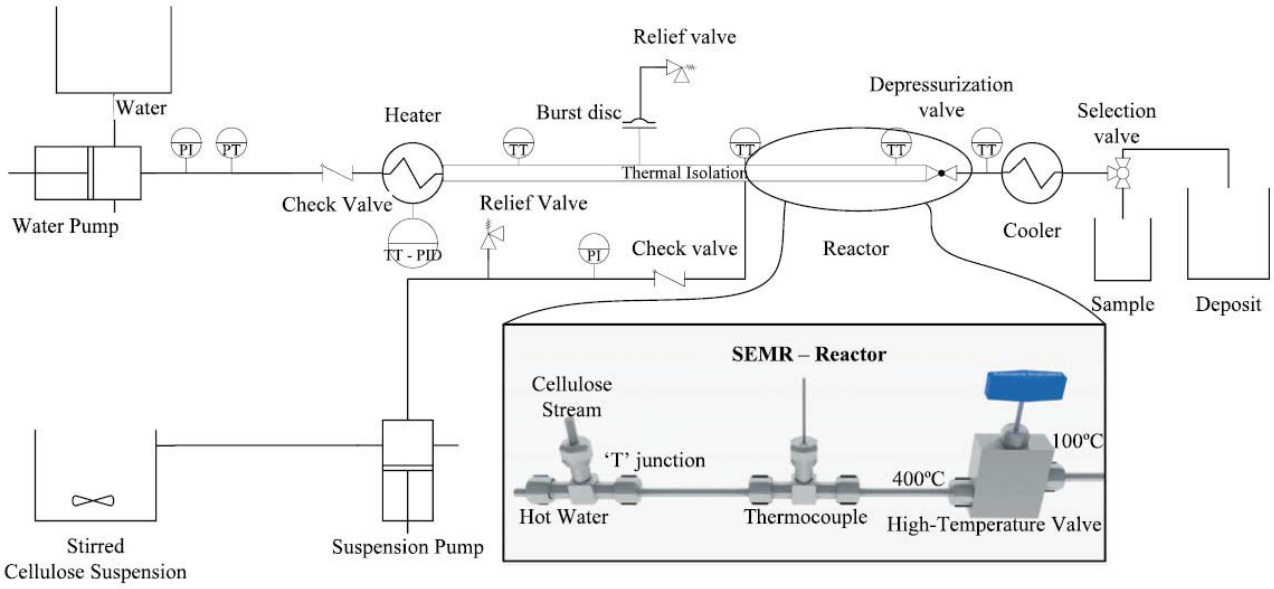


Fig. 1.: Experimental setup. Schema of the PHUN 1 plant [12].

## Summary

The results of this study will be an important part of the environmentally friendly processes field. Once proper amount of oxidation agent will be established, it will be possible to model the industrial process with green energy approach. With the help of the previous published results, new approach in terms of products profile can be next step in future bioeconomy development.

## References

1. O. Bobleter, Hydrothermal degradation of polymers derived from plants. Prog. Polym. Sci. 19 (1994), 797–841.
2. G. Brunner, Near critical and supercritical water. Part I. Hydrolytic and hydrothermal processes. J. Supercrit. Fluids 47 (2009), 373–381.
3. N. Akiya, P.E. Savage, Roles of water for chemical reactions in high-temperature water, Chemical Reviews 102 (2002), 2725–2750.
4. G. Brunner, Chapter 8 – processing of biomass with hydrothermal and super-critical water, in: B. Gerd (Ed.), Supercritical Fluid Science and Technology, Elsevier, Blacksburg (2014), 395–509.
5. G. Brunner, Chapter 2 – properties of pure water, in: B. Gerd (Ed.), Supercritical Fluid Science and Technology, Elsevier, Blacksburg (2014), 9–93.
6. G. Brunner, Chapter 5 – reactions in hydrothermal and supercritical water, in: B. Gerd (Ed.), Supercritical Fluid Science and Technology, Elsevier, Blacksburg (2014), 265–322.
7. A.A. Peterson, F. Vogel, R.P. Lachance, M. Fröling, M.J. Antal, J.W. Tester Jr., Thermochemical biofuel production in hydrothermal media: a review of sub- and supercritical water technologies, Energy & Environmental Science 1(2008), 32–65.
8. D. Bröll, C. Kaul, A. Krämer, P. Krammer, T. Richter, M. Jung, H. Vogel, P. Zehner, Chemistry in supercritical water, Angewandte Chemie International Edition 38 (1999), 2998–3014.
9. A. Loppinet-Serani, C. Aymonier, F. Cansell, Supercritical water for environ-mental technologies, Journal of Chemical Technology & Biotechnology 85 (2010), 583–589.
10. M. Akizuki, T. Fujii, R. Hayashi, Y. Oshima, Effects of water on reactions for waste treatment, organic synthesis, and bio-refinery in sub- and supercritical water, Journal of Bioscience and Bioengineering 117 (2014), 10–18.
11. H. Machida, M. Takesue, R.L. Smith Jr., Green chemical processes with supercritical fluids: properties, materials, separations and energy, Journal of Supercritical Fluids 60 (2011), 2–15.
12. D.A. Cantero, M.D. Bermejo, M.J. Cocero, High glucose selectivity in pressurized water hydrolysis of cellulose using ultra-fast reactors, Bioresource Technology 135 (2013), 697–703.

# Influence of Initiators on Temperature Distribution in High-Pressure Polyethylene Autoclaves

Lorenz Schmidt, Markus Busch

Ernst-Berl-Institut, Technische Universität Darmstadt,

markus.busch@pre.tu-darmstadt.de

## Introduction

Low-density polyethylene is a bulk product produced by free-radical polymerization of ethene at pressure up to 3000 bar and temperatures up to 300 °C. To start the reaction, peroxides are used which provide the required starting radicals by their decomposition. Those initiators have different decay rates depending on their chemical structure. With a higher temperature, the decay rate of the initiators rises, which increases the concentration of radicals in the reactor. Thus, more chains are started, which in turn leads to an enhanced conversion. At a constant initiator concentration, the conversion can therefore be increased with a higher temperature. However, this cannot be done unlimited since each initiator has an optimal operating temperature range. Therefore, a wide variation of initiators for radical polymerization is available on the market to achieve an optimum yield at the selected reaction temperature. The maximum of the initiator effectiveness is caused by the further increasing decay rate which exceeds the mixing rate of the reaction system. This creates a concentration gradient of initiator and consequently of radicals in the reactor. Since the amount of initiator in the system remains constant, but the effective reaction volume decreases, the radical concentration increases in this zone. As a result, a temperature gradient is formed. Furthermore, the locally increased radical concentration leads to more termination reactions, which in combination with the smaller effective reaction volume causes a decrease in conversion.[1]

There are already various simulative approaches to the influence of initiator mixing on the temperature, conversion and molar mass distribution. These include work with CFD simulation as well as approaches to describe the results of the concurrence of mixing and reaction by a compartment model.[2] In this work, the influence of initiators and cocktails on the temperature distribution is investigated experimentally.

## Experimental

For the experiments, continuously operated stirred autoclaves are used. The operating conditions during the experiments are at pressures of 2000 bar and temperatures of up to 300 °C. For individual dosing of the initiators, several syringe pumps can be used which allow smallest flows in a range of a few milliliters per hour. Besides the dosing of the initiators along the shaft of the magnetic stirrer, investigations were also carried out with the additional injection from the side of the reactor. To flush the initiator into the reactor a solvent stream was used in this case. To obtain a temperature profile of the reactor as accurately as possible, 6 thermocouples are distributed at different locations in the autoclave. A drawing of the reactor with the different thermocouples inside is shown in Fig. 1..

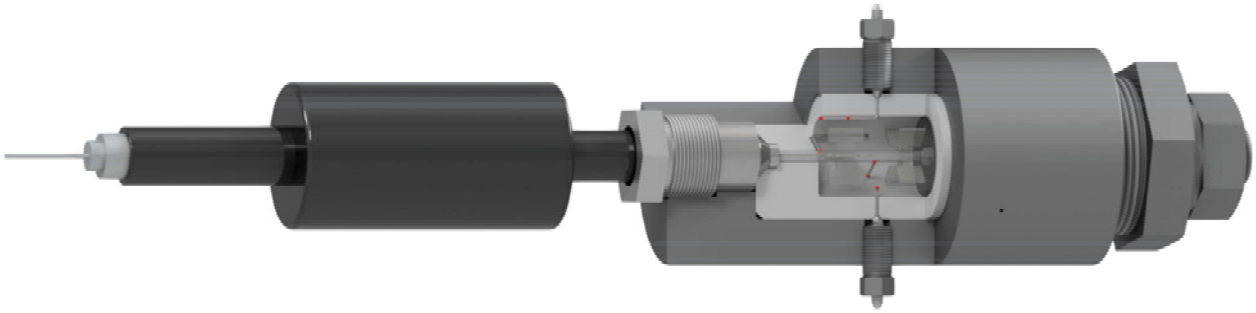

Fig. 1.: Stirred High-Pressure Autoclave with multiple thermocouples.

In the experiment, the jacket temperature is increased successively and the temperature profile in the reactor is monitored by the different thermocouples. As an example, the temperature behavior of the initiator TBPPI is presented here. This initiator is classified as a low-temperature initiator and has a recommended temperature range of 130 °C to 190 °C for the high-pressure polymerization of ethene.[3] Fig. 2. shows the temperature profile in the reactor at a jacket temperature of 170 °C. The homogeneous temperature profile with an increased temperature of approx. 175 °C in the reactor shows the effectiveness of the initiator at this temperature.

Fig. 3. shows the temperature profile at a jacket temperature of 210 °C. Here, a separation of the temperatures in the reactor is visible. Due to the increased temperature, the radical formation takes place faster than the mixing process and therefore, a concentration gradient results. Based on the position of the thermocouples, the radical concentration is

highest directly at the inlet of the reactor and along the stirrer shaft and decreases towards the lower area and the outside.

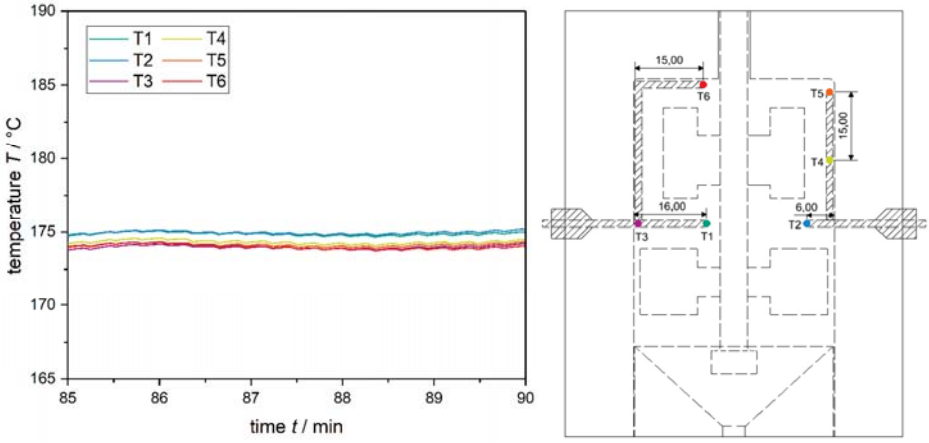


Fig. 2.: Temperature profile at a jacket temperature of 170 °C with a feed rate of 2 kg $h^{-1}$ of ethene and 1.5 mol ppm of TBPPI.

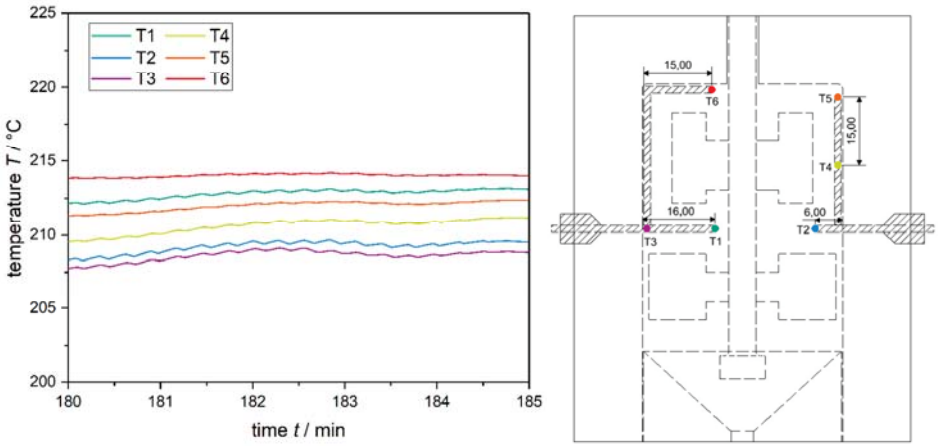


Fig. 3.: Temperature profile at a jacket temperature of 210 °C with a feed rate of 2 kg $h^{-1}$ of ethene and 1.5 mol ppm of TBPPI.

In addition to the formation of a temperature gradient, the curve of the initiator's effectiveness could be observed based on the ethene conversion. In practice, the initiator TAPPI was found to be effective from 170 °C. When the temperature is increased further, hardly any changes are observed. The conversion drops below the maximum at a jacket temperature of 230 °C, which is significantly higher than the recommended temperature of 190 °C. In experiments with the side stream, it was shown that the additional convection of the solvent stream improves the mixing of the initiator. This leads to a more uniform

concentration and temperature profile under similar conditions. Improved mixing thus appears to contribute to a broadening of the operating range of the initiator.

## Summary

In this work, initiators for the radical polymerization of ethene and their mixtures were studied. The temperature profile in the reactor was monitored at several measuring points and conclusions were drawn about the effectiveness of the initiator at different operation points. These observations were also confirmed by the ethene conversion measured at the different process conditions. By introducing a side-stream, the influence of the mixing could be pointed out. The additional convection leads to improved mixing, which results in a more homogeneous temperature distribution under the same conditions. These results will further contribute to the validation of CFD and compartment models.

## References

[1] H. Seidl, G. Luft, *Journal of Macromolecular Science: Part A - Chemistry* 2006, *15*, 1.

[2] G. J. Wells, W. H. Ray, *AIChE Journal* 2005, *51*, 3205.

[3] United Initiators, *Technical Data Sheet* united-initiators.com/products/tappi-75-al/, access: 24.05.2022

# Using Supercritical Carbon Dioxide to Process Biological Tissue into Preserved and Highly Functional Matrices for Tissue Healing and Regeneration

Inês Vasconcelos Silva[1], Raquel Costa[1,2,3]*, Ana Leite Oliveira[1]*

[1] Universidade Católica Portuguesa, CBQF - Centro de Biotecnologia e Química Fina – Laboratório Associado, Escola Superior de Biotecnologia, Porto, Portugal

[3] Instituto de Investigação e Inovação em Saúde, Universidade do Porto (i3S), Porto, Portugal

[4] Department of Biomedicine, Biochemistry Unit, Faculdade de Medicina, Universidade do Porto, Porto, Portugal

*raquel.costa@i3s.up.pt; aloliveira@ucp.pt

## Introduction

The rise in chronic diseases such as diabetes has triggered the development of new therapies aimed at restoring normal tissue function through the use of biomedically engineered smart matrices.[1] Natural and synthetic materials have been developed and applied with the goal of closely mimicking the natural microenvironment of the cell .[2] The extracellular matrix (ECM) houses the living cells in the body and is a composite of a myriad of biomolecules including proteoglycans, glycosaminoglycans (GAGs), collagen, growth factors, cytokines and chemokines.[3] This structure provides cues for cell attachment, proliferation, differentiation, and ultimately tissue regeneration.[4] Since the ECM has a complex 3D structure, to replicate both its physical and compositional characteristic, is extremely challenging. As a result, the application of decellularized tissue and/or organs is becoming increasingly popular.[5] Ideally decellularization allows for the removal of the immune inducing components leaving an intact and well-preserved matrix behind, which can be used without risk to the intended host.[3]

Current decellularization protocols are over dependent on harsh chemicals to reach standards of cell removal, which can damage ECM composition, structure and bioactivity.[6–8] The process is typically complex and can take weeks to complete.[9] Therefore, there is a high demand to improve decellularization processes, its efficiency and ECM final quality. Supercritical carbon dioxide ($scCO_2$), has emerged as a valuable tool to create faster and more effective methodologies to process biological tissue. At relatively low temperature

and pressure (31.1ºC and 7.39MPa), $CO_2$ enters the supercritical state, which confers properties such as high transfer rate and diffusivity, making it an ideal solvent for processing sensitive materials, resulting in faster overall processes.[3] Although some studies have been made using $scCO_2$ assisted decellularization, such as aorta, heart, cornea, and skin, this innovative approach is still in its infancy.[3] Sterilization is also necessary to achieve the required safety of the biological products and $scCO_2$ has been proposed for terminal sterilization of sensitive biomaterials and biological tissue[10], and is currently one of six methodologies being assessed by FDA, as the next standard sterilization process. This project outlines a complete pipeline for processing a biological tissue, placenta, proposing a pioneer strategy to valorize ECM, which combines, decellularization, sterilization and drying using $scCO_2$ technology. The placenta is a specialized organ surrounded by the amniotic and chorion membranes, that are typically classified as medical waste, and they can be harvested without causing any direct harm to the donor and with few ethical considerations. [11–14] Furthermore, the supply is almost limitless with an estimated annual global output of 15 million $m^2$ in amniotic membrane and 60000 $m^3$ in placenta each year.[15] This material is therefore a promising source of ECM for tissue engineering and regenerative medicine applications that stands in stark contrast with other organ and/or tissues in shorter supply. Additionally, the placenta ECM composition offers interesting properties such as anti-inflammatory[16], antibacterial[16], anti-oxidant[20], antiscarring[18], anti-apoptotic[19], wound protective[18] and fibrosis suppression[20] which makes it atractive for a myriad of applications, such as skin[21], bone[22] and liver[27].
In our work, the obtained decellularized placenta will be further processed into a functional hydrogel and a bioink will be developed by the incorporation of cells of interest to create functional tissue microenvironment, looking at every step necessary from source material to final product.

## Experimental

The following research project is divided into three separate but interconnected stages: The development and optimization of $scCO_2$ assisted protocols for the production of dECM powder, the characterization of the resulting material and *in vitro* studies.

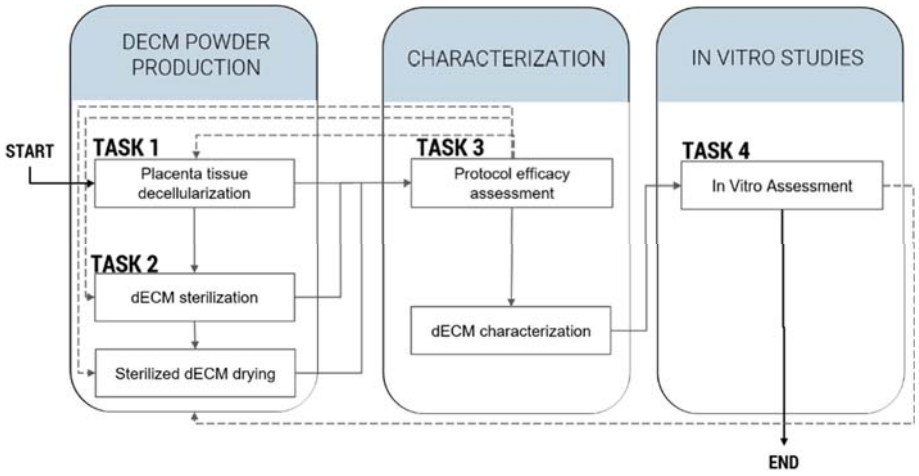


**Figure 1.** Schematic overview of the proposed workflow. The project is divided into four tasks, and grouped into three general stages of development.

Development and optimization of a $scCO_2$-assisted decellularization process - This task consists in tissue harvesting, washing of blood residues and dissection, namely separation of the amniochorionic membrane from the placenta (figure 2). Decellularization will use $scCO_2$ combined with different co-solvents (ethanol/ultrapure water/others). Operational parameters (temperature/pressure/time/depressurization rate) will be explored until an optimal protocol is reached. $scCO_2$ will be used in continuous flow, increasing physical dragging of cellular components. Results will be compared against standard protocols in terms of cell removal efficiency/EMC components preservation.[24] Decellularization efficacy will be assessed by the metrics established by Crapo, *et al*.

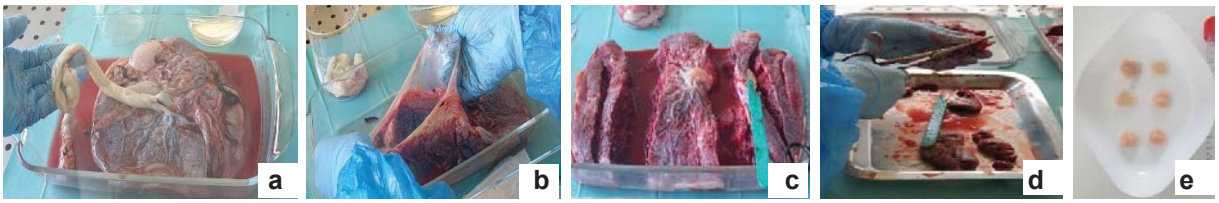


**Figure 2.** Macroscopic images of initial placenta tissue pre-treatment and treatment, (a) placenta fetal side, (b) manuel membrane removal, (c) dissection, (d) mincing and (e) placenta fragments after decellularization and washing.

Sterilization and drying of placental tissue by $scCO_2$-assisted methods - To sterilize dECM, operational parameters and co-solvents (peracetic acid/hydrogen peroxide) will be explored. [25] Efficiency will be assessed using standards of sterility assurance level ($10^{-6}$ CFU reduction), according to ISO14937:2009.[26] Sterilized-dEMC will be dried, to improve stability, extend shelf-life, decrease storage and shipping associated with cold chain requirements.[27] Protocols will be adapted from other works. [28–30]. Studies on dECM powder stability at 4ºC to -80ºC will be conducted.

Characterization of dECM placenta powder - In this task, the biochemical, mechanical and structural integrity of the samples will be performed. For structural characterization, the ultrastructure and pore size will be evaluated using scanning and transmission electron microscopies. Mechanical properties will be evaluated by dynamic Mechanical Analysis. For the biochemical characterization, total collagen, sGAG and elastin quantification and staining will be performed. Growth factor quantification associated with wound healing will be evaluated ELISA assays. Proteomics analysis will be conduct to identify ECM major components.

*In vitro* assays of dECM placenta powder - Biocompatibility will be accessed by direct contact assays using Human Dermal Fibroblasts (HDF) following ISO10993-5:2009. *In-vitro* effect of dECM materials in human cells such as dermal microvascular endothelial cells (HMEC-1), HDF, keratinocytes (HaCat) and mesenchymal stromal cells (MSC). These cells are implicated in wound repair and skin regeneration. Placenta dECM will be investigated for its effects to improve vascular growth with encapsulated HDFs, ECM assembly, MSC differentiation, keratinocyte epithelialization in hyperglycemic context, by acting in a paracrine manner.

## Summary

While decellularized scaffolds are already available commercially, slow decellularization times and the over-reliance on harsh and detrimental chemicals have impeded its widespread use. This project outlines a complete pipeline for processing of biological tissue, proposing a pioneer strategy to valorise extracellular matrix (ECM) and increase process efficiency, combining, decellularization, sterilization and drying using $scCO_2$ technology. Placental tissue will be used as a rich source of ECM and biological cues. Through conjugation with polyphenols and enzymatic crosslinking, the resulting decellularized ECM will be further processed into a hydrogel with improved bioactivity and *in situ* forming capability, which will be used in the context of chronic wound healing. Cell embedding will be attempted due to the moderate hydrogel processing conditions, resulting in a new bioink enabling 3D-bioprinting of viable and rich skin tissue microenvironment.

## Acknowledgments

This research was supported by National Funds from Fundação para a Ciência e a Tecnologia (FCT), through project UID/Multi/50016/2020, and Doctoral Research Grant 2021.05919.BD and this work was also financed through project TEX4WOUNDS (POCI-01-0247-FEDER-047029), under the Incentive System for Research and Technological Development, R&DT Projects in co-promotion (Notice SI/17/2019). Work carried out in the framework of the COST Action CA18224 “Green Chemical Engineering Network towards upscaling sustainable processes” (GREENERING), funded by the European Commission.

## References

1. Blair, N. F., Frith, T. J. R. & Barbaric, I. Regenerative Medicine: Advances from developmental to degenerative diseases. in *Personalised medicine* (ed. El-Khamisy, S.) vol. 1007 225–239 (Springer, 2017).
2. Chandra, P. K., Soker, S. & Atala, A. Tissue engineering: current status and future perspectives. in *Principles of Tissue Engineering* 1–35 (Academic Press, 2020). doi:10.1016/b978-0-12-818422-6.00004-6.
3. Duarte, M. M. *et al.* Contributions of supercritical fluid technology for advancing decellularization and postprocessing of viable biological materials. *Mater. Horizons* (2022) doi:10.1039/D1MH01720A.
4. Xing, H., Lee, H., Luo, L. & Kyriakides, T. R. Extracellular matrix-derived biomaterials in engineering cell function. *Biotechnology Advances* vol. 42 (2020).
5. Choudhury, D., Tun, H. W., Wang, T. & Naing, M. W. Organ-Derived Decellularized Extracellular Matrix: A Game Changer for Bioink Manufacturing? *Trends Biotechnol.* **36**, 787–805 (2018).
6. Grauss, R. W., Hazekamp, M. G., Van Vliet, S., Gittenberger-De Groot, A. C. & DeRuiter, M. C. Decellularization of rat aortic valve allografts reduces leaflet destruction and extracellular matrix remodeling. *J. Thorac. Cardiovasc. Surg.* **126**, 2003–2010 (2003).
7. Cartmell, J. S. & Dunn, M. G. Effect of chemical treatments on tendon cellularity and mechanical properties. *J. Biomed. Mater. Res.* **49**, 134–140 (2000).
8. Roosens, A. *et al.* Impact of Detergent-Based Decellularization Methods on Porcine Tissues for Heart Valve Engineering. *Ann. Biomed. Eng.* **44**, 2827–2839 (2016).

9. Porzionato, A. *et al.* Tissue-engineered grafts from human decellularized extracellular matrices: A systematic review and future perspectives. *International Journal of Molecular Sciences* vol. 19 (2018).
10. Soares, G. C. *et al.* Supercritical CO 2 technology: The next standard sterilization technique? *Materials Science and Engineering C* vol. 99 520–540 (2019).
11. Huppertz, B. The anatomy of the normal placenta. *J. Clin. Pathol.* **61**, 1296–1302 (2008).
12. Carlson, B. M. Placenta. in *Reference Module in Biomedical Sciences* 1–8 (Elsevier, 2014). doi:10.1016/B978-0-12-801238-3.05435-0.
13. Malek, A. & Bersinger, N. A. Human placental stem cells: biomedical potential and clinical relevance. *J. Stem Cells* **6**, 75–92 (2011).
14. Pogozhykh, O., Prokopyuk, V., Figueiredo, C. & Pogozhykh, D. Placenta and Placental Derivatives in Regenerative Therapies: Experimental Studies, History, and Prospects. *Stem Cells Int.* **2018**, (2018).
15. *Regenerative Medicine Using Pregnancy-Specific Biological Substances*. *Regenerative Medicine Using Pregnancy-Specific Biological Substances* (Springer London, 2011). doi:10.1007/978-1-84882-718-9.
16. Kawakatsu, M., Urata, Y., Goto, S., Ono, Y. & Li, T.-S. Placental extract protects bone marrow-derived stem/progenitor cells against radiation injury through anti-inflammatory activity. *J. Radiat. Res.* **54**, 268–76 (2013).
17. Bak, D. ho *et al.* Antioxidant effect of human placenta hydrolysate against oxidative stress on muscle atrophy. *J. Cell. Physiol.* **234**, 1643–1658 (2019).
18. Hong, J. W., Lee, W. J., Hahn, S. B., Kim, B. J. & Lew, D. H. The effect of human placenta extract in wound healing model. *Ann. Plast. Surg.* **65**, 96–100 (2010).
19. Bak, D. H. *et al.* Anti-apoptotic effects of human placental hydrolysate against hepatocyte toxicity in vivo and in vitro. *Int. J. Mol. Med.* **42**, 2569–2583 (2018).
20. Igarashi, K., Sugimoto, K. & Hirano, E. Placental extract suppresses the formation of fibrotic deposits by tumor necrosis factor alpha and transforming growth factor beta-induced epithelial-mesenchymal transition in ARPE-19 cells. doi:10.1186/s13104-021-05824-0.
21. Tiwary, S. K. *et al.* Effect of placental-extract gel and cream on non-healing wounds. *http://dx.doi.org/10.12968/jowc.2006.15.7.26937* **15**, 325–328 (2013).

22. Inglis, S., Schneider, K. H., Kanczler, J. M., Redl, H. & Oreffo, R. O. C. Harnessing Human Decellularized Blood Vessel Matrices and Cellular Construct Implants to Promote Bone Healing in an Ex Vivo Organotypic Bone Defect Model. *Adv. Healthc. Mater.* **8**, (2019).

23. Liu, K. X., Kato, Y., Kaku, T. I. & Sugiyama, Y. Human placental extract stimulates liver regeneration in rats. *Biol. Pharm. Bull.* **21**, 44–49 (1998).

24. Leonel, L. C. P. C. *et al.* Decellularization of placentas: Establishing a protocol. *Brazilian J. Med. Biol. Res.* **51**, (2018).

25. Wehmeyer, J. L., Natesan, S. & Christy, R. J. Development of a Sterile Amniotic Membrane Tissue Graft Using Supercritical Carbon Dioxide. *Tissue Eng. - Part C Methods* **21**, 649–659 (2015).

26. ISO - ISO 14937:2009 - Sterilization of health care products — General requirements for characterization of a sterilizing agent and the development, validation and routine control of a sterilization process for medical devices. https://www.iso.org/standard/44954.html.

27. Maltesen, M. J. & van de Weert, M. Drying methods for protein pharmaceuticals. *Drug Discov. Today Technol.* **5**, e81–e88 (2008).

28. Bleuel, E. P., Roebers, T. P. C., Schulting, E. & Den Dunnen, W. F. A. Solvent-free tissue processing using supercritical carbon dioxide. *Histopathology* **61**, 1198–1208 (2012).

29. Zambon, A. *et al.* Dry acellular oesophageal matrix prepared by supercritical carbon dioxide. *J. Supercrit. Fluids* **115**, 33–41 (2016).

30. Giobbe, G. G. *et al.* Preservation over time of dried acellular esophageal matrix. *Biomed. Phys. Eng. Express* **4**, 065021 (2018).

# Extraction of Active Components from Cranberry (*Vaccinium vitis-ideaea*) and Determination of Antimicrobial Potential

Azra Osmić, Matjaž Finšgar, Gal Slaček, Taja Žitek, Maša Knez Marevci, Željko Knez

Faculty of Chemistry and Chemical Engineering, University of Maribor,

Smetanova ulica 17, 2000 Maribor

Laboratory for separation processes and production design, Laboratory for Analytical Chemistry and Industrial Analysis

azra.osmic@um.si

## Introduction

Cranberry (*Vaccinium vitis - idaea)* is a small evergreen shrub belonging to the Ericaceae group.[1] Recent research suggests that berry fruits are a rich source of numerous phytochemicals with a wide range of bioactivity and effects on human health. Several berry fruits have recently attracted attention because of their effects in vitro and/or their associations in observational studies with lower risk for some chronic diseases. Randomized clinical trials have advanced in recent years to the point where meta-analyses of these results have now been conducted. Cranberries have a wide range of health benefits for humans. Cranberries are a treasure trove of vitamins (A, B1, B2, B3, K), minerals (sodium, potassium, calcium, magnesium and phosphorus) and fibre. They contain a huge percentage of water (> 80 %) in 10 % carbohydrate. Other 10 % represent flavonoids, organic acids and a small amount of ascorbic acid. [1]

Cranberry (*Vaccinium macrocarpon*) is a particularly rich source of (poly)phenols that have been associated in vitro with: antibacterial, antiviral, antimutagenic, anticarcinogenic, antitumorigenic, antiangiogenic, anti-inflammatory (*E. coli, S. aureus, etc.*), and antioxidant properties. Cranberry contains PAC type A and PAC type B. PAC Type A, which contains a second bond via chroman’s oxygen, is liked to have antimicrobial effect in preventing urinary tract infections with *Escherichia coli (E. coli)*. PAC Type B, on the other hand, is a short-chain polymer of anticyanidin units containing multiple basic structures linked by a single ether bond.[2–4]

The aim of the research work was, in the first part, to identify the optimal conditions for the extraction of cranberry and, in the second part, to achieve high activities of the compounds by the most appropriate extraction method. In the present research, the extracts from cranberry from Alfred Galke GmbH (Samtgemeinde Bad Grund, Germany)

were prepared by conventional methods (Soxhlet extraction, Ultrasonic extraction, cold maceration) with three different solvents (water, ethanol, and ethanol : water (70:30)). In the supercritical extraction, carbon dioxide ($CO_2$) was used as the solvent and ethanol, water and an ethanol : water mixture (70:30) as co-solvents. The antimicrobial potential, defined by the determination of minimum inhibitory concentration (MIC), was also measured for the selected extract.

## Experimental

Total phenolic compounds in the cranberry extracts were determined with Folin – Ciocalteu reagent, using gallic acid as a standard phenolic compound. [5] Proanthocyanidins were analysed by a UV spectrophotometry (UV – VIS spectrophotometer, BIOTEK SYNEGRY 2) based on acid hydrolysis and colour formation. [6] Antioxidant activity was determined by the 2,2-diphenyl-1-picrylhydrazyl (DPPH) method. Measurements of antimicrobial potential was performed using the microdilution method. [7,8] Antimicrobial potential was measured on Gram-negative bacteria *Staphylococcus aureus* (MRSA) (ATCC 25923, ATCC, Wesel, Germany), Gram-positive bacteria *Escherichia coli* (ATCC 25922, ATCC, Wesel, Germany) and fungi *Candida albicans* (ATCC 60193, ATCC, Wesel, Germany). [9]

## Summary

- **Yield of extraction**: comparisons of four different extractions (SOX, CM, UZ, SCF) with three different solvents (ethanol, ethanol : water (70:30), water) are shown in Fig 1.

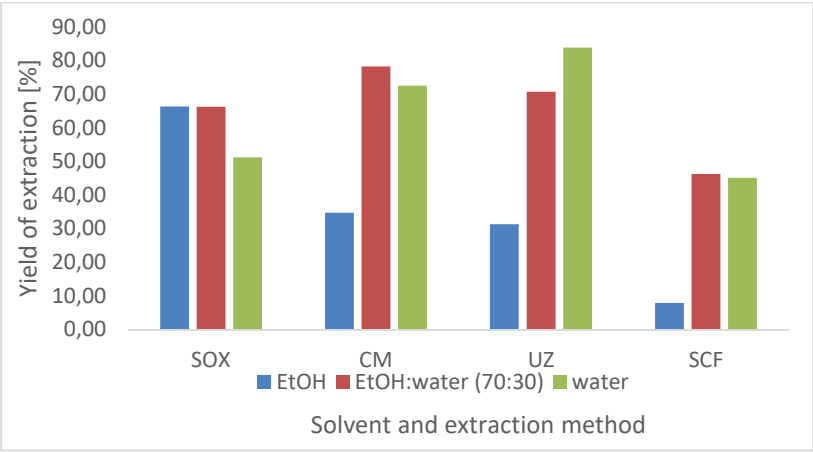


*Figure 1: Yield of extraction.*

- **Antioxidant activity, total phenols and proanthocyanidins:** the total phenolic content is calculated as the equivalent of gallic acid in mg per gram of the selected material (Fig. 2). The content of the proanthocyanidins in mg per gram of material selected (mPAC/g material) are shown in Fig. 3 and the extract solution concentrations required for inhibitory efficacy are shown in Fig. 4.

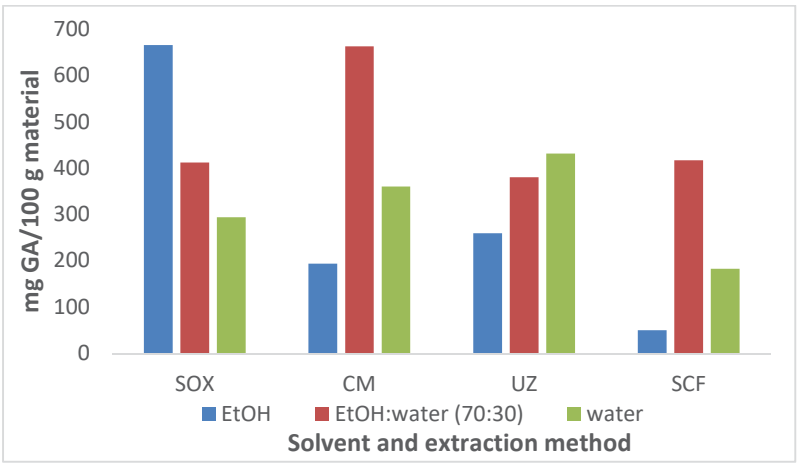


*Figure 2: Total phenolic content of cranberry.*

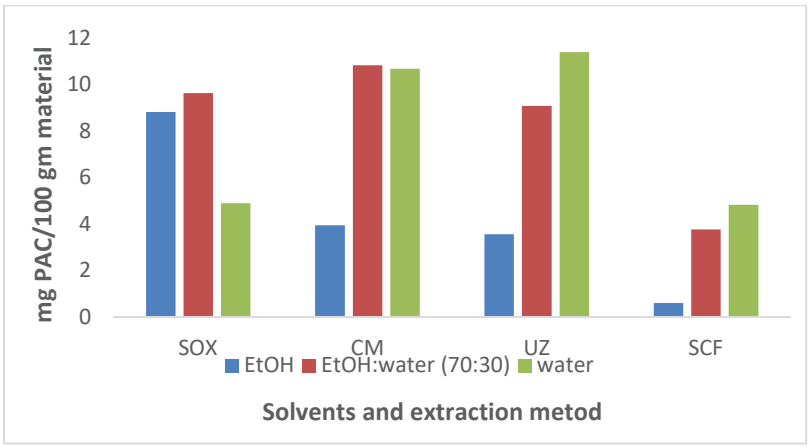


*Figure 3: Proanthocyanidin content in cranberry.*

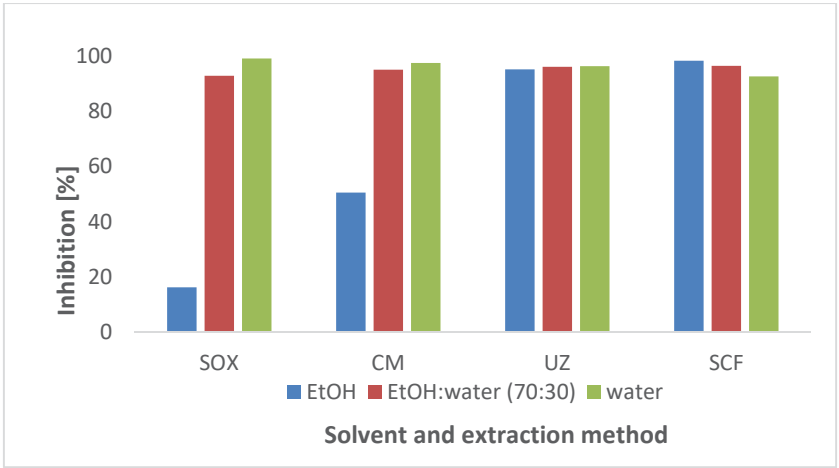


*Figure 4: Antioxidant activity in cranberry.*

- **Antimicrobial potential**: The antimicrobial potential was determined on two bacteria (*Staphylococcus aureus* (Fig. 5) and *Escherichia coli* (Fig. 6)) and one fungus (*Candida albicans* (Fig. 7)). In rows A and B, was applied the extract obtained by the SOX method (GS), in rows C and D, the extract obtained by the CM method (GCM) was applied, then in rows E and F, the extract obtained by the UZ method (GU) and in rows G and H, the extract obtained by supercritical fluid extraction (GSCF).

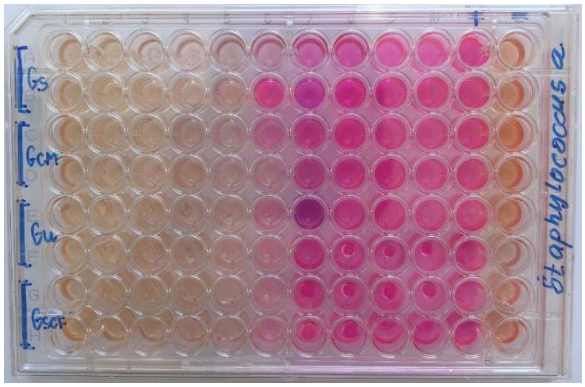


*Figure 5: bacterial Staphylococcus aureus.*


*Figure 6: bacteria Escherichia coli.*


*Figure 7: fungi Candida albicans.*

Extract obtained by ultrasonic extraction contained the highest proportion of total phenols (703.54 mg/100 g ext). The MIC of the extract for Gram positive bacteria, *Staphylococcus aureus*, was 1.934 mg/mL, for Gram negative *Escherichia coli* was 4.105 mg/mL, and for *Candida albicans* it was 16.35 mg/mL.

The most suitable conventional method is ultrasonic extraction, in which water was used as a solvent. The results show that the extracts have antimicrobial potential against *Staphylococcus aureus*, reaching the highest inhibition threshold.

**Other skills**

- X-ray Powder Diffraction (XRD)
- Thermogravimetric analysis (TGA)
- The attenuated total reflectance – Fourier transform infrared spectroscopy (ATR-FTIR)

**References**

[1] R. Raz, B. Chazan, M. Dan, Cranberry Juice and Urinary Tract Infection, Clin. Infect. Dis. 38 (2004) 1413–1419. https://doi.org/10.1086/386328.

[2] R.A. Dixon, D.-Y. Xie, S.B. Sharma, Proanthocyanidins--a final frontier in flavonoid research?, New Phytol. 165 (2005) 9–28. https://doi.org/10.1111/j.1469-8137.2004.01217.x.

[3] A.B. Howell, Bioactive compounds in cranberries and their role in prevention of urinary tract infections, Mol. Nutr. Food Res. 51 (2007) 732–737. https://doi.org/10.1002/mnfr.200700038.

[4] B. Johnson-White, L. Buquo, M. Zeinali, F.S. Ligler, Prevention of nonspecific bacterial cell adhesion in immunoassays by use of cranberry juice, Anal. Chem. 78 (2006) 853–857. https://doi.org/10.1021/ac051700v.

[5] M. Škerget, P. Kotnik, M. Hadolin Kolar, A. Rižner Hraš, M. Simonič, Ž. Knez, Phenols, proanthocyanidins, flavones and flavonols in some plant materials and their antioxidant activities, in: Food Chem., 2005. https://doi.org/10.1016/j.foodchem.2004.02.025.

[6] L. Majhenič, M. Škerget, Ž. Knez, Antioxidant and antimicrobial activity of guarana seed extracts, in: Food Chem., 2007. https://doi.org/10.1016/j.foodchem.2007.01.074.

[7] P. Molyneux, The use of the stable radical Diphenylpicrylhydrazyl (DPPH) for estimating antioxidant activity, 26 (2003).

[8] R.A. Onyeagba, O.C. Ugbogu, C.U. Okeke, O. Iroakasi, Studies on the antimicrobial effects of garlic (Allium sativum Linn), ginger (Zingiber officinale Roscoe) and lime (Citrus aurantifolia Linn), Afr. J. Biotechnol. 3 (2004) 552–554. https://doi.org/10.4314/ajb.v3i10.15016.

[9] T. Žitek, B. Daris, M. Finšgar, Ž. Knez, D. Bjelić, M. Knez Marevci, The Effect of Polyphenolics in Extracts from Natural Materials on Metabolic Activity of Metastatic Melanoma WM-266-4 Cells, Appl. Sci. 10 (2020) 3499. https://doi.org/10.3390/app10103499.

## Registered Lecturers


| | |
|---|---|
| Prof. Zeljko Knez | University of Maribor, Slovenia<br>zeljko.knez@uni-mb.si |
| Prof. Urban Bren | University of Maribor, Slovenia<br>urban.bren@um.si |
| Dr. Amra Perva | University of Maribor, Slovenia<br>amra.pervac@um.si |
| Dr. Masa Knez- Marevci | University of Maribor, Slovenia<br>masa.knez@um.si |
| Ao.Prof. Thomas Gamse | Graz University of Technology, Austria<br>Thomas.Gamse@TUGraz.at |
| Dr. Eduard Lack | Natex Prozesstechnologie, Austria<br>office@natex.at |
| Dr. Helena Sovova | Institute of Chemical Process Fundamentals, Czech Republic, helsov@seznam.cz |
| Prof. Marcus Petermann | Ruhr University Bochum, Germany<br>petermann@fvt.ruhr-uni-bochum.de |
| Prof. Thomas Müller | Ruhr University Bochum, Germany<br>mueller@ls-csc.rub.de |
| Prof. Markus Busch | Technical University Darmstadt, Germany<br>markus.busch@pre.tu-darmstadt.de |
| Prof. Eberhard Schlücker | University Erlangen Nürnberg, Germany<br>sl@ipat.uni-erlangen.de |
| Prof. Sabine Grüner-Lempart | University of Applied Sciences Weihenstephan-Triesdorf, Germany, sabine.gruener-lempart@hswt.de |
| Dr. Carsten Zetzl | Hamburg University of Technology, Germany<br>zetzl@tuhh.de |
| Prof. Pavel Gurikov | Hamburg University of Technology, Germany<br>pavel.gurikov@tuhh.de |
| Prof. Maria Jose Cocero | University of Valladolid, Spain<br>mjcocero@iq.uva.es |

| | |
|---|---|
| Prof. Angel Martin Martinez | University of Valladolid, Spain<br>mamaan@iq.uva.es |
| Prof. Martial Sauceau | Ecole des Mines d'Albi, France<br>martial.sauceau@mines-albi.fr |
| Prof. Edit Szekely | Budapest University of Technology and Economics, Hungary, edit.szekely@edu.bme.hu |
| Dr. Erika Vagi | Budapest University of Technology and Economics, Hungary, vagi.erika.maria@vbk.bme.hu |
| Dr. Alessandro Zambon | University of Padua, Italy<br>alessandro.zambon@unipd.it |
| Prof. Irena Zizovik | Wroclaw University of Science and Technology, Poland<br>irena.zizovic@pwr.edu.pl |

## Registered Participants

| | | |
|---|---|---|
| Azra Osmic | SI | University of Maribor |
| Vid Ravnik | SI | University of Maribor |
| Zala Stukovnik | SI | University of Maribor |
| Jon Alarik Scherf | AT | Graz University of Technology |
| Julija Struncnik | AT | Graz University of Technology |
| Lorenci Gjurgjaj | AL | Ivodent Academy |
| Jeta Lica | AL | Ivodent Academy |
| Altin Mele | AL | Ivodent Academy |
| Joline Hansen | DE | Ruhr University Bochum |
| Ka Loi Lin | DE | Ruhr University Bochum |
| Dennis Panke | DE | Ruhr University Bochum |
| Marcel Jungbluth | DE | Technical University Clausthal |
| Jonas Degenkolb | DE | Technical University Darmstadt |
| Denise Eryildirim | DE | Technical University Darmstadt |
| Laura Euler Bueno | DE | Technical University Darmstadt |
| Lena Gockel | DE | Technical University Darmstadt |
| Moritz Imhoff | DE | Technical University Darmstadt |
| Alexander Klimeck | DE | Technical University Darmstadt |
| Isabel Marie Kronshorst | DE | Technical University Darmstadt |
| Aaron Röblitz | DE | Technical University Darmstadt |
| Lorenz Schmidt | DE | Technical University Darmstadt |
| Nicola Julian Schreiner | DE | Technical University Darmstadt |
| Lara Gibowsky | DE | Hamburg University of Technology |
| Maira Chinchilla | ES | University of Valladolid |
| Enkeledo Menalla | ES | University of Valladolid |
| Alina Satpayeva | ES | University of Valladolid |
| Elisa Mialich | IT | University of Padova |
| Patience Abugu | PL | Wroclaw University of Science and Technology |
| Ahmed Elrashidy | PL | Wroclaw University of Science and Technology |
| Beatriz Bernardes | PT | Universidade Católica Portuguesa |
| Marta Sofia Duarte | PT | Universidade Católica Portuguesa |
| Ines Vasconcelos | PT | Universidade Católica Portuguesa |